A Unified Approach to Nuclear Matter and Quark Matter

Sarah I. Howie

Supervisor: Prof. A. W. Thomas

Department of Physics,

University of Adelaide,
Australia

and

Thomas Jefferson National Accelerator Facility,

Newport News, Virginia,
United States of America.

September 2006

Abstract

The properties of hadronic and quark matter are studied as a function of density using a chiral model based on quark degrees of freedom. Nucleons are described as quark - diquark states in the Faddeev approach and this description is extended to infinite nuclear matter in the mean field approximation. We calculate the properties of two flavour quark matter, allowing for the possibility of colour superconductivity in the form of a spin zero condensate (i.e. the 2SC phase). These calculations are performed using the proper-time regularisation method. We find that the phase diagrams for asymmetric matter in this description can have charge neutral phase transitions from the hadronic phase to the deconfined phase, depending on the pairing strength for quarks in the 2SC phase. We study the evolution of the phase diagrams as a function of the pairing strength. The properties of nuclear matter are significantly improved once we take into account the self-energy of the nucleon. We also find that the structure of the nucleon has important consequences for the phase diagram. The charge neutral equations of state are used to produce compact star configurations by solving the Tolman-Oppenheimer-Volkoff (TOV) equations. We use these solutions to investigate the possibility of hybrid stars.

Statement of Originality

This work contains no material which has been accepted for the award of any other degree or diploma in any university or other tertiary institution and, to the best of my knowledge and belief, contains no material previously published or written by another person, except where due reference has been made in the text.

I give consent to this copy of my thesis, when deposited in the University Library, being available for loan and photocopying.

Acknowledgements

Firstly, I would like to thank Wolfgang Bentz, who has been very dedicated to this project and a tremendous help to me throughout its duration. I have learned a great deal from him and I have enjoyed many interesting discussions with him during his visits to Adelaide and to Jefferson Lab. He was also a wonderful host during my stay at the University of Tokai, in Japan. I am very grateful to the people at Jefferson Lab and The University of Adelaide, who have all contributed in many different ways to the progress of this work. In particular, Ian Cloet, who has been exceedingly helpful and generous in sharing his time and knowledge. I am thankful for all of my friends and family who have encouraged me along the way and especially for my husband, who was prepared to move to the other side of the world for the sake of this work. Most of all, I would like to thank my supervisor, Tony Thomas, who has been a great teacher and a true friend. I am especially appreciative of the many unique opportunities that he has provided for me and my fellow students over the years. Primarily thanks to him I can say, that I have very much enjoyed and benefited from my time as a student.

Contents

1

Introduction

In the standard model of physics which has been developed over the last century, there are various branches to explore, with many fascinating puzzles. In Quantum Chromodynamics (QCD), the structure of matter begins with just a few different particle types, interacting in a way which allows them to form into bound states. Out of the mathematically intractable theory of quark and gluon interactions comes order in the form of hadrons. Exactly how this happens is an unsolved problem in QCD. The hadrons constitute the smallest known level of non-trivial structure accessible to experiment. They are combinations of either two or three quarks confined by very powerful forces operating at distances of the order of 10^{-15} metres or less. At the next level of structure we find that hadrons can also bind with each other. In particular, neutrons and protons can cluster together to form stable bound states. In this thesis we investigate these levels of structure, using the Nambu - Jona-Lasinio (NJL) model. This is a chirally symmetric model based on point-like interactions between quarks. We use the NJL model to describe the nucleon and study how a system of interacting nucleons changes as a function of density [1]. We also consider the idea that quarks may be deconfined if this system is sufficiently compressed, as may be the case inside compact stars.

Historically models of dense matter were formulated in terms of point-like nucleons, long before the discovery of quarks [2–4]. With the great success of the theory of QCD came the realisation that such models are not entirely accurate in neglecting quark and gluon degrees of freedom, especially when they are applied to high density systems like compact stars. However, QCD is very difficult to incorporate into finite density studies. In the weak coupling regime, where quarks experience asymptotic freedom, QCD is well understood, but at low momentum transfer, where the coupling is strong, full QCD calculations become intractable [5]. Lattice Gauge Theory has been extensively employed in this regime, using supercomputers to simulate QCD on a discretised lattice [6]. Unfortunately, this approach is problematic in the finite density plane of the QCD phase diagram. At finite chemical potential the fermion determinant is no longer positive definite, so it cannot be used as a probability weight in the functional integral. This is referred to as *the sign problem*. There has been some success in dealing with this issue, but so far only for very small

chemical potentials [7]. Thus Lattice Gauge Theory cannot be used to produce an equation of state for nuclear matter or quark matter. In order to study the properties of these phases, the most fruitful approach has been to construct models that as far as possible share the properties of QCD. One attraction of the NJL model, is that it is based on quark degrees of freedom and it shares some of the dominant symmetries and symmetry breaking features of low-energy QCD. By construction, it is non-renormalisable, due to the point-like nature of the quark interactions. We choose the proper-time cut-off scheme to regularise the model [8], as this technique has particular advantages for the description of nuclear matter [1]. In this thesis we work with the assumption of two flavours, but the methods used herein may also be extended to include strangeness in the confined and deconfined phases [9–11].

By employing a quark level model which mimics the behaviour of low-energy QCD, we are able to derive the properties of hadrons, hadronic matter and quark matter within a single framework, using the approach of Bentz et. al. [12]. Nucleons are described as a quark - diquark system using the Faddeev approach. The couplings that control quark correlations within nucleons also play a role in quark matter where attractive channels lead to color superconductivity. It has recently been proposed that if quark matter exists in nature, it is likely to be in a colour superconducting state [13, 14]. This behaviour is analogous to a conventional superconductor, only it is quarks rather than electrons which form into Cooper pairs. The superconducting gap in the quark energy spectrum can be very large (of order 100 MeV), but it has a strong dependence on the pairing strength between quarks. In two flavour quark matter, theoretical studies show that there is a scalar attraction between quarks corresponding to the one-gluon exchange and this is the dominant channel for Cooper pairing in this phase [11]. At present colour superconductivity is almost impossible to investigate experimentally, due to the difficulties in producing quark matter.

Most experimental results in finite density physics have been obtained at or near nuclear saturation density ($\rho_0 = 0.17$ fm^{-3}). For example, nuclear binding energies and the properties of nuclei have been extensively studied [15–19]. The properties of matter far above saturation density are challenging to discern from experiments, because such dense matter can only be formed for a fleeting moment of time and its components cannot be directly measured (only its decay products). Heavy ion experiments probe an especially complex region of the phase diagram, where QCD is non-perturbative and simplifying assumptions are few. At present it is an issue of debate whether deconfined quark matter has been produced in experiments at CERN [20] and/or the Relativistic Heavy Ion Collider (RHIC) at Brookhaven [21]. Proposed experiments for the Large Hadron Collider (LHC) at CERN are expected to produce a quark-gluon

plasma in the near future. From this facility much knowledge can be gained about the behaviour of matter at very high temperatures, however, it is not possible to access the low temperature part of the phase diagram using heavy ion collisions.

Compact stars offer a unique opportunity to test our model of nucleons and dense matter at zero temperature. Though typically compact stars have surface temperatures of approximately 10^6 Kelvin, in terms of nuclear physics calculations, the influence of temperature is negligible [22]. Compact stars have radii of the order of ten kilometers and masses of the same order of magnitude as the sun. With such a great mass compressed into such a small volume, the gravitational fields associated with these stars are enormous and we must use the theory of General Relativity to describe them. In this work we use the Tolmann-Oppenheimer-Volfkoff (TOV) equations [23, 24], to obtain compact star properties for the equations of state we derive.

From an observational point of view it is an excellent time to be working in the field of compact star physics, because there is a great deal of new information emerging on a daily basis. There are several major detection surveys being conducted around the world, through which thousands of compact stars have already been identified and extensively studied. The largest system proposed to be used for this purpose, the Square Kilometer Array (SKA), is an international project approved for construction in 2010. It is anticipated that tens of thousands of compact stars will be discovered using this array [25]. Through this project and others, the study of compact stars is sure to remain a very active field in astrophysics for many years to come. We can expect improved estimates of bulk properties such as masses and radii, coupled with significant improvements in the precision of pulsar timing. It is important that the theoretical effort is maintained to support this rapidly progressing area in astrophysics. Ultimately, an improved knowledge of the behaviour of QCD at high densities is crucial to understanding the physics of supernovae, binary mergers, glitches and many other aspects of compact star phenomenology. In particular, the equation of state is essential input for modelling in all of these areas. In this thesis we work towards a realistic equation of state by including the effects of nucleon structure and taking into account the possibility of deconfinement.

The outline of this thesis is as follows. We give an introduction to the field of finite density physics in Chapter 2, providing a brief overview of the main approaches which have been employed in this area. Chapter 3 is focused on the NJL model, its history and its application to the description of bound states. We use the properties of the pion and the nucleon in the vacuum to fix the parameters of the model which are used in this description. We begin with a quark - scalar diquark picture of the nucleon, neglecting the axial vector diquark

(spin 1) channel. In Chapter 4 we explain how to hadronise the NJL Lagrangian density using the method of Reinhardt [26]. Deriving the equation of state for symmetric nuclear matter, we use empirically known properties of the system to fix the remaining coupling constants of the model. Including electrons in chemical equilibrium, we also calculate the charge neutral equation of state for the hadronic phase. We derive the properties of the quark matter phase in Chapter 5, introducing the phenomenon of colour superconductivity.

In Chapter 6 the properties hadronic matter and quark matter are compared, using asymmetric phase diagrams to illustrate the preferred phases as a function of baryon and isospin chemical potentials. Here we study the possible phase transitions from the nuclear matter phase to the quark matter phase as a function of the pairing strength for quarks in quark matter. The transitions are characterised by globally charge neutral mixed phases which may contain varying proportions of negatively and positively charged matter, as a function of baryon density. We calculate the equations of state for these mixed phases using the method of Glendenning [27]. The hybrid star configurations associated with these equations of state are presented in Chapter 7. Finally, in Chapter 8, we improve our model for the nucleon, by including the axial vector diquark channel for quark pairing. We also analyse the effects of including the nucleon self-energy in these calculations. We show that there are substantial improvements in the saturation properties of the model. There are also important consequences for the phase diagram and the properties of compact stars. Indeed, the structure of the nucleon has significant implications in this model. We show that deconfinement does occur within (two-flavour) compact stars, when we fix the pairing strength in quark matter, using the properties of the nucleon.

2

Finite Density Physics

The study of nuclear matter at finite density involves the description of a system of interacting particles and is usually referred to as the many-body problem. The problem draws on many aspects of fundamental physics including quantum mechanics, special relativity, thermodynamics and Quantum Chromodynamics (QCD). Early studies of the many-body problem in nuclear physics were aimed at calculating the properties of nuclei. Long before the discovery of quarks and the subsequent development of QCD, nuclei were extensively researched in terms of nucleon degrees of freedom.

In contemporary physics the description of matter at high densities is typically divided into two distinct phases, the hadronic phase and the quark matter phase. These two phases differ primarily by the property of quark confinement. In the hadronic phase (or nuclear matter (NM) phase), matter is composed of neutrons, protons and other hadrons, as we find inside nuclei, for example. In the quark matter (QM) phase, hadrons are not present. Rather the quarks are deconfined. In this chapter we give an overview of the many-body problem and some of the approaches more commonly employed to study it. Beginning with an introduction to QCD, we include a discussion of the non-relativistic potential models and the relativistic mean field theories in Sections 2.2 and 2.3. Finally, in Section 2.4, we consider how quark degrees of freedom may be incorporated into nuclear matter calculations and provide a motivation for doing so.

2.1 Quantum Chromodynamics

In order to investigate the properties of matter at the subatomic level we must first understand the basic rules for particle interactions and behaviour. Quantum Chromodynamics (QCD) sets up a clear framework to describe interactions between quarks in terms of gluon exchange. Reviews of QCD are found in references [5], [28] and [29]. There are three possible colour charges for quarks (conventionally labeled red, blue and green in the literature) and six different flavours (up, down, strange, charm, bottom and top). QCD is a non-abelian gauge theory. That is, unlike Quantum Electrodynamics (QED), where the force carriers (photons) are charge neutral, in QCD the force carriers (gluons)

are colour charged, so they interact with each other as well as with the quarks. The QCD Lagrangian density has the form,

$$\mathcal{L} = \bar{\psi}(i\not{D} - m_0)\psi - \frac{1}{4}G^{\mu\nu}_a G^a_{\mu\nu}, \tag{2.1}$$

where $\not{D} = D_\mu\gamma^\mu = (\partial_\mu - igA^a_\mu T_a)\gamma^\mu$ and $G^a_{\mu\nu}$ is the field-strength tensor. Here g is the QCD coupling constant and A^a_μ represent the gluon fields. The matrices T_a ($T_a \equiv \lambda_a/2$), appearing in the derivative operator, are the generators of the $SU(3)_{colour}$ Lie algebra. The eight colour matrices, λ_a, are given in Appendix A and obey the following relations,

$$[\lambda_a, \lambda_b] = 2if_{abc}, \quad \mathrm{Tr}(\lambda_a\lambda_b) = 2\delta_{ab}, \quad \mathrm{Tr}\lambda_a = 0, \tag{2.2}$$

where f_{abc} are the structure constants.

The quark fields are given by the column vector,

$$\psi(x) = \begin{pmatrix} \psi_R(x) \\ \psi_B(x) \\ \psi_G(x) \end{pmatrix}$$

The diagonal matrix m_0 in the QCD Lagrangian contains the current quark masses of each quark flavour. In low energy hadronic physics (i.e. where the scale is ~ 2 GeV^2) only the two lightest quark flavours contribute to the dynamics, because their masses are relatively small ($m_u \sim m_d \sim 5$ MeV), in contrast to the other quark flavours. Actually the similarity of these light quark masses reflects the almost perfect SU(2) flavour symmetry of nature and the fact that they are both almost zero is related to the fundamental property of chiral symmetry. The strange quark mass is an order of magnitude larger ($m_s \sim 100$ MeV) and the charm, bottom and top quarks are themselves much more massive than the nucleon[1]. Because up and down quarks are so light it is clear that they play a special role in low energy QCD. Nucleons, the building blocks of nuclei, are colour charge neutral combinations of up and down quarks which are bound by the strong force.

QCD has many interesting features that distinguish it from all other types of interactions encountered in modern physics. Because the colour matrices, λ_a, do not commute (see Eqn. 2.2), gauge transformations in color space require that the the gluon fields transform as,

$$A^\mu_a \to A^\mu_a - \frac{1}{g}\partial^\mu\theta_a + f_{abc}\theta_a A^\mu_c, \tag{2.3}$$

[1]The masses of charm, bottom and top quarks are estimated as $m_c \sim 1.5$ GeV, $m_b \sim 5$ GeV and $m_t \sim 180$ GeV, respectively. At present it is not known why the quarks have these particular masses or indeed why there is such a huge variation in the masses associated with the different flavours.

in order that the Lagrangian density be invariant. Here $\theta_1, \theta_2 \ldots \theta_8$ are real parameters associated with the colour gauge transformations $\psi \rightarrow \tilde{\psi} = U\psi$ where the transformation operator is given by,

$$U = \exp\left(-\mathrm{i}\frac{\lambda_\mathrm{a}\theta_\mathrm{a}}{2}\right). \tag{2.4}$$

Furthermore the invariance of the Lagrangian density with respect to these color transformations also implies that the field strength tensor takes the form,

$$G^a_{\mu\nu} = \partial_\mu A^a_\nu - \partial_\nu A^a_\mu + g f^a_{bc} A^b_\mu A^c_\nu. \tag{2.5}$$

Here we see explicitly that the exchange particles (gluons) are self-interacting. Indeed the interaction term in the Lagrangian density ($G^{\mu\nu}_a G^a_{\mu\nu}$) gives rise to a four-gluon vertex.

It is important to note here how the coupling between particles in QCD depends on the energy scale under consideration. Renormalization in QCD introduces a scale, μ, which is related to the coupling constant, g, according to,

$$\mu\frac{d}{d\mu}g(\mu) = \beta(g). \tag{2.6}$$

For small values of g, the function β is determined by perturbation theory as,

$$\beta(g) = -\frac{\beta_0}{(4\pi)^2}g^3 - \frac{\beta_1}{(4\pi)^4}g^5 + \ldots \tag{2.7}$$

$$\beta_0 = 11 - \frac{2}{3}N_f, \qquad \beta_1 = 102 - \frac{38}{3}N_f, \quad \text{etc}, \tag{2.8}$$

where N_f is the number of active flavours at the energy scale under consideration. The effective coupling constant for QCD (labelled with a subscript "s" to indicate the "strong" interaction) is given by,

$$\begin{aligned}\alpha_s(\mu) &= \frac{g^2(\mu)}{4\pi} \\ &= \frac{12\pi}{(33-2N_f)ln(\mu^2/\Lambda^2_{QCD})}\left[1 - \frac{6(153-19N_f)}{(33-2N_f)^2}\frac{ln\left[ln(\mu^2/\Lambda^2_{QCD})\right]}{ln(\mu^2/\Lambda^2_{QCD})}\right] + \ldots\end{aligned} \tag{2.9}$$

where the constant, Λ_{QCD}, is usually taken to be approximately 200 MeV depending on the number of active flavours [30]. For very high energy processes such as deep inelastic scattering (DIS), perturbation theory works well because QCD becomes asymptotically free. i.e. the running coupling constant, $\alpha_s(\mu)$, becomes small as μ becomes large. Thus the high energy regime is reasonably

well described by theory. However, in the low energy regime ($\lesssim$ 1 GeV) the coupling becomes large and perturbation theory does not work. Here the remarkable properties of quark confinement and chiral symmetry breaking give rise to the spectrum of bound massive particles observed in nature. Moreover, because of the non-perturbative interactions among quarks and gluons the QCD vacuum has a non-trivial structure. It is found that quark - anti-quark pair and gluon condensation both occur in the ground state. The quark - anti-quark condensation is related to the spontaneous breaking of a fundamental symmetry of the Lagrangian density (chiral symmetry), producing finite expectation values for the chiral condensates. Gluon condensation arises because the QCD Lagrangian has dilational symmetry (it is invariant under scale transformations) and this symmetry is broken at the quantum level [30].

The key point to take away from this brief introduction to QCD is the importance of the symmetries and how they are broken, because these effects are so powerful (and central) in explaining the physics of QCD. For a summary, Table 2.1 lists the relevant symmetries for two flavour QCD. According to Noether's theorem a symmetry in the Lagrangian density gives rise to a conserved current, J^μ, which satisfies the relation $\partial_\mu J^\mu = 0$. In Table 2.1 the conserved currents listed in the fourth column are a consequence of the invariance of the Lagrangian density under the transformations listed in the third column. The $U_V(1)$ symmetry implies the conservation of baryon number observed in nature. The "$U_A(1)$ puzzle" in the second row refers to the question of why there is no obvious candidate for the Goldstone boson corresponding to the axial symmetry observed in nature[2]. The observed isospin symmetry in nature (third row of Table 2.1) simplifies the study of 2-flavour matter at finite density because it means that up and down quarks have almost the same mass. Indeed, neutrons and protons have almost the same effective masses and their masses can be equated for the purposes of calculating the equation of state. Finally, listed in the fourth row of Table 2.1, is chiral symmetry. This symmetry is found to be spontaneously broken at zero density, but at high densities and/or temperatures chiral symmetry is restored and the quark mass approaches zero (or, to be precise, the value of the current quark mass).[3]

Incorporating these attributes of QCD is very important, but in practice it

[2]It is now widely believed that this issue was resolved by 't Hooft who claimed it could be explained through instanton effects [31]. However, there are also strong arguments to the contrary [32].

[3]It is evident that the large mass of the nucleon may be attributed to the process of dynamical mass generation. This process, which involves the spontaneous breaking of chiral symmetry, can lead to constituent quark masses of the order of 300 - 400 MeV (as discussed in Chapter 3 in the context of the NJL model).

Symmetry	Group	Transformation	Current	Observation
Baryonic	$U_V(1)$	$\Psi \rightarrow e^{-i\alpha}\Psi$	$\bar{\Psi}\gamma^\mu\Psi$	conserved
Axial	$U_A(1)$	$\Psi \rightarrow e^{-i\beta}\gamma_5\Psi$	$\bar{\Psi}\gamma^\mu\gamma_5\Psi$	"$U_A(1)$ problem"
Isospin	$SU_V(2)$	$\Psi \rightarrow e^{-i\tau.\omega/2}\Psi$	$\bar{\Psi}\gamma^\mu\tau^k\Psi$	approx. conserved
Chiral	$SU_A(2)$	$\Psi \rightarrow e^{-i\tau.\theta\gamma_5/2}\Psi$	$\bar{\Psi}\gamma^\mu\gamma_5\tau^k\Psi$	spont. broken

Table 2.1: The symmetries of two flavour QCD.

is not necessarily easy to translate this to a calculable description of low energy physics. For example, how can we use QCD to calculate the spectrum of baryons and mesons? To describe a single hadron in terms of quarks and gluons explicitly is extremely complex (we do not even know how to account for confinement in terms of particle dynamics). Hadronic matter is arguably even more complex, because there we must consider interactions over different scales and how the interactions (and the particles themselves) are modified by the density of the medium. In an attempt to grapple with these complexities, a variety of models have emerged, each with its own strengths and weaknesses. The next few sections are devoted to an overview of two distinct approaches that are widely used today, namely the *non-relativistic nucleon-nucleon potential models* and the *relativistic mean field theories*, such as the Walecka model (QHD).

2.2 Non-Relativistic Approaches

Early studies in nuclear physics focused on the determination of the interaction of two nucleons as a function of their separation. The nucleon-nucleon (N-N) interaction was characterized by point-like non-relativistic neutrons and protons interacting via two-body potentials. The two-body potentials were typically formulated to include the phenomenology of strong short-range repulsion, intermediate-range attraction and long-range one-pion-exchange (OPE) [33].

In the 1970s potentials were constructed by the Bonn and Paris groups. Very accurate potentials which used the data from over 100 N-N scattering experiments at several laboratories (up to energies of about 350 MeV), were also constructed by the Nijmegen (Netherlands) and Argonne (USA) groups [17]. These potentials have been applied to the study of nuclei using various extentions of the Schrödinger-based nuclear shell model of Mayer and Jensen [3]. This approach has been quite successful in describing properties of finite nuclei [19, 34]. Recently, the Argonne group used a Green's function Monte Carlo (GFMC) method to obtain a suitable wavefunction which gives the correct

binding energies for light nuclei ($N < 12$) to within a few MeV accuracy [35]. In this method the many-body Hamiltonian takes the form,

$$H = \sum_i \frac{-i\hbar}{2M_i}\Delta_i^2 + \sum_{i<j} v_{ij} + \sum_{i<j<k} V_{ijk}, \tag{2.10}$$

where the sum is over the number of particles in the nuclei being considered. The second term contains the two-body interaction components determined by N-N scattering data. The interaction depends on the total spin, isospin, orbital and total angular momenta of the nucleons. Written in full this two body potential contains at least 14 distinct terms,

$$v_{ij} = \sum_{p=1,14} v^p(r_{ij}) O_{ij}^p, \tag{2.11}$$

where the operators ($O_{ij}^p = \mathbf{1}, \tau_\mathbf{i} \cdot \tau_\mathbf{j}, \sigma_\mathbf{i} \cdot \sigma_\mathbf{j}, \ldots$) are defined by spin, isospin and angular momentum operators. Following the usual theoretical guidelines the functions $v^p(r_{ij})$ are assumed to have the forms of short, intermediate and one pion exchange potentials [19]. The last term in the Hamiltonian (2.10) gives the correction expected from three-body forces anticipated to arise inside nuclei [36]. Nuclear systems are subsequently described by the solution of the many-body Schrödinger Equation,

$$-\frac{i}{\hbar}\frac{\partial}{\partial t}\Psi(x_1, x_2, \ldots x_A, t) = H\Psi(x_1, x_2, \ldots x_A, t) \tag{2.12}$$

which is solved by variational techniques. Computationally this is a highly demanding process, increasing rapidly with the number of nucleons involved. Current limitations in computing power limit the scope of this method to describe $N < 12$ systems, but the results agree very well with experiment for these nuclei [35]. For example the binding energies and charge radii for light nuclei are predicted to within 10% of experimental values. The saturation properties for infinite nuclear matter are quite good - though it is found to be underbound [37]. Potential models have also been applied to neutron star calculations [38,39], but this seems dubious given the central densities obtained for such stars.

One advantage of using these methods is that it avoids the need for using a mean field approximation, which may be unrealistic at low densities. However, on the negative side, the method does require a large number of parameters [19]. Naturally, if there are a lot of parameters in a model it is possible to achieve good fits to experimental data. Thus, in principle, one can achieve a more accurate equation of state near saturation density using potential models. For some purposes the most important thing may be the accuracy of the equation of state at low density. However, since the matter inside compact stars is likely to

reach densities an order of magnitude larger than the saturation density, what is more desirable is a formalism for the equation of state that obeys special relativity and respects the fundamental symmetries of QCD.

It is clear that in the study of matter under extreme conditions such as high density and/or high temperature, a relativistic approach to the many-body problem is more realistic. In particular, the physical examples of heavy ion collisions and compact star matter cannot be reasonably described by non-relativistic models, since the relativistic propagation of particles should be taken into account [40]. The value of these non-relativistic potential models lies in their ability to accurately reproduce the properties of light nuclei. The application of these models is also an impressive achievement from a computational point of view.

2.3 Relativistic Mean Field Theories

A popular approach to the nuclear many-body problem is to use quantum field theory to describe the interactions between particles in a Lorentz covariant formalism. The first such models were developed in the 1950's by Johnson and Teller [2] and Duerr [4], in order to include relativistic effects in nuclear forces. The most well known relativistic mean field theory (RMFT) to arise since then has been Quantum Hadrodynamics (QHD). In its original form [41] QHD is a very simple model and serves as a useful illustrative example of how RMFT's are formulated. It is a Lorentz invariant model that describes the exchange of mesons between hadrons using quantum field theory. In this particular model some general simplifying approximations are made as to the nature of the particles and the fields in order that the equations of motion may be self-consistently solved. Namely the particles are assumed to be point-like and the scalar and vector fields are assumed to be uniform on the scale of nucleon-nucleon interactions. This is known as the mean field approximation (MFA). The coupling constants for these interactions are fixed to reproduce the properties of nuclear matter at saturation density.

The dynamics of the nucleon-nucleon interaction are dominated by an attractive scalar force and a repulsive vector force associated with scalar and vector meson exchange. In nature the vector meson corresponds to the omega meson (which has a mass, m_ω, of approximately 783 MeV in the vacuum). Originally the scalar attraction was attributed to the exchange of the so called sigma meson (with a mass, m_σ, of approximately 500 - 600 MeV). It is currently debated whether this scalar force is due to two pion exchange [42] or, if in fact, the original view was correct [43]. Nevertheless, with these phenomenologically mo-

tivated aspects of the nucleon-nucleon interaction in mind, the QHD Lagrangian density can be expressed as,

$$\begin{aligned}\mathcal{L}_{QHD} &= \bar{\Psi}_N[\gamma_\mu(i\partial^\mu - g_\omega\omega^\mu) - (M - g_\sigma\sigma)]\Psi_N \\ &+ \frac{1}{2}(\partial_\mu\sigma\partial^\mu\sigma - m_\sigma^2\sigma^2) - \frac{1}{4}F^{\mu\nu}F_{\mu\nu} + \frac{1}{2}m_\omega^2\omega_\mu\omega^\mu, \end{aligned} \tag{2.13}$$

where we define $F_{\mu\nu} = \partial_\mu\omega_\nu - \partial_\nu\omega_\mu$ and the couplings for the scalar (σ) and vector (ω) fields are given by g_σ and g_ω respectively. An interesting point to note from the first term is that the scalar field shifts the mass of the nucleon, M and the vector field shifts the energy. The equations of motion for the scalar, vector and nucleon fields ($\bar{\Psi}_N$ and Ψ_N) can be readily obtained from the Lagrangian via the Euler-Lagrange equations,

$$\frac{\partial\mathcal{L}}{\partial\phi_i} - \frac{\partial}{\partial x^\mu}\left[\frac{\partial\mathcal{L}}{\partial(\partial\phi_i/\partial x^\mu)}\right] = 0, \tag{2.14}$$

where $\phi_i \equiv \phi_i(x_\mu)$ are the fields. This yields the following non-linear quantum field equations,

$$(\partial_\mu\partial^\mu + m_\sigma^2)\sigma = g_\sigma\bar{\Psi}_N\Psi_N \tag{2.15}$$

$$\partial_\mu F^{\mu\nu} + m_\omega^2\omega^\nu = g_\omega\bar{\Psi}_N\gamma^\nu\Psi_N \tag{2.16}$$

$$[\gamma^\mu(i\partial_\mu - g_\omega\omega_\mu) - (M - g_\sigma\sigma)]\Psi_N = 0 \tag{2.17}$$

$$\bar{\Psi}_N[\gamma^\mu(i\overleftarrow{\partial}_\mu - g_\omega\omega_\mu) - (M - g_\sigma\sigma)] = 0 \tag{2.18}$$

These equations are very complicated to solve. However, if one makes the simplifying assumption that the meson fields do not depend on position (i.e. the mean field approximation), then the field operators can be replaced by their expectation values so that,

$$\sigma \rightarrow \langle\sigma\rangle \equiv \sigma_0 \tag{2.19}$$

$$\omega_\mu \rightarrow \langle\omega_\mu\rangle \equiv \delta_{\mu0}\omega_0 \tag{2.20}$$

In uniform matter at rest, the expectation value of the spatial component of the vector field $\langle\vec{\omega}\rangle$ vanishes due to rotational invariance (here we are assuming that the system is both uniform and static, meaning that all positions and directions are equivalent). Reinserting the constants σ_0 and ω_0 into equations (2.15) - (2.16), gives the field equations in the mean field approximation,

$$\sigma_0 = \frac{g_\sigma}{m_\sigma^2}\langle\bar{\Psi}_N\Psi_N\rangle \quad and \quad \omega_0 = \frac{g_\omega}{m_\omega^2}\langle\Psi_N^\dagger\Psi_N\rangle, \tag{2.21}$$

which can be solved self-consistently and used to obtain the equation of state for nuclear matter. This mean field approximation should become increasingly

valid as the density increases, because the source terms in the field equations will become larger [44]. One of the benefits of using a relativistically covariant formalism is that the equation of state will automatically respect causality, by construction, which is not the case for Schrödinger-based potential models. Furthermore, very few parameters are needed to describe the system. For example, as presented in the previous section, QHD only requires two parameters, g_σ and g_ω. These can be adjusted to give the correct binding energy ($E_B = -17$ MeV) and saturation density ($\rho_0 = 0.17$ fm^{-3}) for nuclear matter. The model can also be extended to include other effects such as rho meson exchange, scalar self-interactions and kaon and pion condensation [22]. Yet it remains simple to formulate and requires comparatively little computational effort to calculate the properties of hadronic matter. The NJL model as presented in this thesis, has many similarities to QHD, with the additional benefits that it is chirally symmetric and it also has the power to describe the quark structure of the nucleon in a Lorentz covariant manner.

2.4 Quark Level Models

One shortcoming of most descriptions of nuclear matter to date, is the absence of explicit quark degrees of freedom. It is sometimes argued that at saturation density the quark degrees of freedom are redundant in describing the interaction between nucleons. Thus nucleons are treated as point-like particles. Often such models are extrapolated up to very high densities - even ten times normal nuclear matter density - to be used in neutron star calculations. It is highly questionable whether under these conditions nucleon degrees of freedom are still valid. Of course, in effective field theories internal degrees of freedom can, to an extent, be included implicitly and it is not necessarily a simple task to differentiate between quark effects and long-range effects in a nuclear medium. So there is some debate about what are the preferred degrees of freedom to describe matter at saturation density. However, it is clear that once the interquark separation is small enough, there is no compelling argument to use nucleon degrees of freedom. Put simply, as matter approaches high enough densities a quark should no longer be able to tell which "nucleon" it belongs to, so to speak, because it becomes as close to the quarks from neighbouring nucleons as it is to the quarks in its original color singlet bound state. This is an argument for deconfinement, but even before deconfinement there is a very good case for using quark degrees of freedom in the description of nuclear matter - even below normal nuclear matter density ($\rho_0 = 0.17$ fm^{-3}).

In 1983 the discovery of the EMC effect [16,45,46] indicated that the structure

of a nucleon bound within a nucleus is different from a nucleon in free space[4]. Despite many attempts to account for this effect in terms of Fermi motion and binding effects of nucleons [48–52], the most likely conclusion appears to be that the internal quark structure of the nucleon depends on the nuclear environment [53–55].

Another indicator that quark degrees of freedom are important in the description of nuclear matter is the fact that chirally symmetric models formulated in terms of point-like nucleons, do not have a natural mechanism for saturation. This problem is known as the "chiral collapse" and occurs in both the Nambu-Jona − Lasinio (NJL) model [56] and the linear sigma model [57]. It means that the system doesn't have the essential balance of attractive and repulsive forces necessary to produce a minimum in the binding energy per nucleon as a function of density. In this scenario, stable nuclei are not possible. However if the internal structure of nucleons is taken into account, this issue can be resolved [1].

Contemporary approaches for incorporating quark degrees of freedom in hadronic matter involve first using a model to calculate the properties of the nucleon and then extending this to infinite nuclear matter in the mean field approximation.

One example of a quark level model used to describe the nucleon is the bag model. In bag models hadrons consist of three quarks which are confined to a finite region of space (a sphere of radius R). The confinement is not a dynamical result of the underlying theory, but is imposed through the application of appropriate boundary conditions to constrain the motion of the quarks to the interior of the hadron. The radius of the bag, R, and the bag constant, B, parameterize such models. The bag constant is an input parameter for the vacuum energy density and the radius of the bag is determined by minimising the bag energy with respect to R. In 1988, Guichon developed a model that applied the MIT bag model of the nucleon [58] to the many-body problem in the mean field approximation. This has become known as the Quark Meson Coupling (QMC) model [59]. It is essentially an extension to the original QHD model which incorporates the quark structure of the nucleon. In fact QMC has been very successful in explaining the EMC effect, the properties of nuclear matter and of finite nuclei, because it takes into account the scalar polarizability of the nucleon [60, 61].

Another approach to describing the nucleon in terms of quarks is the chiral

[4]To be precise, what was found by the European Muon Collaboration (EMC) was that the ratio of the isoscalar structure functions, F_{2N}^A/F_{2N}, differs substantially from 1. This implies that the structure of a nucleon in a deuteron is different from a nucleon in medium (i.e. inside a nucleus of atomic number A). This effect has since been observed for nuclei ranging from helium to lead [47].

quark soliton model [62], which has also been extended to finite density with the introduction of vector meson exchange term in the mean field approximation [55]. In this model confinement is implemented by the chiral (pion) field instead of using a bag. Again there is a satisfactory agreement with the EMC effect, which has not been achieved without nucleon substructure [55].

The method adopted in this thesis is to use a Faddeev description of the nucleon [63], using the NJL model [64, 65] to describe the interactions between quarks. The quarks are confined by means of an infra-red cut-off in the proper-time regularisation scheme [8]. In this picture nucleons are in a quark - diquark configuration. At finite density the nucleon evolves internally as a function of the quark mass in accordance the the Faddeev equation. The properties of the nucleon are thus determined self-consistently within the medium.

3

Nambu - Jona-Lasinio model

Historically the NJL model goes back to two pioneering papers by Nambu and Jona-Lasinio in 1961 [64, 65], predating the development of QCD and even the discovery of quarks. Since then it has been applied to many different problems in nuclear physics and low-energy QCD. Detailed reviews of the NJL model are given in references [30], [66], [67] and [68]. It is arguably one of the most important models to be developed in these areas because it has led to numerous physical insights and discoveries. It has contributed significantly to our understanding of the properties of the vacuum, the QCD phase diagram (including the regions of finite temperature and finite chemical potential) and the role of symmetries, symmetry breaking and fundamental algebraic relations. The nature of the pion as a Goldstone boson [69] of QCD has been elucidated through the NJL model and the remarkable success of the constituent quark model can now be interpreted physically in light of the mass generation mechanism illustrated within the model.

Considering that explicit gluonic degrees of freedom are neglected in the NJL model (to some extent they are taken into account within the coupling constants of the model), it may seem surprising that it has been so useful in describing QCD, especially since it does not necessarily give rise to quark confinement[1]. The striking impact that the NJL model has had at low energies can be attributed to the extent to which it shares the symmetry properties of the underlying theory of QCD. In this chapter we give a historical introduction to the model. We then outline how the model can be used to describe diquarks and hadrons in terms of quark degrees of freedom. We use familiar techniques in quantum field theory to construct describe these particles. The Bethe-Salpeter equation is used for two-body systems (diquarks and mesons) and the Faddeev Equation for three-body systems (nucleons). In Section 3.2 we outline the importance of our choice of regularisation method. Sections 3.3 and 3.4 describe the method of calculating two-body and three-body systems of quarks corresponding to low-energy QCD.

[1] The confinement of quarks inside hadrons involves complex non-linear interactions between gluons, which are not included in the simple NJL model framework which is characterised by point-like interactions between quarks. However, it is possible to crudely implement confinement using an appropriate cut-off scheme to restrict the infra-red (very low energy) behaviour of quarks [70].

3.1 Introduction to NJL model

The NJL model was originally inspired by the theory of superconductivity developed by Bardeen, Cooper and Schrieffer [71] and Bogoliubov [72]. In the BCS-Bogoliubov theory the energy gap between the ground state and the excited states of a superconductor is generated by phonon-mediated electron-electron interactions in the superconducting material. This theoretical framework has been very successful in explaining and predicting the properties of conventional superconductors. Nambu and Jona-Lasinio developed the idea that the physical mass of a quasi-particle (nucleon) could be generated analogously to the energy gap in a superconductor through interactions between originally massless fermions. This comes about through the spontaneous breaking of chiral symmetry. In the early 1960's there were already indications of a (partially) conserved axial vector current (PCAC) indicating the existence of this fundamental symmetry at the level of the Lagrangian density [57]. Note that chiral symmetry (or approximate chiral symmetry), requires that in the Lagrangian density, fermions be massless (or almost massless), whereas the nucleon actually has a comparatively large empirical mass [67]. This arrangement can be accommodated naturally in the NJL model through the dynamical generation of mass, as follows. The empirical mass of the nucleon does not appear in the Lagrangian density, which is given by,

$$\mathcal{L} = \bar{\Psi}(i\partial\!\!\!/ - m_N)\Psi + G[(\bar{\Psi}\Psi)^2 + (\bar{\Psi}i\gamma_5\tau\Psi)^2]. \tag{3.1}$$

In this case m_N represents the bare mass (which is relatively small, reflecting the approximately conserved chiral symmetry), G is the coupling constant and Ψ and $\bar{\Psi}$ are the nucleon fields. The equation of motion for a nucleon is obtained from this Lagrangian density in the usual way, through the Euler-Lagrange equation. In the mean field approximation this reduces to a Dirac equation of the form,

$$(i\partial\!\!\!/ - m_N + 2G\langle\bar{\Psi}\Psi\rangle)\Psi = 0, \tag{3.2}$$

where $\langle\bar{\Psi}\Psi\rangle$ is the scalar condensate. From this Dirac equation we can make the identification

$$M_N = m_N - 2G\langle\bar{\Psi}\Psi\rangle, \tag{3.3}$$

for the effective mass of the nucleon. We refer to this as the Gap equation for the fermion mass, not to be confused with the Gap equation associated with the colour superconducting quark matter discussed in Chapter 5. Note that even if we had set the bare nucleon mass (m_N) to zero to begin with, we would still have obtained a large, dynamically generated nucleon mass, $M_N = -2G\langle\bar{\Psi}\Psi\rangle$.

With the development of QCD, the NJL model was later reformulated in terms of quark degrees of freedom because it shares some of the important fea-

tures of low energy QCD. The role of the pion as a Goldstone boson is elucidated through the NJL model. In a perfectly conserved symmetry this Goldstone boson arising from the spontaneous symmetry breaking would be massless. In nature the pion has a small mass (relative to the other hadrons) corresponding to the presence of the small current quark masses appearing in the Lagrangian. Through the same process as seen in the original NJL model, the large constituent quark mass ($M \approx 400$ MeV) is generated by the passage of the light quark ($m \approx 10$ MeV) through the quark condensate in the vacuum.

The NJL model is ingenious in the way it mimics these important properties of QCD. As a result it also satisfies numerous results of current algebra, including the Gell-Mann–Oakes–Renner relation [73], the Goldberger-Treiman relation [74] and the KSFR relation [75,76], which are requirements of QCD. The Gell-Mann–Oakes–Renner relation is given by,

$$f_\pi^2 m_\pi^2 \approx -\frac{(m_u + m_d)}{2}\langle \bar{u}u + \bar{d}d\rangle \tag{3.4}$$

where f_π is the pion decay constant and m_π is the pion mass. Assuming that the quark masses are approximately given by $m_u = m_d = 7 \pm 2$ MeV, we find that the chiral condensate is,

$$\langle \bar{\psi}\psi\rangle^{1/3} = -(225 \pm 25)\text{MeV}. \tag{3.5}$$

The Gell-Mann–Oakes–Renner relation is satisfied in the NJL model because it is a consequence of chiral symmetry [73]. The non-zero ground state expectation value implies that the QCD vacuum contains a condensate of quark and anti-quark pairs.

When expressed in terms of quark degrees of freedom, the NJL model can be used to describe diquarks and baryons within a relativistically covariant formalism. It has been successfully used to calculate many observables, including the meson spectrum [68, 70] and the light baryon spectrum [67], the pion form factor [67] and nucleon structure functions [54]. It has also been extensively applied to finite density and finite temperature studies [11, 30, 66]

In finite density studies, the NJL model has been most widely used to investigate the properties of quark matter [11]. In the study of nuclear matter the model showed some serious deficiencies. In particular, it was found that the model did not account for the stability of nuclear matter. In other words, nuclei would either collapse or expand indefinitely, depending on the magnitude of the vector coupling strength [77]. Unlike the familiar Walecka model, discussed in Section 2.3, the NJL model had the important property of chiral symmetry, which is related directly to the existence of the non-trivial vacuum. However, in the resulting equation of state it was the term for the vacuum which was fatal to

the stability of nuclear matter. In fact, once the negative energy fermion states are included, the minimum corresponding to the saturation density shifts to the region of zero effective fermion mass [56]. For this reason (and the fact that the model is non-renormalizable), the NJL model was not widely used in the study of nuclear matter for some time. However, as outlined in the previous chapter, this issue is common to all chirally symmetric field theories that use point-like nucleons. It is referred to as the "chiral collapse." In this thesis we resolve this problem in two ways. Firstly, we use the Faddeev approach to incorporate the structure of the nucleon. Secondly, we make a specific choice of regularisation method which simulates quark confinement and gives rise to nuclear saturation.

3.2 Regularisation

Because the NJL model is not renormalisable, we must choose a regularisation method in order to obtain meaningful results. That is, when calculating Feynman diagrams involving point-like interactions between quarks, at the very least, an ultra-violet cut-off is necessary to obtain finite solutions to integrals over quark momenta. Furthermore, an infra-red cut-off may also be introduced. For example, if we consider the quark propagator,

$$S_F(x-y) = -i\langle T[\psi(x)\bar{\psi}(y)]\rangle = \int \frac{d^4p}{(2\pi)^4}\frac{e^{ip(x-y)}}{\not{p} - m + i\epsilon}, \tag{3.6}$$

where we have defined $\not{p} = \gamma_\mu p^\mu$ and the integral is in Minkowski space. In a local 4-point interaction we have,

$$S_F(0) = -i\langle\bar{\psi}\psi\rangle. \tag{3.7}$$

Thus the gap equation, $M = m_q - 2G_\pi\, N_c\, N_F\, \langle\, \bar{\psi}\psi\rangle$, is given by,

$$M = m_q + 2G_\pi N_c N_F \mathrm{Tr}\int \frac{d^4p}{(2\pi)^4}\frac{1}{\not{p} - M + i\epsilon}, \tag{3.8}$$

where M is the dynamically generated constituent quark mass, m_q is the current quark mass and G_π is the scalar coupling constant. There are several possible regularisation schemes available for solving such four-dimensional integrals and indeed there are different ways of implementing them[2]. Therefore "the NJL model" is not really a unique model, because each regularisation procedure

[2]Regularisation schemes that have been used in the literature include the 3-momentum (non-covariant), Euclidean 4-momentum, Pauli-Villars, proper-time and recently, using a (Gaussian) form factor in Euclidean space [78].

will produce different quantitative results and sometimes give different qualitative results as well. While there are many regularisation independent features of the NJL model[3], it is important to consider the implications of the non-renormalisability of the model. The fact that the choice of regularisation method effects the results may seem disappointing in some respects (historically it certainly was), but the point is that one may use physical insight to motivate the choice. As Hatsuda and Kunihiro point out [79], the ultra-violet cut-off has a physical interpretation in QCD. It corresponds to the scale of chiral symmetry breaking ($\lesssim 1$ GeV). It is no coincidence that the region where chiral symmetry is dynamically broken is where NJL has been so successful, i.e. in describing the low energy properties of mesons etc.

Another scale of QCD relevant to the very low energy (infra-red) region is the scale of confinement. This physical phenomenon motivates the use of an infra-red cut-off in addition to the compulsory ultra-violet cut-off [70]. One of the early criticisms of the NJL model was that it did not incorporate confinement. For some purposes this can be overlooked but it limits the application of the model and reduces its appeal considerably. However, Ebert et. al. [70, 80] have shown that the property of confinement can be included within the NJL model by using the proper time regularisation method with a finite infra-red cut-off. Recently Bentz and Thomas successfully extended this approach to describe saturating symmetric nuclear matter [1].

In the proper-time regularisation scheme introduced by Schwinger [8], the following prescriptions are used,

$$lnA \longrightarrow -\int_{\frac{1}{\Lambda_{UV}^2}}^{\frac{1}{\Lambda_{IR}^2}} \frac{d\tau}{\tau} e^{-\tau A} \tag{3.9}$$

$$\frac{1}{A^n} \longrightarrow \frac{1}{(n-1)!} \int_{\frac{1}{\Lambda_{UV}^2}}^{\frac{1}{\Lambda_{IR}^2}} d\tau \tau^{n-1} e^{-\tau A} \tag{3.10}$$

where Λ_{UV} is the ultra-violet cut-off, Λ_{IR} is the infra-red cut-off and A is a function of quark momentum. For example, using the second prescription (see Appendix B), Eqn. 3.8 reduces to,

$$M = m_q - \frac{G_\pi N_c N_F M}{2\pi^2} \int_{\frac{1}{\Lambda_{UV}^2}}^{\frac{1}{\Lambda_{IR}^2}} \frac{d\tau}{\tau^2} e^{-\tau M^2} \tag{3.11}$$

Some important advantages of the proper-time scheme are that from the begin-

[3]For example, the Gell-Mann–Oakes–Renner relation [73], the Goldberger-Treiman [74] relation are satisfied in both three and four dimensional cut-off schemes.

ning it preserves Lorentz-, chiral- and vector-gauge invariance [81][4]. This is not the case if we use the 3-momentum cut-off scheme, for example, which from the outset is not a Lorentz covariant method.

In the calculations that follow, Λ_{IR} is an input parameter. It should be chosen to reflect the confinement scale of QCD, which is of the order of Λ_{QCD} (~ 200 MeV). As long as the model is not overly sensitive to this choice or any other input parameter, it may reliably be used to make predictions within the low energy sector. Indeed the model produces minimal variation in results within the range $150 < \Lambda_{IR} < 300$ MeV. The essential effect of the infra-red cut-off is to remove unphysical quark decay thresholds [70]. At the level of the quark propagator this can be illustrated simply using Eqn. (3.10). The pole in the quark propagator in Euclidean space, $S_F = (i\not{p} - M)/(p_E^2 + M^2)$, becomes,

$$\frac{1}{p_E^2 + M^2} = \int_{\frac{1}{\Lambda_{UV}^2}}^{\frac{1}{\Lambda_{IR}^2}} d\tau e^{-\tau(p_E^2+M^2)} = \frac{e^{-\frac{p_E^2+M^2}{\Lambda_{IR}^2}} - e^{-\frac{p_E^2+M^2}{\Lambda_{UV}^2}}}{p_E^2 + M^2}. \tag{3.12}$$

Clearly the original pole in the propagator at $-p_E^2 = p^2 = M^2$ is now cancelled by a corresponding zero in the numerator. The physical meaning of this mathematical novelty is that there is no solution for the mass corresponding to a freely propagating quark. In this sense the introduction of a finite infra-red cut-off simulates (albeit in a crude way) the dynamical process of quark confinement. In this thesis we do not apply the proper-time regularisation directly to the quark propagator, rather it is applied to momentum integrals over entire diagrams, however the effect is the same (i.e. to remove the poles that correspond to nucleons decaying into free quarks).

3.3 Mesons and Diquarks

In terms of quark degrees of freedom the NJL Lagrangian density is given by,

$$\mathcal{L}_{NJL} = \bar{\psi}(i\not{\partial} - m)\psi + \sum_{\alpha} G_\alpha (\bar{\psi}\Gamma_\alpha \psi)^2, \tag{3.13}$$

where $\bar{\psi}$ and ψ are the quark fields, m is the current quark mass and G_α are the coupling constants associated with the various interaction channels. Because of the symmetries of the gamma matrices ($\Gamma = \mathbf{1}, i\gamma_5, \gamma_\mu, \gamma_\mu\gamma_5 ...$), this Lagrangian density can be expressed in a variety of equivalent forms using Fierz

[4]That is, if we include all channels in the Lagrangian density, then the these properties are preserved in the proper-time method.

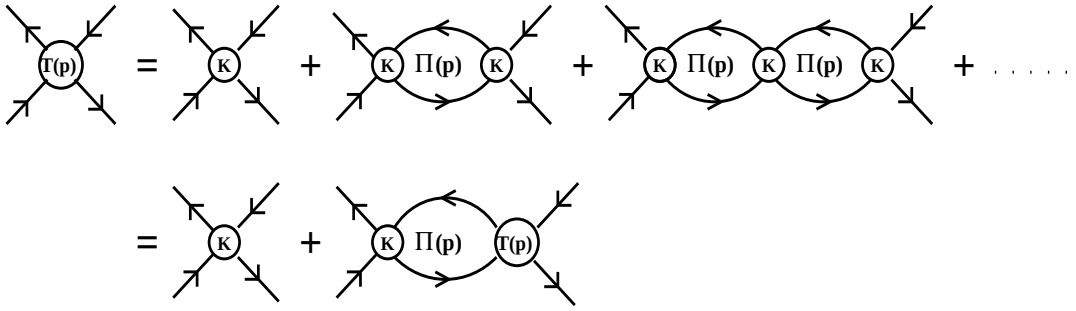

Figure 3.1: Particle interactions in the Bethe-Salpeter approach.

transformations [82]. Here we decompose the Lagrangian density into $\bar{\psi}\psi$ and $\psi\psi$ terms.

$$\mathcal{L}_{NJL} = \bar{\psi}(i\partial\!\!\!/ - m)\psi \tag{3.14}$$
$$+ G_\pi(\bar{\psi}\psi)^2 - G_\pi(\bar{\psi}\gamma_5\tau\psi)^2 \tag{3.15}$$
$$- G_\omega(\bar{\psi}\gamma^\mu\psi)^2 - G_\rho(\bar{\psi}\gamma^\mu\tau\psi)^2 \tag{3.16}$$
$$+ G_s(\bar{\psi}\gamma_5 C\tau_2\beta^A\bar{\psi}^T)(\psi^T C^{-1}\gamma_5\tau_2\beta^A\psi) \tag{3.17}$$
$$+ G_a(\bar{\psi}\gamma_\mu C\tau\tau_2\beta^A\bar{\psi}^T)(\psi^T C^{-1}\gamma_\mu\tau_2\tau\beta^A\psi) \tag{3.18}$$

In order of appearance the above terms correspond to the non-interacting, scalar, pseudoscalar, vector and isovector terms and the last two terms correspond to the scalar diquark and the axial vector diquark channels. The color matrices β^A are specified by the choice (A=2,5,7) indicating that these are attractive, color anti-symmetric channels (see Appendix A for matrix definitions). In the nuclear matter phase this will lead to color singlet nucleons and in the quark matter phase this will lead to color superconducting pairs.

Meson and diquark masses are determined using the Bethe-Salpeter equation[5]. Using the Lagrangian density of the NJL model given above, we may consider how quarks interact in each channel. As an example, let us take the omega meson. In using the Bethe-Salpeter equation we are assuming that the quark and the anti-quark in this bound state may interact with each other an indefinite number of times over a very long (essentially infinite) period of time. Using Feynman diagrams this can be treated as an infinite series of ladder diagrams [83], which in the NJL model (which is characterised by point-like interactions) becomes an infinite series of bubble graphs. As illustrated in Fig. 3.1, this infinite series reduces to the compact expression referred to as the Bethe-Salpeter

[5]There are alternative methods such as auxiliary-field path integral techniques and mean field methods where meson spectra are determined as collective excitations in the vacuum [30].

equation. In terms of matrices this diagram can be expressed as,

$$T_\omega(p^2) = K_\omega + K_\omega \Pi_\omega(p^2) K_\omega + \ldots \tag{3.19}$$

where $T_\omega(p^2)$ is the T-matrix for the interaction, K_ω is the kernel and $\Pi_\omega(p^2)$ represents the bubble graph. Multiplying by the identity,

$$\mathbf{1} = [\mathbf{1} - K_\omega \Pi_\omega(p^2)]^{-1}[\mathbf{1} - K_\omega \Pi_\omega(p^2)], \tag{3.20}$$

on the left results in the expression,

$$T_\omega(p^2) = [\mathbf{1} - K_\omega \Pi_\omega(p^2)]^{-1} K_\omega \tag{3.21}$$

The mass of the meson in the vector channel is then determined by the pole in the T-matrix,

$$\mathbf{1} - K_\omega \Pi_\omega(p^2 = m_\omega^2) = 0, \tag{3.22}$$

where the bubble graph is given by,

$$\Pi_\omega^{\mu\nu}(p^2) = i \ \mathrm{Tr} \int \frac{d^4p}{(2\pi)^4} \left[\gamma^\mu S\left(\not{k} + \frac{\not{p}}{2} \right) \gamma^\nu S\left(\not{k} - \frac{\not{p}}{2} \right) \right]. \tag{3.23}$$

The quark propagator is defined by,

$$S(\not{k}) = \frac{1}{\not{k} - M + i\epsilon} \tag{3.24}$$

and the kernel, K_ω, is given by $2G_\omega$ since we are including both direct and exchange terms in the Fierz invariant form of the Lagrangian density. The pole in the T-matrix at $p^2 = m_\omega^2$ corresponds to the particle's mass because this is the momentum for which the particle is on-shell.

Similarly the other meson and diquark masses can be determined from their respective Bethe-Salpeter equations. Note that the results depend on the constituent quark mass, the infra-red cut-off and the ultra-violet cut-off, through the bubble graph. In section 3.5 we show how to use the empirical values for the pion mass and pion decay constant to relate the quark mass and the cut-off parameters at zero density.

At finite density QCD is expected to undergo a chiral phase transition, where the dynamically generated quark mass decreases[6]. In order to describe the nucleon in medium we need to know how its internal degrees of freedom change as a function of density. Hence we calculate the diquark masses over a range

[6] At very high densities we expect that the approximate chiral symmetry of the Lagrangian should be restored. In the hadronic phase this restoration is only partial in the model we are using. The symmetry is fully restored in the deconfined quark matter phase.

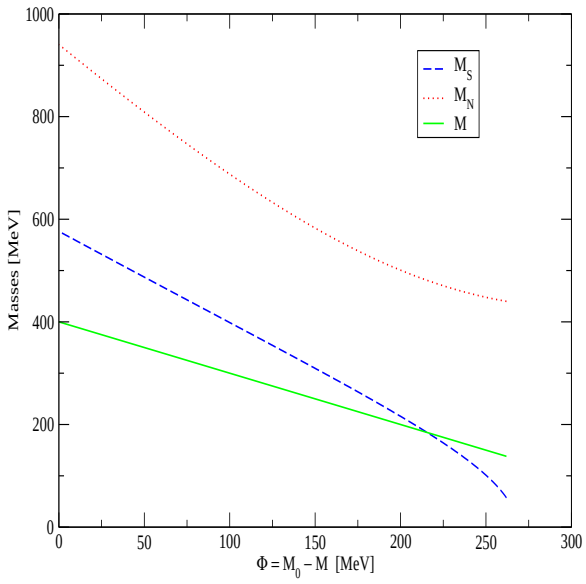

Figure 3.2: Scalar diquark and nucleon masses as a function of the scalar potential, $\Phi = M_0 - M$, with $G_s = 0.51\, G_\pi$, $M_0 = 400$ MeV and $\Lambda_{IR} = 200$ MeV.

of quark masses, corresponding to finite density behaviour. The dashed line in Fig. 3.2 shows the scalar diquark mass as a function of the scalar potential, $\Phi = M_0 - M$. Note that the scalar diquark mass also depends on the choice of the coupling constant, G_s, since it is determined by the position of the pole in the Bethe-Salpeter equation, $\mathbf{1} - 2\, G_s\, \Pi_s(p^2 = M_s^2) = 0$. In Fig. 3.2 the coupling constant, $G_s = 0.51\, G_\pi$, is chosen to give the correct nucleon mass (940 MeV) at zero density (with $M_0 = 400$ MeV and $\Lambda_{IR} = 200$ MeV). This result corresponds to using a quark - scalar diquark picture of the nucleon in the Faddeev approach.

3.4 Nucleons in the Faddeev Approach

In the early 1960's Faddeev developed a method to tackle the 3-body problem in a paper entitled "*Scattering theory for a three particle system*" [63]. The first numerical study of the Faddeev Equation for the nucleon, using a model of the kind employed here, was reported in Ref. [84]. The basic method is to sum over all possible interactions between quarks using quantum field theoretic

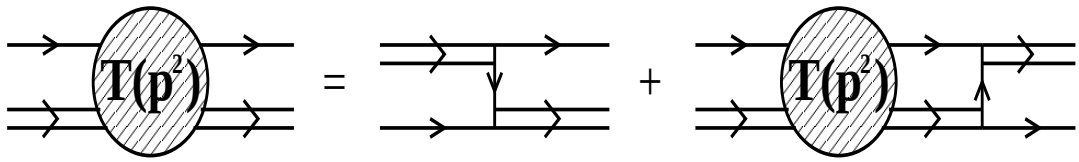

Figure 3.3: The Faddeev equation for the nucleon.

procedures. The exact three-quark Bethe-Salpeter equation contains complicated two-body and three-body interactions (even without including gluons, it is already an extremely complex problem). However, using the ladder approximation the problem reduces to a simpler form where only separable two-body interactions are involved. This assumption will only be realistic if effective three-body forces really are negligible compared to effective two-body forces between valence quarks inside the nucleon.

It may seem like an over-simplification, but it turns out that this picture of the nucleon has considerable appeal, both theoretical and observational[7]. For example, a simple two particle (quark-diquark) description of the baryon nicely reproduces the light baryon spectrum [86], while the three particle counterpart predicts an abundance of missing resonances [87]. Indeed, the widespread consensus that quark pairing is favorable in high density quark matter lends some support to the idea of quark pairing within the nucleon [85]. Moreover, in this model we may also consider the possibility of a connection between the pairing of quarks within the nucleon and the pairing of quarks anticipated in color superconducting quark matter.

Similarly to the Bethe-Salpeter equation, the Faddeev equation can be expressed as an infinite series of quark - diquark bubble graphs, $\Pi_N(p^2)$. For simplicity we will begin with case of a quark - scalar diquark description of the nucleon. In this case the bubble graph is given by (See Appendix C),

$$\Pi_N(p^2) = \int \frac{d^4k}{(2\pi)^4} S(\not{k})\tau_s(\not{p} - \not{k}). \tag{3.25}$$

where τ_s is the T-matrix for the scalar diquark. As illustrated in Fig. 3.3, the geometric series of bubble graphs can again be reduced to a finite expression for the nucleon T-matrix. Thus the nucleon is pictured as a quark and a diquark

[7]For a discussion on the evidence in favour of diquarks see Ref. [85].

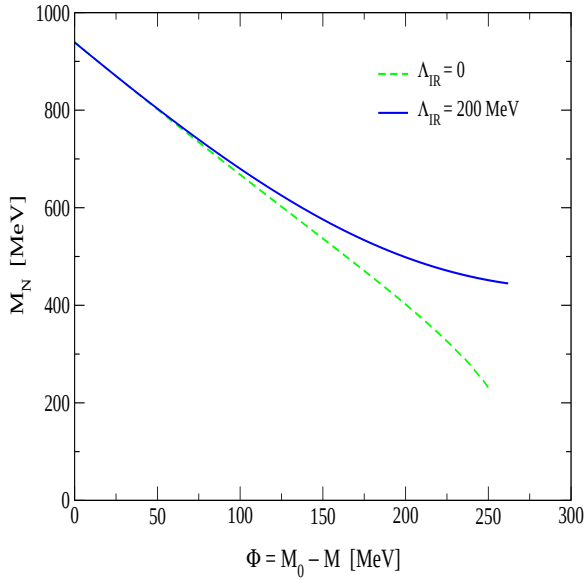

Figure 3.4: The nucleon mass as a function of the scalar potential, $M_0 - M$.

interacting via quark exchange. Due to the numerical complexity of solving the Faddeev equation in the proper-time regularisation scheme, the quark propagator (associated with quark exchange) is taken to be momentum independent, i.e. $S(\not{k}) = -1/M$. The nucleon mass is then determined by the pole in the T-matrix,

$$T_N(p^2) = \frac{3}{M}\frac{1}{1+\frac{3}{M}\Pi_N(p^2)}. \tag{3.26}$$

In Ref. [1], Bentz et. al. have shown that a linear interpolation between $-1/M$ and $-1/M_0$ for the quark propagator[8], reproduces the exact Faddeev result, as obtained in Refs. [82] and [88]. In regularising the integral in the expression for $\Pi_N(p^2)$, it is crucial that we use a finite infra-red cut-off to avoid unphysical quark decay thresholds [1]. As shown in Fig. 3.4 the nucleon mass develops an increased curvature of opposite sign when Λ_{IR} is introduced. Physically this means that the composite nucleon has a non-zero scalar polarizability which (as in the QMC model [59]) opposes the applied scalar field. In finite density calculations this behaviour is essential to the stability of symmetric nuclear matter. This is dramatically illustrated by Fig. 3.5, which shows the binding energy curves for the calculations with $\Lambda_{IR} = 0$ and 200 MeV. The curvature in

[8]Using linear interpolation the momentum independent quark propagator is expressed as $1/M \longrightarrow (1/M_0)(M_0+c)/(M+c)$. With $c = 700$ MeV the agreement with the exact Faddeev result is very good [1].

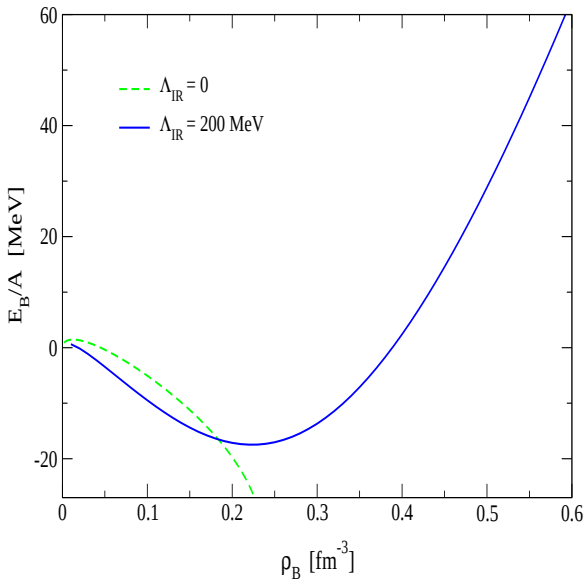

Figure 3.5: Binding energy curves for two choices of Λ_{IR}. Without the finite infra-red cut-off symmetric nuclear matter does not saturate.

the nucleon mass as a function of decreasing quark mass (i.e. increasing density) prevents the collapse. The scalar polarisability of the nucleon [89] is something that is only seen in models that include nucleon structure, because it is purely due to internal degrees of freedom within the nucleon.

3.5 Fixing Parameters

The method used for fixing parameters in the model proceeds as follows. First the constituent quark mass at zero density and the infra-red cut-off are chosen. To begin with we take $M_0 = 400$ MeV and $\Lambda_{IR} = 200$ MeV. The model is not sensitive to these choices. Using 350 MeV or 450 MeV for the quark mass gives similar results and within the range $150 < \Lambda_{IR} < 300$ MeV the results are not significantly changed either. Once M_0 and Λ_{IR} are chosen the ultra-violet cut-off, Λ_{UV}, is calculated using the matrix element for pion decay, with the requirement that the pion decay constant, f_π, is 93 MeV at zero density. The

decay width for pion decay satifies the relation,

$$\Gamma_\pi \propto \ |\langle\pi(q)|A_\mu(0)|0\rangle\langle 0|\mathcal{A}_\mu(0)|\mu,\bar{\nu}\rangle|^2 \ \propto \ \frac{1}{\tau_\pi}, \tag{3.27}$$

where τ_π is the lifetime of the pion. The pion decay constant is related to the first matrix element since the pion decays via the axial vector current $A_\mu = \bar{\psi}\ \gamma_\mu\ \gamma_5\ \psi$, according to the relation

$$\langle 0|A_\mu(0)|\pi(q)\rangle = i f_\pi q_\mu \tag{3.28}$$

From this we obtain, in the proper time regularisation scheme (see Appendix B),

$$f_\pi = \frac{3}{4\pi^2} M\sqrt{g_\pi}\int_0^1 dx \int_{\frac{1}{\Lambda_{UV}}}^{\frac{1}{\Lambda_{IR}}} d\tau \frac{1}{\tau} e^{-\tau(M_\pi^2(x^2-x)+M^2)} \tag{3.29}$$

where we have introduced the Feynman parameter, x, in order to simplify the integral. The pion mass, M_π, is taken to be 140 MeV and the constituent quark mass $M = M_0$ (their values at zero density). The coupling constant g_π is given by the relation,

$$g_\pi = \frac{-2}{\partial\Pi_\pi(q^2)/\partial q^2}\Big|_{q^2=M_\pi^2}, \tag{3.30}$$

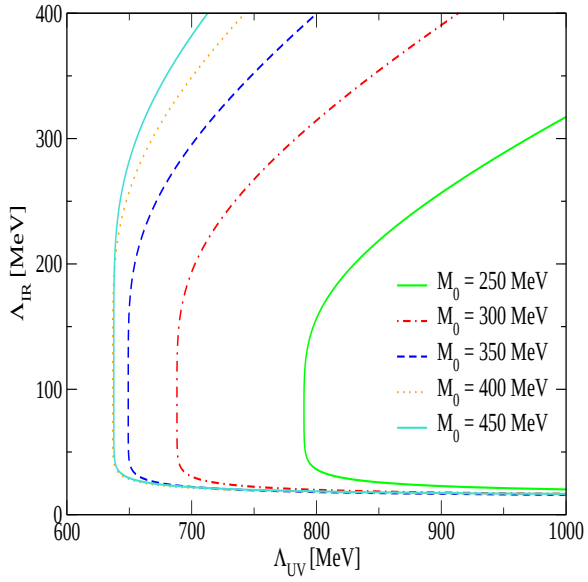

Figure 3.6: Relationship between the ultra-violet and infra-red cut-offs for various choices of the quark mass.

where the pseudoscalar bubble graph is,

$$\Pi_\pi(k^2) = i \,\mathrm{Tr} \int \frac{d^4q}{(2\pi)^4}[\gamma_5 S(\not{q})\gamma_5 S(\not{q} - \not{k}))]. \tag{3.31}$$

After taking the derivative we insert Eqn. (3.30) into Eqn. (3.29) and solve for the ultra-violet cut-off, Λ_{UV}. From Fig. 3.6 it is clear that if Λ_{IR} is taken to be too small then the ultra-violet cut-off increases sharply. However, the results for 200 and 300 MeV are very similar - for example, the saturation density differs only by about 0.01 fm^{-3} for these choices (i.e. the position of the minima in Fig. 3.5). Thus we find that Λ_{UV} is around 650 MeV in this model and is not overly sensitive to the initial choice of Λ_{IR}.

The next step is to determine G_π, the pseudoscalar coupling constant. The value of G_π is fixed by the pole in the Bethe-Salpeter equation for the pion at zero density,

$$1 + 2G_\pi \Pi_\pi(k^2 = M_\pi^2) = 0, \tag{3.32}$$

where Π_π is the pseudoscalar bubble graph. Using these equations we establish G_π according to the properties of the pion in the vacuum. We may then calculate the current quark mass, m_q. This is given by the solution to the gap equation,

$$M = m_q + \frac{G_\pi N_c N_F M}{2\pi^2} \int_{\frac{1}{\Lambda_{UV}^2}}^{\frac{1}{\Lambda_{IR}^2}} d\tau \frac{1}{\tau^2} e^{-\tau M^2} \tag{3.33}$$

where $M = M_0$ and in these calculations $N_c = 3$ and $N_F = 2$. In this way the constant m_q is determined by the value of the constituent quark mass at zero density. With this regularisation scheme it is around 15 - 20 MeV, depending on the initial choices of M_0 and Λ_{IR}. Following the determination of Λ_{UV}, G_π and m_q, we calculate the coupling constant G_s from the Faddeev equation for the nucleon, fixing it by the nucleon mass at zero density.

4

Nuclear Matter

The fact that particle states are quantised (i.e. quantum mechanics) and that no two fermions can be in the same state (the Pauli exclusion principle), means that each nucleon occupies a unique state inside a nucleus, just as electrons occupy quantised energy levels in an atom. Even without any interactions, quantisation and the Pauli exclusion principle prevent nuclei, indeed stars, from collapsing immediately. However, in addition to this there are attractive and repulsive interactions between nucleons, mediated by long and short range forces. In symmetric nuclear matter these forces balance to give a stable (zero pressure) state where the density does not change with perturbations in the number of particles. This is referred to as nuclear saturation.

A realistic approach to the description of matter inside stars must be grounded in our knowledge of the bulk properties of matter at saturation density. This is where most of our empirical information comes from. At saturation density the equation of state should agree with these properties as far as is possible. However in the pursuit of an accurate model for the system it pays to be patient in attaining precise agreement with all of these properties simultaneously. In particular, it is preferable to use a minimal number of parameters and take care to preserve more fundamental aspects of QCD such as chiral symmetry. Quantitative precision is of course important, but it should be sought in conjunction with qualitative understanding. With a relativistic, chirally symmetric model, that agrees well with phenomenology, we have a consistent framework to describe matter. A comparison with some of the bulk properties of matter should indicate whether the model has deficiencies or problems in describing the real world. If so we may be able to identify what is missing from the dynamics, or which approximations may be breaking down, for example.

In this chapter, Section 4.1 deals with the properties of infinite symmetric nuclear matter and explains how they are related to the semi-empirical mass formula and the equation of state. In Section 4.2 we derive the equation of state for the NJL model with composite nucleons using path integral techniques. In Section 4.3 we present the results of these calculations. Here we consider the case when the nucleon is treated as a quark - scalar diquark system.

4.1 Properties Nuclei and Nuclear Matter

The stability of nuclei in nature is dependent on the balance of attractive and repulsive forces between nucleons. In a nucleus the favored ratio of neutron number, N, to proton number, Z, depends on the atomic number, A. Smaller nuclei (such as carbon for example) favour equal numbers of neutrons and protons. Ultimately this is due to the isospin symmetry of nature at the fundamental level. In QCD the isospin symmetry means that up quarks are almost interchangeable with down quarks (since the Lagrangian density is invariant with respect to transformations that interchange them, up to the small mass difference, $m_d - m_u$). On the scale of nucleons this translates to neutrons and protons being almost interchangeable, having almost identical masses. Then it is primarily Fermi statistics that dictates that the lowest energy levels for each species are occupied symmetrically, in preference to asymmetric configurations (which would require more energy). In larger nuclei other effects become important. As the proton number increases the repulsive Coulomb forces are large enough to destabalise a symmetric system. A larger fraction of neutrons are required to dilute the repulsion between protons. However this effect is tempered by the input of energy associated with isospin asymmetry so that stable isotopes only exist within a restricted range of proton and neutron numbers, known as the valley of beta stability. In the situation of a compact star, the conditions of chemical equilibrium and charge neutrality lead to a highly asymmetric composition (a very large neutron to proton ratio).

In constructing an equation of state to describe compact star matter there are several empirically known properties that can be used to constrain model parameters and/or provide a test for how well the model works. It is helpful to consider the origin of some of these properties in terms of a of a simple equation for a nucleus which includes the effects of Coulomb repulsion, surface energy and nucleon asymmetry. Such an equation was formulated in the 1930's by Weizsäcker [90] in the context of the liquid drop model of the nucleus. It is commonly referred to as the semi-empirical mass formula[1] This formula gives the total mass of a nucleus in terms of neutron and proton numbers (N and Z),

$$M(A,Z) = A[\frac{4}{3}\pi r_0^3 \epsilon_0 + a_{sym}(\frac{N-Z}{A})^2] + 4\pi r_0^2 A^{2/3}\epsilon_{surf} + \frac{3e^2Z^2}{5r_0A^{1/3}} \qquad (4.1)$$

[1]More detailed models using a lot more parameters can be used that incorporate a vast amount of information from experimental data on nuclei [18, 91], for example the nucleons are slightly more densely packed in the interior of the nucleus compared to the outer region (skin) [92]. However, the semi-empirical mass formula gives the dominant contributions which are important for our purposes.

where ϵ_0 is the energy density at saturation and r_0 is a constant which is determined by the approximate relation for the radius of nuclei, $R = r_0 A^{1/3}$. Indeed the energy density remains approximately constant as a function of A for stable nuclei and the saturation density is related to the constant r_0 according to,

$$\rho_0 = \left[(4\pi/3)r_0^3\right]^{-1} \sim 0.17 \text{ fm}^{-3}. \tag{4.2}$$

The term for the surface energy contribution, $4\pi\ r_0^2\ A^{2/3}\ \epsilon_{surf}$, arises because nucleons at the surface of a nucleus feel less attraction from other nucleons than those on the inside. The last term in the semi-empirical mass formula is due to the Coulomb repulsion between protons, where e is the proton charge.

If we take the case of an extremely large value of A we can investigate the properties of an effectively infinite system of symmetric ($N = Z$) nuclear matter. Assuming that the surface energy and Coulomb energy terms do not contribute we are left with the relation, $M(A,Z)/A = \frac{4}{3}\pi\ r_0^3\ \epsilon_0\ \sim 922$ MeV, where $r_0\ \sim 1.16$ fm and $\epsilon_0 \sim 141$ MeV fm^{-3}, are determined by fitting experimental data for finite nuclei [18]. Thus the binding energy per nucleon (B/A) associated with removing a nucleon of mass 939 MeV, from a system of infinite symmetric nuclear matter, in the absence of the Coulomb force, would be approximately 17 MeV. In the equation of state this means that the binding energy per nucleon (i.e. the energy density per unit density, ϵ/ρ), should also have a minimum at saturation density corresponding to the binding energy,

$$E_b = (\epsilon/\rho)_0 - M_N. \tag{4.3}$$

The second term in the semi-empirical mass formula (Eqn. (4.1)) gives the energy associated with having different numbers of neutrons and protons in the system. Best fits to data from asymmetric nuclei imply that the asymmetry energy coefficient, a_{sym}, is approximately 32.5 MeV. Since the rho meson contributes uniquely to the asymmetric forces in nuclear matter this energy may be used to determine the strength of the rho-nucleon coupling in nuclear matter (Of course, if one goes beyond the Hartree level, other mesons also contribute). The asymmetry energy coefficient is related to the equation of state according to,

$$a_{sym} = \frac{\partial^2(\epsilon/\rho)}{\partial\alpha^2}|_{\alpha=0}, \tag{4.4}$$

where α is defined as $(\rho_p - \rho_n)/\rho_B$. So again this quantity can either be used as input or as a test for nuclear matter models. In this thesis it is used it to fix ${G_\rho}^2$.

[2] Alternatively, in the NJL model the meson-nucleon coupling constants can be determined by the meson masses by solving Bethe-Salpeter equations for each interaction channel.

In addition to these properties of nuclear matter there are two other key quantities, which are less accurately known. These are the incompressibility, K, (also known as the compression modulus) and the nucleon mass at saturation density, $M_N(\rho_0)$. Here these quantities are calculated as tests for the model. The nucleon mass is determined by first minimizing the effective potential with respect to quark mass and with this quark mass as input, calculating the corresponding nucleon mass through the Faddeev equation. From experimental evidence the nucleon mass in medium is determined to be between 600 and 800 MeV at saturation density [93]. The incompressibility is related to the equation of state through,

$$K = 9\left[\rho^2 \frac{d^2}{d\rho^2}\left(\frac{\epsilon}{\rho}\right)\right]_{\rho=\rho_0} \tag{4.5}$$

which is a measure of the changing curvature of the binding energy (i.e. the stiffness or the softness of the equation of state at saturation density). Experimental results for the compressibility have been obtained through the study of monopole excitations in nuclei. These studies suggest a value of approximately 200 - 300 MeV [22, 93].

4.2 Deriving of the Equation of State

The equation of state for a given system such as nuclear matter, is the relationship between the pressure and the energy density. This relationship is essential for us to understand the properties of nuclei and neutron stars. There are several ways to derive the equation of state for a model from its Lagrangian density. The simplest method is to calculate the energy-momentum tensor $\mathcal{T}^{\mu\nu}$ through the relation,

$$\mathcal{T}^{\mu\nu} = \frac{\partial \mathcal{L}}{\partial(\partial_\mu \phi_i)}\partial^\nu \phi_i - \eta^{\mu\nu}\mathcal{L}, \tag{4.6}$$

where there is a sum over all of the fields, ϕ_i. Then in the case of a perfect fluid, the pressure and the energy density are related simply to the space-like and time-like diagonal components of $\mathcal{T}^{\mu\nu}$ according to the relation,

$$\mathcal{T}^{\mu\nu} = P\delta_{\mu\nu} + (\mathcal{E} + P)u_\mu u_\nu. \tag{4.7}$$

In this method Pressure is given by $P = 1/3\langle\Phi_0|\mathcal{T}^{ii}|\Phi_0\rangle$ and the energy density is given by $\mathcal{E} = \langle\Phi_0|\ \mathcal{T}^{00}|\Phi_0\rangle$ where $|\Phi_0\rangle$ denotes the ground state of the system. Detailed examples of this method are outlined in Refs. [22, 40], in which the equation of state for Quantum Hadrodynamics is derived.

In the model we are using obtaining the equation of state is not so simple, because at the level of the Lagrangian density we are beginning with quark fields. In the absence of a complete and practical solution to QCD at low energies, the nuclear many-body system is most efficiently described in terms of hadronic degrees of freedom. Therefore our first step is to hadronize the Lagrangian density following the approach of Reinhardt [26]. This procedure is explained in Appendix D.1. After hadronization the Lagrangian no longer contains quark fields, but there is no restriction on incorporating quark degrees of freedom within this framework through the hadrons themselves. In fact, the internal properties of nucleons may significantly influence the bulk properties of the system.

We derive the equation of state for nuclear matter using path integral techniques as described in Ref. [12][3]. In order to hadronize the Lagrangian density, auxiliary fields for mesons, diquarks and nucleons are introduced into the generating functional of the model. In the process of integrating over the quark fields and the auxiliary fields we generate "trace-log" terms in the effective action, S_{eff} (see Appendix D.1). Because we are working in the mean field approximation the fields associated with the scalar, vector and isovector mesons[4] are approximated by,

$$\Sigma = -2G_\pi\langle NM|\bar{\psi}\psi|NM\rangle = M - m, \tag{4.8}$$

$$\omega^\mu = 6G_\omega\langle NM|\bar{\psi}\gamma^\mu\psi|NM\rangle \equiv \omega^0\delta_{\mu 0}, \tag{4.9}$$

$$\rho^\mu = 2G_\rho\langle NM|\bar{\psi}\gamma^\mu\tau_3\psi|NM\rangle \equiv \rho^0\delta_{\mu 0}, \tag{4.10}$$

where the spatial components of the vector fields vanish for nuclear matter at rest. The hadronized effective action with nucleon fields, $\bar{N}$ and N, is then given by (see Appendix D.1),

$$\begin{aligned} S_{eff} = &- i\,(Tr\,ln\,S_0^{-1} - Tr\,ln\,G_N^{-1}) \\ &+ \bar{N}G_N^{-1}N + \int d^4x\left[-\frac{(M-m)^2}{4G_\pi} + \frac{\omega_0^2}{4G_\omega} + \frac{\rho_0^2}{4G_\rho}\right], \end{aligned} \tag{4.11}$$

where the quark propagator is expressed in momentum space as,

$$S_0(k) = \frac{1}{\not{k} - M - \not{\omega} - \tau_3\not{\rho}} \tag{4.12}$$

[3] An alternative approach is to use a hybrid model for nuclear matter, where the expectation value for any local operator is separated into vacuum and valence components, $<\rho|\,\hat{\mathcal{O}}|\rho> = <\,\hat{\mathcal{O}}>_{vac} + <\,\hat{\mathcal{O}}>_{val}$. This method has also been applied by several authors to obtain hadronic equations of state [1,59,94]. We use the path integral formalism here to illustrate in a more detailed way how a hadronic equation of state is derived from a quark based theory.

[4] The pseudoscalar (pion) field is assumed to have zero expectation value in nuclear matter, because of the spin dependence of the pion nucleon coupling. i.e. the pion exchange contribution averages to zero in the mean field approximation.

and the pole part of the nucleon propagator, G_N, behaves as,

$$\hat{G}_N^{-1} \;\rightarrow\; \not{p}_N - M_N. \tag{4.13}$$

Renormalizing the nucleon fields, $\bar{N}$ and N, we may introduce chemical potentials for the nucleons through the kinetic term in the effective action (Eqn. (4.11)),

$$\bar{N} G_N^{-1} N \rightarrow \bar{\tilde{N}}(\not{p} - M_N + \mu_N^* \gamma^0)\tilde{N}, \tag{4.14}$$

where the matrix for the chemical potentials is given by,

$$\mu_N^* = \begin{pmatrix} \mu_p^* & 0 \\ 0 & \mu_n^* \end{pmatrix}, \tag{4.15}$$

The effective neutron and proton chemical potentials in medium are defined as, $\mu_n^* = \mu_n - 3\omega^0 - \rho^0$ and $\mu_p^* = \mu_p - 3\omega^0 + \rho^0$, respectively. We then integrate over the nucleon fields and use the resulting effective action to determine the effective potential, V. By construction the effective potential is the function whose minimum defines the vacuum expectation values of the quantum fields. It is related to the effective action by,

$$S_{eff} = -\int d^4x V. \tag{4.16}$$

We calculate the effective potential for nuclear matter using Eqn. (4.11) to obtain,

$$V^{NM} = V_{vac} + V_N + V_\omega + V_\rho. \tag{4.17}$$

The first term corresponds to the vacuum contribution (derived from the quark loop term, -i $Tr\ ln\ S_0^{-1}$). The trace is taken over colour, flavour and Dirac space, so that we have,

$$Tr\, ln\, (\not{k}_q - M) = ln\, Det\, (\not{k}_q - M) = 2N_c N_F\, ln\, (\not{k}_q^2 - M^2) \tag{4.18}$$

where $\not{k}_q = \not{k} - \not{\omega} - \tau_3 \not{\rho}$. Incorporating also the first term in the integral of Eqn. (4.11) we obtain,

$$V_{vac} \;=\; 12i \int \frac{d^4k}{(2\pi)^4} ln \left[\frac{k^2 - M^2 + i\epsilon}{k^2 - M_0^2 + i\epsilon}\right] + \frac{(M-m)^2}{4G_\pi} - \frac{(M_0 - m)^2}{4G_\pi} \tag{4.19}$$

$$\;=\; \frac{3}{4\pi^2}[C_3(M^2) - C_3(M_0^2)] + \frac{(M-m)^2}{4G_\pi} - \frac{(M_0 - m)^2}{4G_\pi} \tag{4.20}$$

Note that we have subtracted the $M = M_0$ contribution, so that this term vanishes at zero density. The second form for V_{vac} is derived in Appendix B,

using the proper time regularisation scheme. This procedure leads to terms of the form,

$$C_3(M^2) = \int_{\frac{1}{\Lambda_{UV}^2}}^{\frac{1}{\Lambda_{IR}^2}} d\tau \frac{1}{\tau^3} e^{-\tau M^2}. \tag{4.21}$$

which can be solved numerically. The term for the fermi motion of the nucleon arises from the second and third terms in Eqn. (4.11). To simplify the expression for $Tr\, ln\, G_N^{-1}$, we use the relation,

$$Tr\, ln \begin{pmatrix} A & B \\ C & D \end{pmatrix} = Tr\, ln(-BC + BDB^{-1}A), \tag{4.22}$$

to derive the expression,

$$\begin{aligned} V_N &= i \int \frac{d^4p}{(2\pi)^4} \left[Tr\, ln G_N^{-1} - Tr\, ln G_N^{-1}(\mu_N = 0) \right] && (4.23) \\ &= i \int \frac{d^4p}{(2\pi)^4} \Big[Tr\, ln(-\not{p} - M_N + \mu_N^* \gamma^0)(\not{p} - M_N + \mu_N^* \gamma^0) && (4.24) \\ &\qquad - (\mu_N = 0 \ \text{term}) \Big] && (4.25) \\ &= 2i \int \frac{d^4p}{(2\pi)^4} \left[ln \left(\frac{p_0^2 - (E_N(p) + \mu_N^*)^2}{p_0^2 - E_N^2(p)} \right) \right. && (4.26) \\ &\qquad \left. + \ ln \left(\frac{p_0^2 - (E_N(p) - \mu_N^*)^2}{p_0^2 - E_N^2(p)} \right) - (\mu_N = 0 \ \text{term}) \right], && (4.27) \end{aligned}$$

where we have defined $p_\mu = (p_0, p)$ and $E_N(p) = \sqrt{p^2 + M_N^2}$. Because the $\mu_N = 0$ term is subtracted, only a density dependent contribution will survive. After Wick rotation and integration over the time component of momentum, p_0, we obtain the usual nucleon Fermi motion term,

$$V_N = -2 \sum_{N=n,p} \int \frac{d^3p}{(2\pi)^3} (\mu_N^* - E_N(p)) \Theta(\mu_N^* - E_N(p)). \tag{4.28}$$

From the last two terms in Eqn. 4.11 we identify the vector and isovector meson terms in the effective potential are,

$$\begin{aligned} V_\omega &= -\frac{\omega_0^2}{4G_\omega} \equiv -9G_\omega(\rho_n + \rho_p)^2 && (4.29) \\ V_\rho &= -\frac{\rho_0^2}{4G_\rho} \equiv -G_\rho(\rho_p - \rho_n)^2 && (4.30) \end{aligned}$$

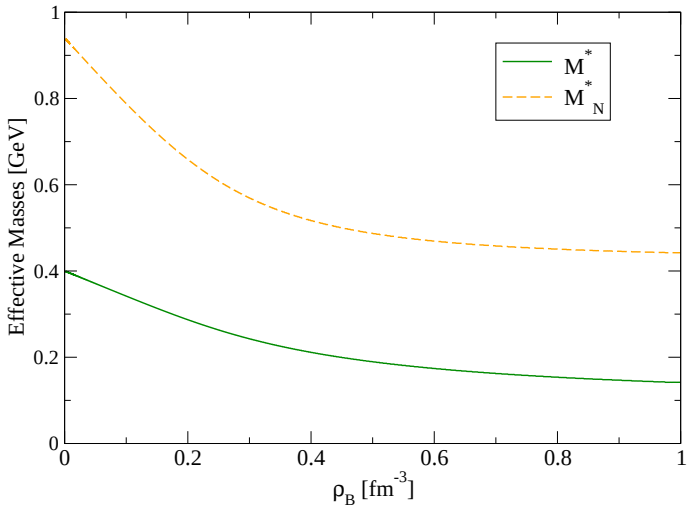

Figure 4.1: The effective masses of quarks and nucleons in medium.

where the expectation values of the fields, ω_0 and ρ_0, are defined by the minima, $\partial V^{NM}/\partial\omega = 0$ and $\partial V^{NM}/\partial\rho = 0$, respectively. In order to construct charge neutral nuclear matter we include also electrons in the form of a non-interacting Fermi gas. This gives an additional contribution to the effective potential,

$$V_e = -\frac{\mu_e^4}{12\pi^2}, \tag{4.31}$$

where μ_e is the electron chemical potential. The effective potential for the model is related to the pressure and energy density according to $P^{NM} = -V^{NM}$ and $\mathcal{E}^{NM} = V^{NM} + \sum_i \mu_i\rho_i$, where μ_i and ρ_i are the chemical potentials and densities of the components of the system which also satisfy the relation $\rho_i = \partial V^{NM}/\partial\mu_i$.

4.3 Symmetric Nuclear Matter

The most basic test for models of finite density nuclear physics is how well they reproduce the known properties of infinite symmetric nuclear matter at saturation density. These properties include the binding energy per nucleon, the compressibility, the effective nucleon mass, the asymmetry energy and the

saturation density itself[5]. In symmetric matter, by definition, we have equal densities of protons and neutrons, so that, $\rho^0 = 2G_\rho(\rho_p - \rho_n) = 0$ ($V_\rho = 0$) and there are no electrons ($V_e = 0$). For a given chemical potential the constituent quark mass M is determined by the condition $\partial V^{NM}/\partial M = 0$, where the quark mass at zero density is $M_0 = 400$ MeV. The nucleon mass M_N in Eqn. (4.28) is a function of M, determined by the pole in the Faddeev equation (Eqn. 3.26). The results of these calculations are shown in Fig. 4.1. The masses decrease as a function of density in accordance with the process of chiral symmetry restoration.

In this model we use the saturation curve (i.e. the dotted line in Fig. 4.2) to determine the vector coupling constant, G_ω. The coupling is adjusted so that the minimum is at the empirical value of the binding energy per nucleon (-17 MeV). The corresponding density at the saturation point (0.22 fm^{-3}), is a little above the experimental range, which is $\rho = 0.17 \pm 0.02$ fm^{-3}. As mentioned previously this is actually in very good agreement, considering that we have adjusted only one parameter (G_ω) to fix the saturation point. In Quantum Hadrodynamics the position of this minimum is used to determine the couplings for scalar and vector mean fields. In the NJL-type model used here we do not have that freedom since the scalar coupling constant, G_π, is already determined by the properties of the pion in the vacuum. The coupling constants for the model are given in Table 4.3.

The effective mass of the nucleon at saturation density ($M_N^* = 695$ MeV) is also in agreement with the experimental range of approximately 600 to 800 MeV. However, the incompressibility at the saturation point ($K = 560$ MeV), is much too high. The experimental evidence to date implies that incompressibility is within the range of 200 to 300 MeV. In other words, our equation of state is significantly too stiff near the saturation density. This suggests that there may be some problems with the approximations and assumptions we have made in formulating this model. It is important to pay attention to such deficiencies, because it is often where models or ideas break down that we can learn a great deal from them. In particular, if we can resolve the reasons why a model breaks down or lacks accuracy. In this case the high incompressibility must be related to the way that the mean fields change with density. Unless we assume density dependent coupling constants we cannot change the form of attractive and repulsive components of the equation of state directly. However, we have already seen that in this model the internal properties of the nucleon can have a significant effect on the equation of state. Thus we need to pay careful attention to our description of the nucleon. Indeed, as shown in Chapter 8, the problem of

[5]Clearly models that do not give rise to saturation cannot make meaningful predictions about any of these properties. This is why the NJL model for point-like nucleons cannot be directly applied to the description of nuclei or nuclear matter.

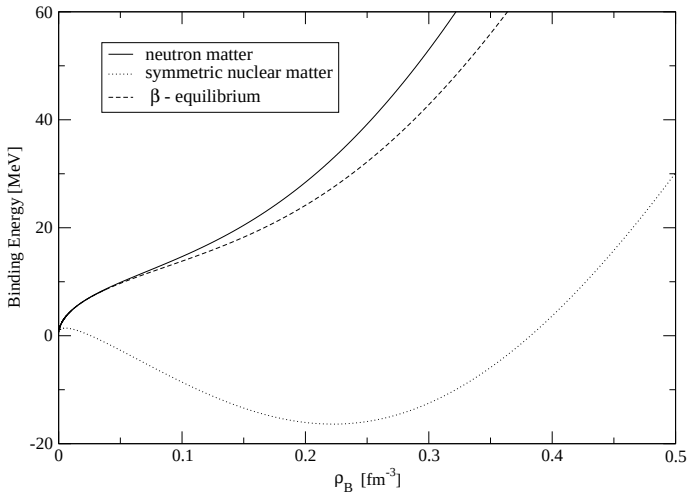

Figure 4.2: Binding energy curves for neutron matter (solid line), matter in β - equilibrium (dashed line) and symmetric nuclear matter (dotted line).

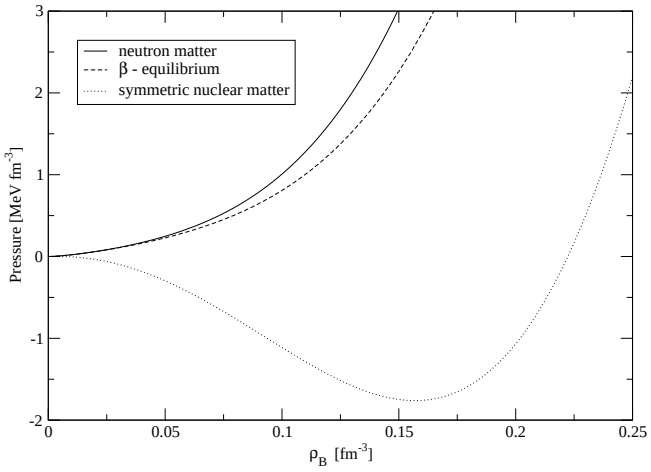

Figure 4.3: Equations of state for neutron matter (solid line), matter in β - equilibrium (dashed line) and symmetric nuclear matter (dotted line).

Table 4.1: Parameters for the calculations of the properties of the nucleon and nuclear matter.

$G_\pi[GeV^{-2}]$	19.60
$G_s[GeV^{-2}]$	$0.51G_\pi$
$G_\omega[GeV^{-2}]$	$0.37G_\pi$
$G_\rho[GeV^{-2}]$	$0.82G_\pi$
$\Lambda_{UV}[MeV]$	638.5
$\Lambda_{IR}[MeV]$	200
$m[MeV]$	16.93

high incompressibility is completely resolved when the self-energy of the nucleon is taken into account.

4.4 Asymmetric Matter

In order to describe neutron stars or asymmetric nuclei, it is important to be able to construct equations of state with different densities of neutrons and protons. In this case V_ρ becomes active in the effective potential. The coupling constant associated with this term is calculated using Eqn. (4.4). In fact, the proton fraction has a considerable effect on the equation of state. This is understood clearly in terms of the contribution from the rho meson, V_ρ. For a given density, if the proton fraction is increased then V_ρ increases. Hence the pressure ($P = -V$) is reduced, as illustrated in Fig. 4.4.

Though the gravitational fields associated with compact stars are extremely strong, for the individual particles inside them, the repulsive Coulomb forces would actually be stronger, for a star with a finite electrical charge. Therefore compact stars must be approximately charge neutral, just as ordinary stars and planets are. Note however, that this is a global constraint, we must still allow for the possibility of localised regions of positively and negatively charged matter inside a compact star [22].

Because of the condition of charge neutrality compact stars have traditionally been treated as "neutron stars," i.e. stars composed entirely of neutrons. This assumes that all protons have decayed into neutrons during the formation of the compact star. However, if we allow electrons we can impose charge neutrality through the constraint, $\rho_e = \rho_p$. Intuitively it seems reasonable that a finite density of protons should be energetically favourable, since each species of

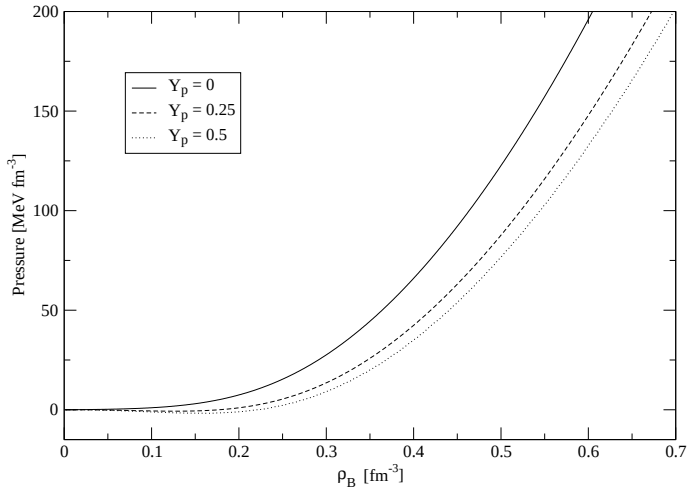

Figure 4.4: Equation of state for nuclear matter for various values of the proton fractions (Y_p).

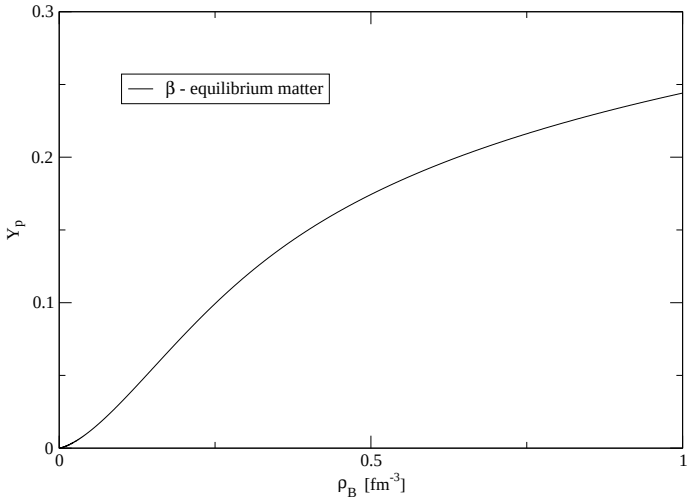

Figure 4.5: Proton fraction for charge-neutral nuclear matter (neutrons, protons and electrons) in chemical equilibrium.

baryon introduces additional degeneracy in the Fermi sea. Furthermore, protons have the same mass as neutrons, so the proton energy well is immediately available to be populated. As noted above, the inclusion of protons in the system decreases the pressure. However, once we include an equal density of electrons to balance the charge, the effect will be partially cancelled. Balancing the effects of introducing protons and electrons in such a way as to minimise the effective potential is exactly equivalent to applying the constraint of chemical equilibrium for the species,

$$\mu_p = \mu_n - \mu_e. \tag{4.32}$$

Fig. 4.5 indicates the resulting proton fraction for matter in β-equilibrium as a function of baryon density. In this model it may reach about one quarter of the baryon fraction at densities relevant to the cores of compact stars.

5

Quark Matter

A surprising feature of QCD is revealed when we study the behaviour of the quarks at large momentum transfer. Essentially, within the confines of the nucleon, the quarks behave almost as though they are free. This phenomenon, discovered by 2004 Nobel prize laureates Gross, Politzer and Wilczek, is known as asymptotic freedom [95]. It means that at short distances, or large momentum transfer, the coupling strength becomes small [96]. Indeed, in the region of densities sufficiently high that nucleons begin to overlap and quarks come much closer together, asymptotic freedom is expected to apply. Even at two or three times normal nuclear matter density this may be the case. In this region we expect the quarks to be in a globally colourless, deconfined phase. Hadronic models of the equation of state are not plausible at these densities due to the proximity of the quarks. Thus quark degrees of freedom should be employed to describe the system. In fact, quark matter is likely to occur within compact stars, since the central densities may well be as high as ten times normal nuclear matter density[1].

It is because of the observed property of asymptotic freedom that quarks are treated as a non-interacting Fermi gas in typical models of quark matter. In the limit that the QCD coupling constant goes to zero the equation of state reduces to the expressions for the Fermi motion of the quarks (i.e. a non-interacting gas) and the energy due to the vacuum. However, as outlined in the following sections of this chapter, quark matter may have far more complexity than this if we take into account the pairing of quarks in the vicinity of the Fermi surface.

5.1 Colour Superconductivity

Deconfinement at zero temperature has not been achieved in experiment, so it is not possible to study the phases of quark matter directly. However, it is quite possible that deconfinement does occur within compact stars. If this is the

[1]There is no experimental upper limit for the central densities of compact stars. Hadronic equations of state tend to give maximum central densities of around ten times nuclear matter density, but equations of state with transitions to quark matter can give significantly higher values [97].

case then we anticipate some form of quark pairing to arise in the deconfined phase. Just as electron pairing gives rise to electrical superconductivity in certain metals [71,98], quark pairing ought to produce colour superconductivity in quark matter. Detailed reviews on the subject of colour superconductivity are given in Refs. [11, 99, 100].

The possibility of quark pairing was first suggested as early as 1975 [101] and was studied in the 1970's by Barrois [102] and in the 1980's by Bailin and Love [103]. However, the topic received little attention until the late 1990's when it was shown that some of the relevant superconducting gaps in the fermion spectrum could be of the order of 100 MeV [13, 14]. Such pairing is favourable because it reduces the free energy of the system. This can be understood in the following way. Consider an infinite system of non-interacting fermions. At zero temperature the fermions will occupy all available states up to the Fermi energy, E_F. This energy defines the "Fermi surface" of the system. Now the Free Energy is given by,

$$F = E - \mu N, \tag{5.1}$$

where E is the total energy, μ is the chemical potential and N is the number of particles. Thus for non-interacting particles the Free energy cost associated with adding or removing a particle, vanishes at the Fermi surface ($E_F - \mu = 0$). Moreover, if there is some attraction between the particles this will lead to the formation of Cooper pairs, which reduces the Free energy. So, in the NJL model, pair formation is certainly favourable in the colour anti-symmetric, spin-0 channel (the same channel that the scalar diquarks are derived from), which is known to be attactive[2].

When pairing occurs near the Fermi surface, the single particle excitation energies are modified by the formation of an energy gap, Δ. In fact, in the NJL model with proper time regularisation the relevant gap is particularly large, even up to several hundred MeV for densities applicable to hybrid stars (see Fig. 5.1). Note that the condensation energy associated with the superconductivity is only a small fraction of the total energy, since the condensation energy is not proportional to Δ, but to Δ^2/E_F, but the effect is certainly big enough to be it important to the equation of state (see Fig. 5.3) and consequently to hybrid star and/or quark star properties.

Pairing is favoured in channels that do not break rotational symmetry, which is why spin-singlet pairing is preferred. The dominant channel of pairing in two flavor quark matter should be through the Lorentz-invariant scalar ($J^P = 0^+$), corresponding to the second to last term in the NJL Lagrangian density

[2]This channel has been found to be attractive through studies of one gluon exchange as well as instanton induced interactions [14, 104].

(Eqn. (3.17)). The condensates arising from this channel are given by the expectation values of the diquark fields,

$$\Delta_a = \langle \psi^T C^{-1} \gamma_5 \tau_2 \beta_a \psi \rangle, \tag{5.2}$$

where the matrices β_a are proportional to the Gell-Mann matrices given in Appendix A, such that $\beta_a = \sqrt{3/2}\lambda_A$, where $a = 1, 2$ and 3 corresponds to $A = 2, 5$ and 7. This means we are considering only the color anti-symmetric (attractive) channels. The well known 2SC phase occurs in the $a = 1$ channel, where we get a large expectation value for the spin-0 condensate, as illustrated in Fig. 5.1. The 2SC phase is favoured in two flavour quark matter because it reduces the free energy of the system. This is the pairing channel we refer to throughout this thesis, except where otherwise stated.

Given that the Cooper pairs are anti-symmetric in both colour and spin, they must also be anti-symmetric in flavour so that the resulting wavefunction for the pair is anti-symmetric. In other words any given Cooper pair in the 2SC phase, consists of an up quark and a down quark with opposite spins and two different colours (by convention we choose red and green, leaving the blue quarks unpaired). We do not include axial vector diquark (spin-1) condensation in two flavour quark matter, as this would break rotational invariance. In three flavour quark matter the condensates for spin-1 have been shown to be much smaller than for spin-0 pairing (i.e. < 1 MeV), so they do not significantly effect the equation of state anyway. However, these condensates, if present in three flavour quark matter, may effect the cooling rate of compact stars by inhibiting the direct URCA processes [105, 106].

5.2 The many phases of Quark Matter

The calculations presented in this thesis, both for hadronic matter and for quark matter, assume that only two flavours are active in the density region relevant to compact stars. The reason that this assumption is made here and in many other works, is that in the low energy regime, the strange quark (i.e. the third lightest quark) is considerably more massive ($m_s \sim 100$ MeV) than the up and the down quarks ($m_u \sim m_d \sim 10$ MeV). In NJL type models, it has been shown that the large mass of the strange quark tends to inhibit the formation of strange quark matter in the density region relevant to hybrid stars [11, 107–109]. However, the study of three flavour quark matter is of considerable importance from a theoretical point of view as it leads to some interesting concepts and ideas in QCD. The idea that strange quark matter is actually the true ground state

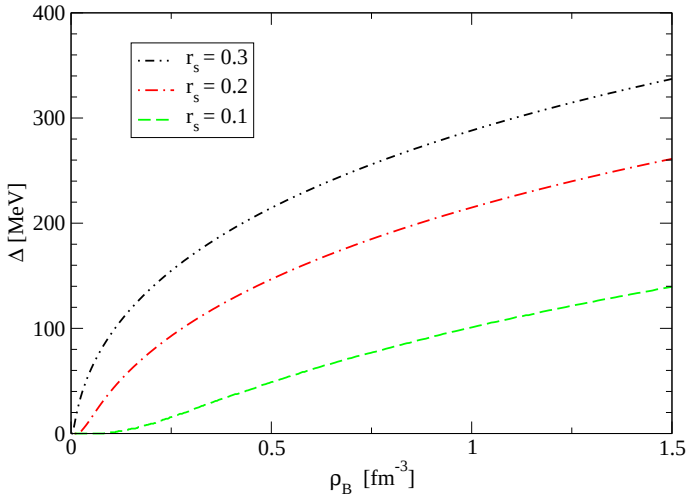

Figure 5.1: The value of the gap in symmetric colour superconducting (2SC) quark matter as a function of baryon density.

of the matter in the universe (i.e. The Strange Matter Hypothesis), has been around since the early 1970's [110, 111][3]. Depending on the bag constant and the behaviour of the strange quark mass at finite density, bag model calculations suggest that the binding energy of strange quark matter may be smaller than that of the most stable nuclei [39],

$$930 \text{ MeV} \geq \left(\frac{E}{A}\right)_{nuclei} > \left(\frac{E}{A}\right)_{SQM} = 830 \text{ to } 915 \text{ MeV}. \qquad (5.3)$$

It may seem like an outlandish conjecture that the observed universe (which is essentially made up of neutrons and protons, i.e. two flavour matter) is actually in a meta-stable state, which may decay into absolutely stable strange quark matter given the right conditions. However, the hypothesis has not been disproven as yet [11, 22]. There are even a few strange quark star candidates that may ultimately validate it, though at this stage they remain controversial. Some key observational features which may be used to identify strange stars, include their capacity to have relatively small radii and/or to have very high rotation rates compared to conventional neutron stars and hybrid stars. The reason for this is that strange quark matter is self-bound. Even without the

[3]The possibility of 3-flavour quark stars was first investigated in 1970 by Itoh [112].

gravitational field associated with its mass-energy, a strange quark star would be stable. Therefore, these stars are much more stable against equatorial mass shedding. Furthermore, the equation of state for strange quark matter is much softer than for hadronic matter, leading to the prediction of comparatively small radii (R 6 - 8 km). For a recent overview of strange quark stars see Ref. [106].

Another significant theoretical realisation in the area of three flavour quark matter is that the preferred pairing structure of cooper pairs in the high density limit should be the Colour-Flavour-Locked (CFL) phase. This phase is possible only at densities that are so high that the up, down and strange quarks can be treated on the same footing (i.e. the effect of the strange quark mass is negligible). The order parameter for the CFL phase is defined by the ansatz,

$$\langle \psi_i^{T\alpha} C\gamma_5 \psi_j^{\beta} \rangle = \Delta_{CFL} \delta_i^{\alpha} \delta_j^{\beta}. \tag{5.4}$$

The Kronecker δ's indicate that the colour indices (α and β) are connected with the flavour indices (i and j). Since there are three colours and three flavours (in equal proportions) maximal pairing is achieved in the CFL phase, producing equal pairing gaps for the u-d, d-s and u-s pairs. Because pairing is associated with a reduction in the energy of the system, the CFL phase is expected to be the most stable phase and is now widely accepted to represent the high density limit of QCD [11, 100, 104, 113].

At zero temperature and normal nuclear matter density strange quarks certainly do not feature in the dynamics of the system. Therefore, it is interesting to study how the low density configuration of QCD evolves into the high density limit (the CFL phase). There is a great deal of activity in approaching this from the top down, beginning with the CFL phase. This involves considering the stresses that arise on the pairing structure as the strange quark mass is increased from zero, so that the chemical potentials of the quark species lose their equality [113]. However, in this thesis we are approaching the problem from the bottom up, starting with hadronic matter and moving to quark matter. There is still a great deal of work to be done in both directions to determine what lies in between. Fortunately this is the density region that is relevant to compact stars, from which there is a continuous stream of observational data to draw.

In compact stars strangeness may play participate through the formation of hyperons, kaon condensates and/or strange quark matter, depending on which of these phase transitions are favoured and in what sequence they appear with respect to density [106, 114–116]. In addition to these ideas there is also the possibility of pseudoscalar condensation [117–120]. Pion condensation is unlikely to be favoured in nuclear matter [121], but it may be relevant for charge neutral quark matter in chemical equilibrium, depending on the behaviour of the pion mass [119, 122]. The competition between the pseudoscalar condensates and

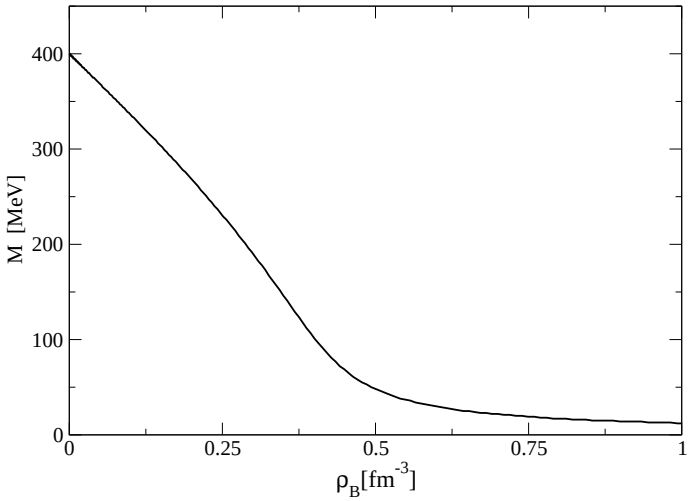

Figure 5.2: The effective quark mass in quark matter as a function of baryon density.

the two-flavor superconducting phase is examined in Ref. [123]. If pion or kaon condensation does occur it is expected to soften the equation of state.

There are numerous possibilities for quark pairing in high density matter, especially if strangeness is introduced. Systematic studies of pairing in two and three flavour quark matter are presented in Refs. [11, 104]. These phases can all be investigated within the framework we are using. Here we wish to concentrate first on the question of whether a unified description of diquark interactions can be achieved for both the nuclear matter and quark matter phases. For this purpose, we consider the idea that two flavour hadronic matter goes directly to two flavour quark matter.

5.3 The Effective Potential

The equation of state for quark matter is derived from the NJL Lagrangian density (Eqn. (3.14)) in the same way as the equation of state for nuclear matter (See Section 4.2 and Appendix D.1), using a few different assumptions in the process. Firstly, we do not introduce baryon fields into the generating functional and secondly, we do not include contributions from omega meson or rho meson

exchange. The reason for the first assumption is obvious by definition (quark matter is not made up of baryons). The reason for the second assumption, which has been made implicitly in almost all investigations of quark matter, is more subtle. It is supported by recent arguments related to the EMC effect [124], which show that in the high energy region, where one has essentially current quarks (as in the present high density case), the mean vector field must indeed be set to zero. Essentially, as quarks become asymptotically free the repulsive effects of the vector fields go to zero. Furthermore, it was shown in Ref. [12] that a finite value of G_ω in the quark matter phase gives rise to a pole for the omega meson mass. Depending on the choice of G_ω, the pole may be present at high density even though it is not present at low density. For example, for the choice $G_\omega = 0.37 G_\pi$ the pole only appears above $\rho_B = 0.8$ fm^{-3}, indicating that vector mesons would spontaneously appear above this density in quark matter. This unphysical scenario is averted by setting G_ω to zero in quark matter. In terms of particle dynamics, this means that nucleons interact via vector meson exchange, but deconfined quarks do not. It is clear that the vector terms in the effective potential must go to zero. The question that remains is exactly how this transition occurs. Does the repulsion decrease slowly or does it go to zero suddenly, at some threshold density? Either way is appears that the behaviour of G_ω should be determined by the nature of the deconfinement transition. In this model, deconfinement is a first order phase transition characterised by a sudden decay of the nucleon at some critical density, where quark matter becomes energetically favourable and at this point we set the vector repulsion terms to zero.

In the most simple mean field description of quark matter, each energy level for the quarks is filled up to the Fermi energy. At the Fermi surface, only a small attraction between quarks leads to the formation of Cooper pairs. This is the picture that emerges if we use the NJL Lagrangian density and allow for the possibility that the gap, Δ, may be non-zero in the colour anti-symmetric ($\bar{3}_c$) channel. The effective potential that emerges for quark matter is given by (see Appendix E),

$$V^{QM} = V_{vac} + V_Q + V_\Delta + V_e, \tag{5.5}$$

where the four terms correspond to the contributions from the vacuum, the Fermi motion of the quarks, the effect of residual quark pairing near the Fermi surface and finally, the contribution from the non-interacting gas of electrons. The term for the vacuum is the same as in the nuclear matter effective potential, which is given in Eqn. (4.20). The Fermi motion of the quarks also has the familiar form

(see Eqn. (4.28)),

$$V_Q = -\sum_{Q=u,d} \gamma_Q \int \frac{d^3k}{(2\pi)^3} \Theta(\mu_Q - E_Q(k))(\mu_Q - E_Q(k)) \tag{5.6}$$

where $E_Q(k) = \sqrt{k^2 + M_Q^2}$ and $\gamma_u = \gamma_d = 6$, since there are 3 colours and the spin degeneracy is 2. The chemical potentials are related according to the definitions,

$$\mu_u = \mu_q + \mu_I \tag{5.7}$$
$$\mu_d = \mu_q - \mu_I \tag{5.8}$$
$$\mu_B = \mu_q/3, \tag{5.9}$$

so that $\mu_q = (\mu_u + \mu_d)/2$ and $\mu_I = (\mu_u - \mu_d)/2$. The contribution to the effective potential from the effects of colour superconductivity is given by (see Appendix E),

$$V_\Delta = \sum_{\alpha=\pm} 2i \int \frac{d^4p}{(2\pi)^4} \left[ln \frac{p_0^2 - (\varepsilon_\alpha + \mu_I)^2}{p_0^2 - (E_\alpha + \mu_I)^2} + ln \frac{p_0^2 - (\varepsilon_\alpha - \mu_I)^2}{p_0^2 - (E_\alpha - \mu_I)^2} \right] + \frac{\Delta^2}{6G_s} \tag{5.10}$$

where the dispersion relations are given by $\varepsilon_\pm(p) = \sqrt{(E_q(p) \pm \mu_q)^2 + \Delta^2}$ and we have defined $E_\pm = |E_q(p) \pm \mu_q|$ and $E_q(p) = \sqrt{p^2 + M^2}$. The dispersion relations imply that all the quark energies are shifted by the gap (or in other words all the quarks are "gapped") however physically this does not mean that all the quarks are paired. To begin with, charge neutral quark matter is asymmetric (there are a lot more down quarks than up quarks) and here we are assuming just colour anti-symmetric, spin-0 pairing, so that the pairs must comprise of two different flavours to be overall anti-symmetric states. Secondly, pairing is only possible near the Fermi surface (where the up and the down quark must have similar chemical potentials) and thirdly, the pairing breaks the colour symmetry of the system. Though quark matter is colour charge neutral the pairing picks out a direction in colour space, so that $SU(3)_c \to SU(2)_c$. Thus all the quark energies are "gapped," but only a small fraction of the quarks are actually paired. We determine the gap and the quark mass for fixed chemical potentials (μ_B and μ_I) by minimising the effective potential with respect to these variables such that,

$$\left.\frac{\partial V(\Delta, M)}{\partial \Delta}\right|_{\mu_B, \mu_I, M} = 0 \quad \text{and} \quad \left.\frac{\partial \mathrm{V}(\Delta, \mathrm{M})}{\partial \mathrm{M}}\right|_{\mu_\mathrm{B}, \mu_\mathrm{I}, \Delta} = 0. \tag{5.11}$$

Note that the value of $G_s = r_s G_\pi$ controls the outcome of this minimization through the last term in Eqn. (5.10).

Note that the nuclear matter and quark matter phases differ essentially by the property of confinement. In Chapter 3 we saw that in this model the effects of confinement are simulated by the application of a finite infra-red cut-off, Λ_{IR}, within the proper-time regularization scheme [1]. In the proper time scheme the infra-red cut-off determines whether nuclear matter does or does not saturate and whether quarks are or are not bound. Therefore we use this parameter as a mathematical indicator of the phase transition. Though this is not a dynamical description of the process, it can be used as a tool to distinguish the phases. In physical terms we can only say that we are effectively imposing a restriction on how far apart quarks can be in the confined phase. To date the physical mechanism or reason for quark confinement has never been calculated. However it appears that the deconfinement transition may be related the the restoration of chiral symmetry. In any case we will set the infra-red cut-off to zero in quark matter as we assume that there is no confinement in this phase.

5.4 The Equation of State

We have used the NJL Lagrangian density to determine the effective potentials for nuclear matter and quark matter. The next step is to compare the equations of state for the two phases. The pressure and energy density in quark matter are given by the thermodynamic relations,

$$P^{QM} = -V^{QM} \tag{5.12}$$

$$\mathcal{E}^{NM} = V^{QM} + \mu_B \rho_B^{QM} + \mu_I \rho_I^{QM} + \mu_e \rho_e \tag{5.13}$$

The baryon and isospin densities are determined by,

$$\rho_B^{QM} = -\frac{\partial V^{QM}}{\partial \mu_B} = -\frac{1}{3}\frac{\partial V_Q}{\partial \mu_q} - \frac{1}{3}\frac{\partial V_\Delta}{\partial \mu_q} \tag{5.14}$$

$$\rho_I^{QM} = -\frac{\partial V^{QM}}{\partial \mu_I} = -\frac{\partial V_Q}{\partial \mu_I} - \frac{\partial V_\Delta}{\partial \mu_I}. \tag{5.15}$$

The derivations of these quantities are included in Appendix E. The gap, Δ, and the quark mass, M, are determined by Eqn. (5.11)[4], yielding the results shown in Figs. 5.2 and 5.1. In these calculations we consider the symmetric case, where $\mu_I = 0$, for illustration.

[4]Note that minimising the effective potential at fixed chemical potentials (μ_B and μ_I) is equivalent to minimising the energy density for fixed densities (ρ_B and ρ_I), since the effective potential and the energy density are connected through the Legendre transformation, Eqn. (5.13).

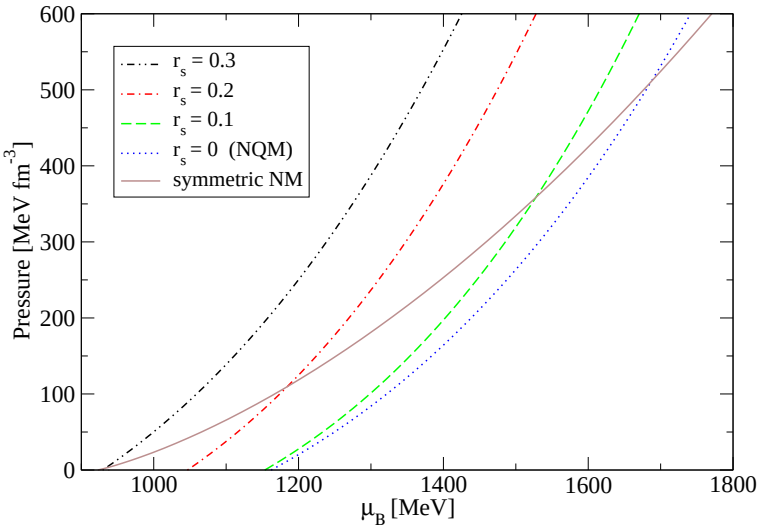

Figure 5.3: The equations of state for symmetric nuclear matter and for symmetric quark matter with various choices of the pairing strength r_s.

The equations of state for this model exhibit phase transitions from the confined phase to the deconfined phase. Plotting the pressure as a function of baryon chemical potential for symmetric matter in both phases (See Fig. 5.3), we find that the position of the phase transition moves to smaller densities and pressures as the pairing strength, r_s, is increased. Note that for any given baryon chemical potential, the phase which has the highest pressure (lowest effective potential) is favoured. Thus it is clear that where there are transitions the system always moves from the nuclear matter phase to the quark matter phase, as expected.

In principle we can combine the effective potentials for nuclear matter and quark matter to make one effective potential, assuming some transition density where the infra-red cut-off would go to zero and the mean vector fields would go to zero also. In this case we would have,

$$V = V^{NM} + V^{QM} \tag{5.16}$$

$$= V_{vac} + V_N + V_\omega + V_\rho + V_Q + V_\Delta + V_e. \tag{5.17}$$

In fact, this is would give equivalent results to those obtained in this thesis. At low density with the finite infra-red cut-off, the quark matter terms V_Q and V_Δ

become small and the nuclear matter components dominate. At high density the nucleons decay (i.e. $V_N \rightarrow 0$) as soon as the infra-red cut-off is put to zero. Assuming that the vector terms (V_ω and V_ρ) go to zero at the same point, we are left with only the quark matter components of effective potential (i.e. Eqn. (5.5)).

We note that most of the recent calculations on SQM have been performed by using the 3-momentum cut-off scheme and in general the gap is found to be around 100 MeV in the intermediate density region [125]. Our work differs in that we have used the proper time regularization scheme, which leads to larger values of the gap (between 300 and 400 MeV in the relevant density region). However, qualitatively the situation is similar to the cases of strong diquark coupling discussed in Ref. [107, 108].

The equations of state for this model with $\mu_I = 0$ allow phase transitions from the confined quark-diquark states employed in the description of nuclear matter to a deconfined phase, which may have diquark condensation in the form of colour superconducting pairs. This prompts us to investigate the possibility of phase transitions in asymmetric matter and in particular, matter in charge neutral chemical equilibrium. If such transitions are possible then they may have important implications for the structure of compact stars.

6

Compact Star Matter

Compact stars are a valuable source of information in the field of dense matter physics. The profile of a compact star unravels nature's equation of state, from the terrestrially familiar densities at the edge of the star, to the extremely high densities in its centre. There are three distinct possibilities for the composition of compact stars. The traditional view is that they are entirely composed of hadronic matter. In this case neutrons would be the dominant species of particle (hence the name "neutron star"). Another conjecture is that compact stars are made entirely of quark matter. In this case we refer to them as "quark stars." We do not expect quark stars to be composed of two flavour quark matter, but if the Strange Matter Hypothesis is correct then some or all of the compact stars in the universe could be made entirely of strange quark matter[1]. The third possibility for the composition of compact stars is that both phases are present, that is, they have a hadronic exterior with quark matter in the centre. In the literature such stars are referred to as "hybrid stars." They are the logical outcome if deconfined matter exists in the centres of compact stars, provided that it is not in the form of absolutely stable strange quark matter.

In this thesis and in Refs. [97] and [127], for the first time, we apply the NJL model to investigate the possibility of hybrid stars[2]. For this purpose we construct phase diagrams for asymmetric matter in chemical equilibrium. We do not impose charge neutrality to begin with, because we must allow for the possibility of mixed phases that contain localised regions of positively and negatively charged matter. Provided that these mixed phases are globally charge neutral and microscopically stable, they may exist within compact stars.

We have seen in the last chapter that the equation of state for symmetric quark matter is sensitive to the value of the pairing strength, r_s, associated with Cooper pairing. In this chapter we investigate how r_s affects the phase

[1] If strange quark matter is the most stable form of matter in the universe, then any form of matter that makes contact with it should be converted into strange quark matter as well. Therefore, if strange quark matter formed in the centre of a compact star, the entire star would be converted, except perhaps, the crust of the star (the outer layer), which may be sustained if it is separated from the rest of the star by Coulomb forces [126].

[2] Actually, there have been many studies of hybrid stars [27, 128–131], but this is the first time that one model has been successfully applied to describe both the confined phase and the deconfined phase.

diagrams of asymmetric matter. To produce a phase diagram, we look for the phase where the effective potential is minimised (i.e. the phase with the highest pressure, since $P = -V$). Physically this procedure can be understood from the point of view that if there are two phases competing for space, the phase with the highest pressure will always expel the other phase until a point of equilibrium is found where the pressures become equal. Indeed this is one of the Gibbs criteria for a mixed phase (the pressure of each phase must be equal for any given density in the mixed phase) [27]. The other condition is that the chemical potentials of the phases are equal. For this reason we generate phase diagrams in the plane of isospin and baryon chemical potential, so that the Gibbs criteria are automatically satisfied along the equal pressure boundaries where the phases meet on the diagram. In this way we can identify the composition of the mixed phases directly. In the following sections we outline the methods employed to produce such phase diagrams, how to interpret the diagrams and how to obtain the corresponding charge neutral equations of state.

6.1 Phase Diagrams

To study the behaviour of asymmetric matter at finite density we wish to compare the effective potentials, $V^{NM}(\mu_B, \mu_I)$, $V^{NQM}(\mu_B, \mu_I)$ and $V^{SQM}(\mu_B, \mu_I)$, where the superscripts, NM, NQM and SQM, represent nuclear matter, normal quark matter ($V_\Delta = 0$) and colour superconducting quark matter ($V_\Delta > 0$) in the 2SC phase. For each set of chemical potentials, (μ_B, μ_I), we choose the phase with the smallest effective potential to be plotted on the phase diagram. The method is as follows. For simplicity we choose values of ρ_p and ρ_n first, so that it is easy to calculate the neutron and proton chemical potentials[3],

$$\mu_n = \sqrt{k_{F_n}^2 + M_n^2} + 18 G_\omega \rho_B - 2 G_\rho (\rho_p - \rho_n) \tag{6.1}$$

$$\mu_p = \sqrt{k_{F_p}^2 + M_p^2} + 18 G_\omega \rho_B + 2 G_\rho (\rho_p - \rho_n) \tag{6.2}$$

The Fermi momenta of the nucleons are given by $k_{F_N} = (3\pi^2 \rho_N)^{1/3}$, where $N = n, p$. The effective quark mass is determined by minimising the energy

[3]This is easier than choosing μ_p and μ_n (or μ_B and μ_I) directly and searching for the corresponding values of ρ_p and ρ_n, that is, inverting Eqns. (6.1) and (6.2). It is also convenient to calculate V^{NM} as a function of ρ_p and ρ_n, since the vector and iso-vector components are expressed in terms of these variables in Eqns. (4.29) and (4.30). Then it is straight forward to calculate the chemical potentials (corresponding to the choice of ρ_p and ρ_n), to be used in the calculation of V^{NQM} and V^{SQM} (i.e. using Eqns. (6.3) and (6.4)).

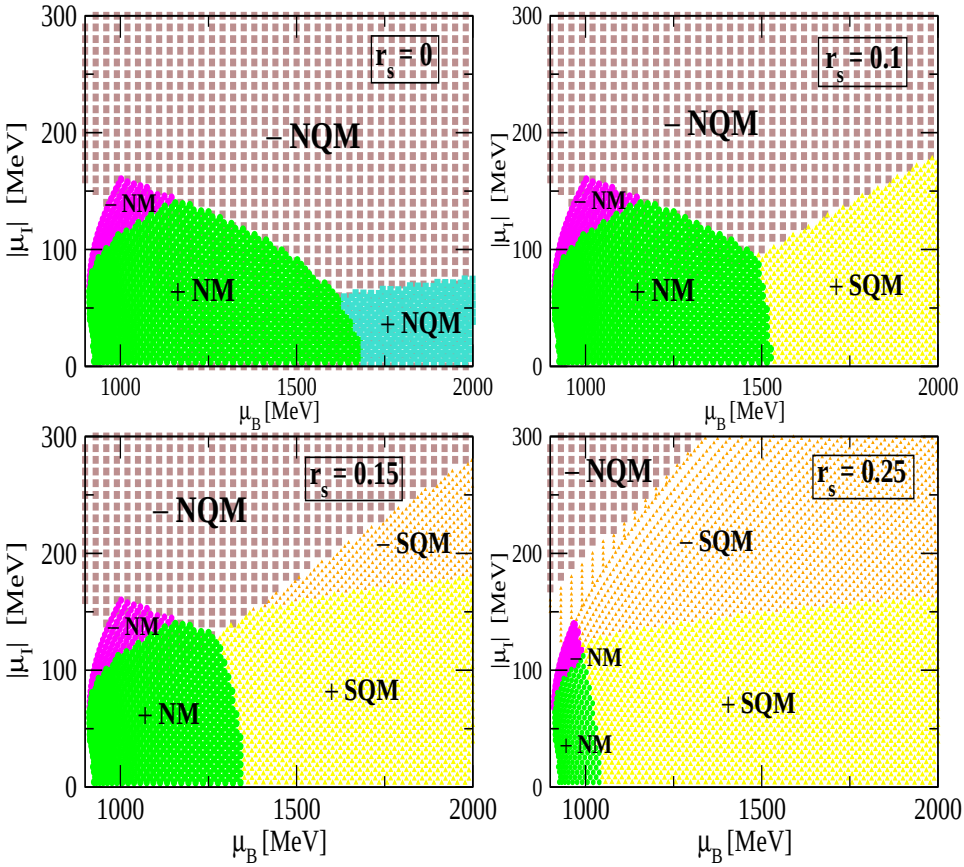

Figure 6.1: Phase diagrams in the plane of chemical potentials μ_B, μ_I for baryon number and isospin for various choices of r_s. The labels NM, NQM and SQM indicate nuclear matter, normal quark matter and superconducting quark matter respectively. The $\pm$ indicate the sign of the total charge density, including the electrons, when the system is in chemical equilibrium.

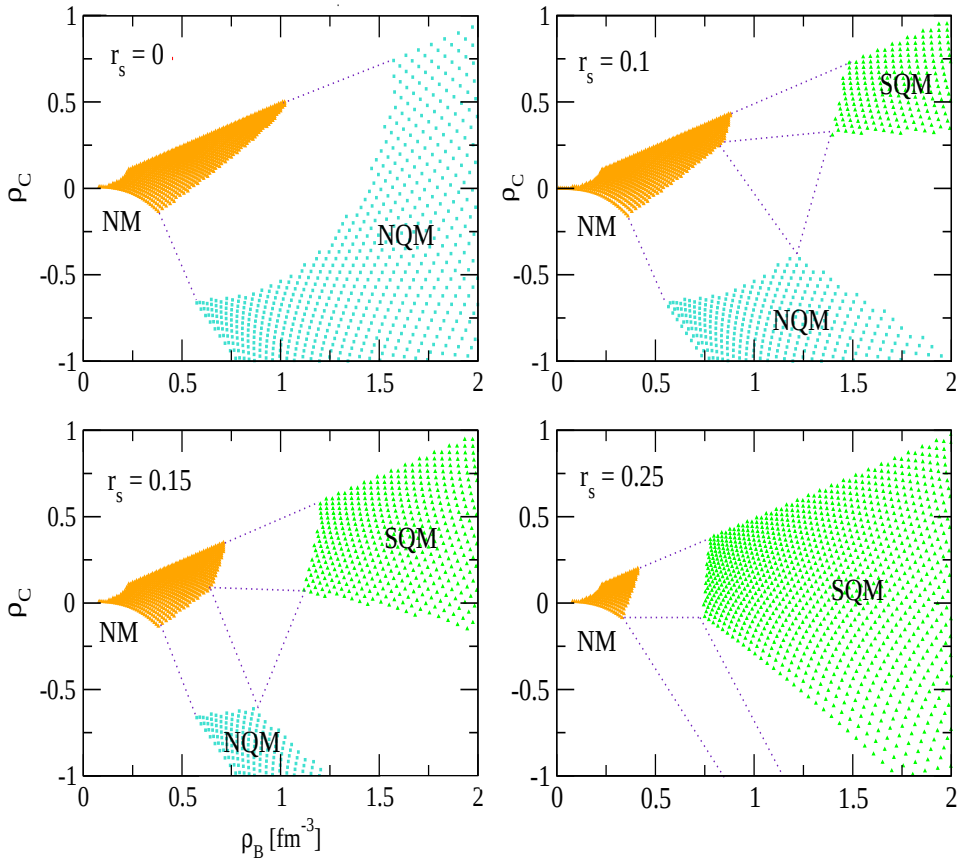

Figure 6.2: Phase diagrams in the plane of densities ρ_B, ρ_C for baryon number and charge for various choices of r_s. The labels NM, NQM and SQM indicate nuclear matter, normal quark matter and superconducting quark matter respectively. The white regions separated by the dashed lines correspond to the mixture of two phases, and the triangular region for the cases $r_s = 0.1$ and 0.15 involves a mixture of three phases. The upper left regions in each diagram are left empty, because we consider only the case $\mu_I < 0$.

density, $\mathcal{E}^{NM} = V^{NM} + \mu_n\rho_n + \mu_p\rho_p$, with respect to M for fixed densities, ρ_p and ρ_n (i.e. the stable solution of $\partial\mathcal{E}^{NM}/\partial M = 0$)[4]. The nucleon mass is a function of the quark mass, $M_N(M)$, as determined by the Faddeev Equation (see Section 3.4). The baryon, quark and isospin chemical potentials are given by[5],

$$\mu_B = \frac{1}{2}(\mu_p + \mu_n), \quad \mu_q = \frac{1}{3}\mu_B \tag{6.3}$$

$$\mu_I = \frac{1}{2}(\mu_p - \mu_n) \tag{6.4}$$

The electron chemical potential is fixed by the condition of β - equilibrium, $\mu_e = \mu_n - \mu_p$[6]. From this condition we find that there are more neutrons than protons for a system in chemical equilibrium, since μ_e must not be negative. Therefore, by definition, the isospin chemical potential is always negative or zero. For this reason, the convention is to plot $|\mu_I| = -\mu_I$, for the y-axis of the phase diagram, as shown in Fig. 6.1. In principle we could extend the phase diagrams to the region where $\mu_I > 0$ by ad-mixing positrons instead of electrons, but clearly the matter in this part of the phase diagram is always positively charged and is not relevant to the charge neutral equation of state. This type of mixture would give rise to extremely large repulsive Coulomb forces which cannot be balanced by the gravitational forces in compact stars [132].

Using the above conventions for the chemical potentials, the baryon and charge densities are defined by,

$$\rho_B^a = -\frac{\partial V^a}{\partial \mu_B} \tag{6.5}$$

$$\rho_C^a = -\frac{1}{2}\left(\frac{\partial V^a}{\partial \mu_B} + \frac{\partial V^a}{\partial \mu_I}\right), \tag{6.6}$$

where $a =$ NM, NQM or SQM. Using the effective potential for nuclear matter, given in Eqn. (4.17), we obtain,

$$\rho_B^{NM} = \rho_p + \rho_n \tag{6.7}$$

$$\rho_C^{NM} = \rho_p - \rho_e. \tag{6.8}$$

[4]This is equivalent to minimising V^{NM} with respect to M, with fixed chemical potentials.

[5]Many authors use the charge chemical potential, $\mu_c = \mu_e$, instead of the isospin chemical potential, μ_I, as the second chemical potential. In studies of hadronic matter, sometimes μ_n and μ_e are used instead of μ_B and μ_I. The results, of course, are independent of this parameterization choice. The different conventions used in the literature are related to one another through Legendre Transformations of the effective potential (i.e. $V = \mathcal{E} + \mu_i\rho_i$).

[6]As the electron mass is very small, we can approximate $\mu_e = \sqrt{k_{F_e}^2 + m_e^2} \approx k_{F_e}$.

The effective potential for quark matter is given by Eqn. (5.5). For normal quark matter ($V_\Delta = 0$) we find,

$$\rho_B^{NQM} = \frac{1}{3}(\rho_u + \rho_d) \tag{6.9}$$

$$\rho_C^{NQM} = \frac{2}{3}\rho_u - \frac{1}{3}\rho_d - \rho_e. \tag{6.10}$$

In colour superconducting quark matter the baryon and charge densities are modified by the term associated with the gap (V_Δ), so that (see Appendix E),

$$\rho_B^{SQM} = \frac{1}{3}(\rho_u + \rho_d) - \frac{\partial V_\Delta}{\partial \mu_B} \tag{6.11}$$

$$\rho_C^{SQM} = \frac{2}{3}\rho_u - \frac{1}{3}\rho_d - \rho_e - \frac{1}{2}\frac{\partial V_\Delta}{\partial \mu_I}. \tag{6.12}$$

We know that the introduction of spin zero pairing at constant baryon density reduces the pressure. Conversely, if we introduce pairing while maintaining a constant pressure, the baryon density increases. That is, $-\partial V_\Delta/\partial\mu_B$ gives a positive contribution to the baryon density in SQM. Furthermore, $-\partial V_\Delta/\partial\mu_I$ gives a positive contribution to the charge density in SQM.

For each point on the phase diagram (μ_B vs $|\mu_I|$), we calculate the baryon and charge densities using the above equations. Fig. 6.1 shows the phase diagrams for several choices of the pairing strength in the SQM phase. The different coloured regions indicate the phases with the lowest effective potential, and the $\pm$ indicate the sign of the total charge density. The corresponding plots in the plane of baryon and charge density are shown in Fig. 6.2. The mixed phases appear as white regions in this Figure. The phase boundaries, which are single lines in Fig. 6.1, appear as two lines facing each other in Fig. 6.2. By connecting the corresponding end points on the boundaries by straight lines (dashed lines in Fig. 6.2), we can divide the white region into sections which correspond to mixtures of the two phases facing each other. The $\mu_I = 0$ axes in Fig. 6.1 correspond to the upper-most line running from NM to QM in Fig. 6.2, and because we consider only the case $\mu_I < 0$ the upper left parts of the diagrams in Fig. 6.2 are left empty. If we extend this diagram to the region where $\mu_I < 0$ by introducing positrons instead of electrons, we obtain positively charged matter in this part of the phase diagram. However, since it does not contribute in a globally charge neutral mixed phase, it is not relevant to the composition of compact stars.

The four diagrams in Fig. 6.1 show the effect of increasing the scalar diquark interaction strength parameterised by the ratio $r_s = G_s/G_\pi$. Starting from the first diagram in Fig. 6.1, the regions occupied by SQM become larger while those of NM and NQM phases become smaller. Notice that the values of r_s used in

quark matter ($r_s = 0 \rightarrow 0.25$), are significantly smaller than the value used to construct the nucleon as a quark - scalar-diquark state ($r_s = 0.51$). If we use $r_s = 0.3$ in SQM then the NM phase is expelled almost completely by the SQM phase even in the low density region. However, since both the scalar attraction inside the nucleon and the scalar pairing in Cooper pairs come from the same term in the Lagrangian density of the model (Eqn. (3.17)), the values of r_s in each phase should be equated. However, the naive quark - scalar-diquark model of the nucleon leads to a phase structure which is entirely consumed by colour superconducting quark matter (i.e. if we use $r_s = 0.51$).

This suggests that there may be shortcomings in our simple description of the nucleon. One consideration is that we have neglected the self-energy of the nucleon, thereby attributing the whole attraction within the nucleon to diquark correlations. Furthermore, as a first approximation we have only included the scalar diquark channel associated with Eqn. (3.17). Including also the axial vector diquark channel (corresponding to Eqn. (3.18)) may also effect the value of r_s required to obtain the bare nucleon mass. We will return to this issue in Chapter 8, where we consider the effects of the axial vector diquark channel and the pion cloud of the nucleon in more detail.

6.2 Equations of State

For each case in Fig. 6.1, the charge neutral equation of state corresponds to the line separating the positively and negatively charged regions. For example, in the first diagram ($r_s = 0$), the charge neutral equation of state begins in the pure NM phase, then there is a mixed (+NM/-NQM) phase and finally a pure NQM phase. Each point on the boundary between the NM and NQM phases satisfies the Gibbs conditions, since $P^{(NM)}(\mu_B, \mu_I) = P^{(NQM)}(\mu_B, \mu_I)$. The equation of state in the mixed neutral phase is found by using the method of Glendenning [27]. Physically this method implies that the mixed phase begins with charge neutral NM, and then as the charge of NM becomes increasingly positive, regions of negatively charged NQM form, such that the mixed phase remains globally charge neutral. Finally, the NQM phase becomes charge neutral and the equation of state completes the transtition to pure NQM. The same sequence of neutral phases can also be seen in the first diagram of Fig. 6.2 by following the horizontal line $\rho_C = 0$.

As we increase the pairing strength in the SQM phase, the regions where SQM is the ground state extend. When $r_s = 0.1$ (the second diagram in Fig. 6.1), we have a mixed (+NM/-NQM) phase, and then come to a triple point where all

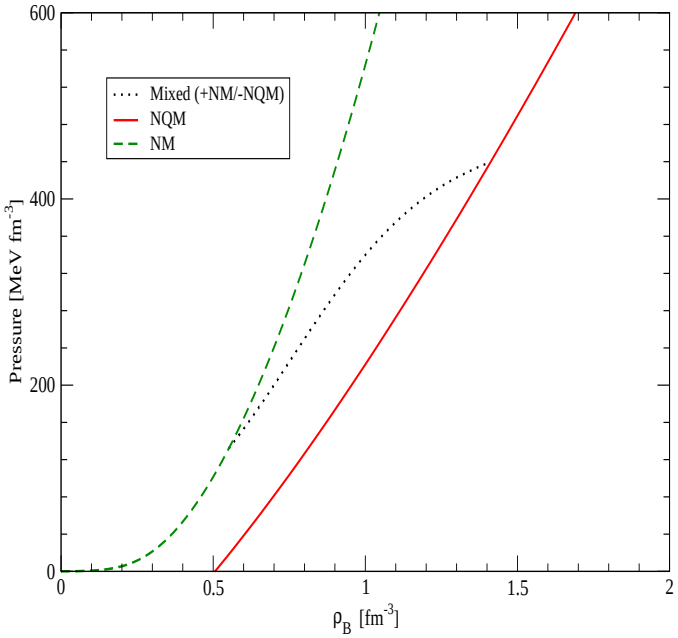

Figure 6.3: The equation of state for charge neutral nuclear matter in chemical equilibrium (dashed line). The equation of state for normal quark matter (solid line), which is a charge neutral mixture of up quarks, down quarks and electrons in chemical equilibrium. The mixed phase (dotted line) satisfies the Gibbs conditions for a two component system.

three phases meet. This is the same situation as investigated in Ref. [129], and leads to a region of constant pressure in the equation of state, where all three phases are mixed. Note that the triple point (a single point in the (μ_B, μ_I) plane), corresponds to a large triangular region in the (ρ_B, ρ_C) plane, as illustrated in Fig.2. When the $\rho_C = 0$ line passes through the triangular region, all three phases are present. The volume fraction of SQM begins at zero on the left hand side of the triangle and increases while the volume fraction of NM decreases until it reaches zero on the right hand side of the triangle. The NQM phase occupies the remaining volume fraction, which varies continuously between the boundaries of the triangle. In this region the baryon density is increasing, while the pressure remains constant. However, within compact stars the pressure must always be decreasing as a function of radial position[7]. Thus the three component

[7]General Relativity requires that the pressure is always decreasing as we move away from the centre of the star, in order to satisfy the equations for hydrostatic equilibrium (For further discussion see the next Chapter of this thesis).

mixed phase cannot occupy any finite volume within a star and there will be a discontinuity in the star's density profile (as is the case for equations of state with a Maxwell Construction).

If we further increase the pairing strength to $r_s = 0.15$, a charge neutral SQM state becomes possible. This transition from NM to SQM involves three intermediate mixed phases,

$$\text{NM} \rightarrow \text{+NM/-NQM} \rightarrow \text{+NM/-NQM/+SQM} \rightarrow \text{-NQM/+SQM} \rightarrow \text{SQM} \tag{6.13}$$

Again, the three component mixed phase occurs at the triple point in Fig. 1, which corresponds to the triangle in Fig. 2. At still larger pairing strengths the NQM phase becomes unfavorable and the equation of state involves just NM and SQM. When $r_s = 0.25$ we start with a neutral NM phase, and then enter a (-NM/+SQM) mixed phase before arriving at the neutral SQM phase. In Fig. 1 the line along the mixed phase in this case is only very short, which means that the pressure changes in the mixed phase are small. With $r_s = 0.3$, the SQM phase almost completely expels the NM phase, so that quark matter becomes the ground state of the system, even at densities below the empirical saturation point for nuclear matter. This result is consistent with the findings of Ref. [12] for the isospin symmetric case.

6.3 Mixed Phases

The equation of state as a function of baryon density is constructed subject to the constraint of global charge neutrality. If charge neutrality can be realized within one phase (for example the NM phase), one simply moves along the charge neutral line in the phase diagram (for example the line +NM/-NM) as the baryon density increases. When a phase transition occurs, it is necessary to construct a mixed phase, which is composed of positively and negatively charged components belonging to two different phases [27]. In a two component mixed phase the volume fractions for NM and QM (say) must add up to unity,

$$\chi^{NM} + \chi^{QM} = 1. \tag{6.14}$$

Furthermore, charge neutrality requires that,

$$\rho_C^{NM}\chi^{NM} + \rho_C^{QM}\chi^{QM} = 0. \tag{6.15}$$

Combining Eqns. (6.14) and (6.15), we may solve for the NM (or QM) volume fraction. A charge neutral mixture of NM and QM (where QM may refer to

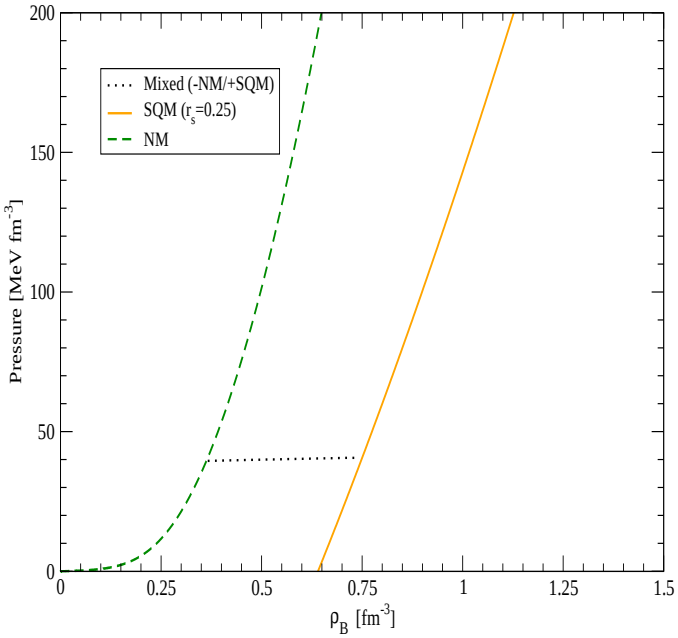

Figure 6.4: The equation of state for charge neutral nuclear matter in chemical equilibrium (dashed line). The equation of state for colour superconducting quark matter (solid line), with $r_s = 0.25$. The mixed phase (dotted line) satisfies the Gibbs conditions for a two component system.

either NQM or SQM), for example, is characterized by,

$$\chi^{NM} = \frac{\rho_C^{QM}}{\rho_C^{QM} - \rho_C^{NM}} \tag{6.16}$$

which ranges from 1 to 0, as the density increases from the point of pure NM (where $\rho_C^{NM} = 0$) to the one of pure QM (where $\rho_C^{QM} = 0$).

The baryon and energy densities for the mixed phase are then expressed by the volume fraction as follows,

$$\rho_B^M = \chi^{NM}\rho_B^{NM} + (1-\chi^{NM})\rho_B^{QM} \tag{6.17}$$

$$\mathcal{E}^M = \chi^{NM}\mathcal{E}^{NM} + (1-\chi^{NM})\mathcal{E}^{QM} \tag{6.18}$$

In principle, all intensive quantities can be calculated using equations of this form. However, it is important to keep in mind that these are volume averaged properties. They are only appropriate to the description of macroscopic physics. For example, the gravitational field of a compact star is insensitive to the details of how matter and energy are distributed within the mixed phase. Therefore,

the volume averaged equation of state can be used to determine masses, radii, etc, provided that it is microscopically stable.

In recent years there has been some debate over whether mixed phases of this form would be microscopically stable [15, 128, 131, 133]. This issue is not simple to resolve because it depends on the microscopic features of the mixed phase. In particular, the repulsive Coulomb forces within the local regions of charged matter must be balanced with the surface tension at the interface of the different regions[8]. Heiselberg et. al. [128] and Voskresensky et. al. [133] showed that the mixed phase can be energetically unfavourable if the surface tension is too large. However, assuming that the surface tension is reasonable, the mixed phase may also minimise its energy by the formation of geometric structures, including drops, rods and slabs [134].

Note that the components of the mixed phase have equal pressures ($P^M = P^{NM} = P^{QM}$) at each point (μ_B, μ_I) on the phase boundary. In this way one moves along the phase boundaries between NM and QM while ρ_B is increasing, until one comes to the point where charge neutral pure QM is realized ($\chi^{NM} = 0$).

In practice, our procedure is as follows. We first find the point where the effective potential for charge neutral NM becomes equal to the one for QM. At this point $\chi^{NM} = 1$, since $\rho_C^{NM} = 0$. From this point we incrementally increase either the neutron or proton density (depending on whether the transition is in the direction of increasing neutron and/or proton density). For example, the transition from NM to SQM ($r_s = 0.25$) is in the direction of increasing neutron density. For each neutron density, we determine the value for proton density required to ensure that we are on the phase boundary. Next we calculate the charge densities of each phase and the resulting volume fraction. The volume averaged properties of the mixed phase are then related to its component phases by Eqns. (6.17) and (6.18). This process continues until we encounter the point where the QM phase becomes charge neutral ($\rho_C^{QM} = 0$), and thus the volume fraction χ^{NM} goes to 0. From here the remainder of the equation of state will be the pure charge neutral QM phase. Note that in the case of $r_s = 0.25$, the phase boundary in this case is rather short, indicating that the pressure is almost constant during the phase transition (see Fig. 6.4). In this respect the transition looks like that of a one component (i.e. one chemical potential) system. In water, for example, the transition from liquid to gas is a constant pressure transition. For these systems it is appropriate to use a Maxwell construction. An example of this is given in Ref. [41], where the equation of state is calculated for pure neutron matter in QHD, including a constant pressure phase transition between

[8] Furthermore, Coulomb screening effects must be taken into account.

the liquid and gas phases of the low density region.

To construct a full equation of state, with NM phase, mixed phase and QM phase, we calculate the charge neutral equations of state for each phase separately, generating tables of values for baryon density, pressure and energy density. Then we amalgamate these tables into one. It is very helpful to have a phase diagram (i.e. μ_B vs $|\mu_I|$) to anticipate the location, direction and extent of phase transitions.

In Figs. 6.3 and 6.4 we show two examples of the charge neutral equations of state, corresponding to the cases $r_s = 0$ and $r_s = 0.25$. Essentially, these cases represent the smallest and largest reasonable values of r_s in the quark matter phase, while ensuring that nuclear matter is the most stable state in the low density region of the phase diagram. The phase transition from NM to NQM illustrated in Fig. 6.3 begins at approximately $3.4\rho_0$. In this case the mixed phase extends over a wide range of pressures and accordingly, it may occupy a large portion of the stars profile. In contrast to this, transition from NM to SQM (with $r_s = 0.25$), gives rise to just a few MeV per cubic Fermi, change in pressure (see Fig. 6.4). In this case the phase transition begins and ends at much smaller densities.

By applying a flavor SU(2) NJL model to both NM and QM phases, we have studied the phase diagram for isospin asymmetric matter at finite density. We emphasize that the model, and in particular the regularization scheme which we used, describes the single nucleon and the saturation of normal NM, and therefore forms a basis to investigate the equation of state at higher densities. We found that, as we vary the pairing strength in QM, several scenarios are possible. The charge neutral equation of state may make a transition to NQM or to SQM, via either one, two or three globally charge neutral mixed phases. These transitions begin at small enough densities (2.3 - $3.4\rho_0$) that the QM phase, or at least the mixed phase, may occur inside neutron stars. In the next chapter we will examine whether these hybrid stars would be gravitationally stable.

7

An Overview of Compact Stars

When a main sequence star reaches a critical point in its evolution, the internal pressure from nuclear reactions can no longer balance the gravitational pressure due to its mass. If the star is massive enough ($M \gtrsim 8\ M_\odot$), the rapid collapse of the core and subsequent outgoing shock wave leads to a spectacular explosion, known as a supernova. Compact stars are formed in the aftermath of such explosions. They are what remains of those main sequence stars that were not so massive that they would collapse into a black hole, yet massive enough that the remnant core would form into something more dense than a white dwarf[1]

The popular name for such an object, "neutron star," relates to the original idea that if such an object could exist, though it may begin as a mixture of protons, neutrons and electrons, the protons would rapidly capture the electrons via the weak interaction, leading to a neutron rich composition. The existence of such astrophysical objects was first suggested in 1934 by Baade and Zwicky [135], not long after the discovery of the neutron by Chadwick [136]. In some early studies, equations of state for pure neutron matter were used to approximate the composition of compact stars [44,137]. However, isospin asymmetric studies of hadronic matter show that it is not particularly accurate to neglect the contribution from protons [138,139]. For example, in the NJL model we are using, Fig. 4.3 shows that a mixture of neutrons, protons and electrons in β-equilibrium produces an equation of state which is much softer than pure neutron matter. As the density becomes very large, around a quarter of the baryons are protons (see Fig. 4.5).

There are many possibilities for the composition of the smallest known stars in our universe and it is possible that they are not all of the same type. Therefore, in this thesis we refer to them as "compact stars". The number of compact stars in our galaxy is expected to be of order 10^9, taking into account the time scales of stellar evolution and the estimated age of our galaxy [140]. However, due to their low luminosities and small diameter the vast majority of these

[1]Many authors include white dwarves (which are typically larger than the earth) under the category of "compact stars" and refer to the smallest most dense stars as "neutron stars" to distinguish them from white dwarves. However, this convention is outdated, since at present it is not clear whether these smaller objects are actually quark stars, hybrid stars, or stars with large fractions of hyperons and/or exotic species.

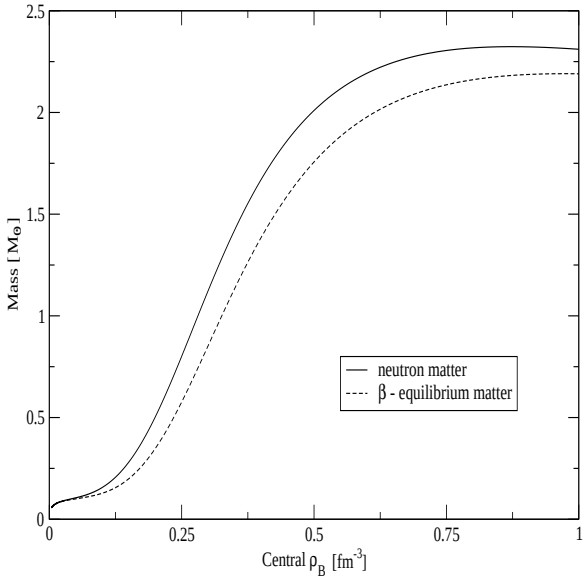

Figure 7.1: Neutron star (solid line) and npe star (dashed line) masses in the NJL model, using a quark - scalar-diquark model of the nucleon.

compact stars are undetectable. Two particular types of compact star that can be detected are radio pulsars and X-ray bursters. A brief overview of these stars is given in section 7.1. In section 7.2 we introduce the equations that describe the curvature of space-time and the arrangement of matter inside compact stars. We solve these equations, using the NJL model as our input equation of state, presenting the results in section 7.3.

7.1 Pulsars and X-Ray Binaries

Given that compact stars are very small (of the order of 10 km in radius), it is very difficult to find them in the optical range, though some have been discovered in this way by chance. Fortunately there are other means of detecting these stars. Over the last 40 years, thousands of compact stars have been identified - most of them in the form of radio pulsars and X-ray bursters. The first compact star to be discovered was a pulsar (PSR 1919+21). It was detected in 1967 by Bell and Hewish, as a pulsating source of radio waves with a period of about 1.3 seconds. The signal varied in intensity over long and short time scales but as Hewish *et. al.*

quickly realised "the most significant feature to be accounted for is the extreme regularity of the pulses" [141]. The time intervals between pulses were found to be constant to at least 1 part in 10^7 (so that they are actually very accurate clocks). The simplest explanation, independently developed by Pacini [142] and Gold [143], was that the pulses are produced by rotating magnetised compact stars. This hypothesis is now accepted, but there are still many open questions about the mechanism for how the radiation is produced [144–146].

Though there are several theoretical models for how the beams are produced, it is widely accepted that the mechanism depends on the strong magnetic field of the star. It is clear that pulsars emit twin beams of energy in opposite directions. The direction of these beams is not necessarily through the poles because the axis of rotation is not usually aligned with the magnetic field. This is the case for most astrophysical objects. The Earth's magnetic field, for example, is angled at approximately 11.3° from the planet's axis of rotation. If a pulsar is in a binary system, in many cases the masses of each star can be determined to a high level of accuracy [147]. A recent summary of available mass measurements is presented in Fig. 7.7, which is taken from Ref. [148]. Binary pulsars have given the most accurate mass estimates for compact stars. Provided that the orbit is at a significant angle to the Earth (i.e. edge-on) it is possible to derive their orbital parameters using the Doppler effect [147]. In particular, because the pulsar is moving around its orbit, sometimes it is moving toward Earth and sometimes away. After many months of observation, estimates of the orbital parameters become very good (i.e. as statistics improve). In 1993, Hulse and Taylor were awarded a Nobel prize for their ground breaking work in deriving a method to determine the masses of pulsars in binary systems to an unprecedented level of accuracy [147]. Some of the mass measurements for binary pulsars are now so accurate that the precision exceeds our knowledge of the gravitational constant. In fact, a method has recently been suggested to test for variability in the gravitational constant using binary pulsars [149]. These systems have also been used in a several ways as tests of general relativity over other theories of gravitation [150].

Another category of compact star system, which is especially useful from a theoretical perspective, is the X-ray binary. These are generally thought to be very old binary systems, with particularly close orbits. The gravitational field of one star tears matter away from the other giving out enormous bursts of X-rays as the matter is accreted onto it's surface. Determining the masses of X-ray bursters is much more difficult than it is for binary pulsars, as evidenced by the large error bars in the top portion of Fig. 7.7.

When X-ray binaries are located within globular clusters (which are standard candles) their distances from the Earth can be estimated. It is possible to

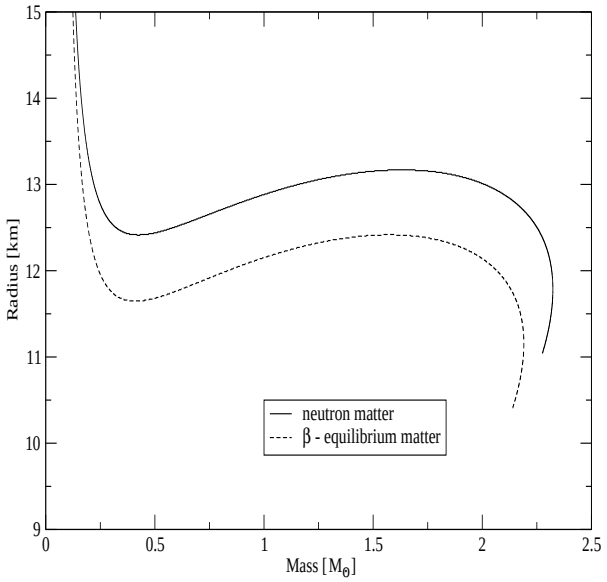

Figure 7.2: Neutron star (solid line) and npe star (dashed line) masses and radii in the NJL model, using a quark - scalar-diquark model of the nucleon.

measure the flux of the bursts and use the distance estimate to infer the temperature. If the bursts are treated as blackbody radiation from a spherical object, constraints for the radius of the star can be deduced.

7.2 General Relativity and Nuclear Physics

Given that compact stars have masses of approximately 1.5 $M_\odot$, the Schwarzschild radius can be estimated as $R_S = 2\ G\ M\ \sim 5$ km, where G is the gravitational constant. This is the same order of magnitude as the physical radius of the star ($R\ \sim 10$ km). Note that $R_S\ >\ R$ would imply that the object is a black hole. The matter inside compact stars is so compressed that the geometry of space-time is significantly modified[2]. Therefore, we must employ Einstein's theory

[2]The curvature of space-time in a compact star is substantial on the scale of metres or kilometres, thereby influencing the large scale structure of the star. However, at the scale of subatomic particle interactions which operate at distances of the order of 10^{-15} metres (i.e. the Fermi scale), the curvature does not influence the behaviour of particles in any local Lorentz frame. They behave just as they would in a flat space-time, even in a hypothetical star with $R\ \sim\ R_S$. Black holes ($R_S\ >\ R$), of course, are a separate issue. Reconciling

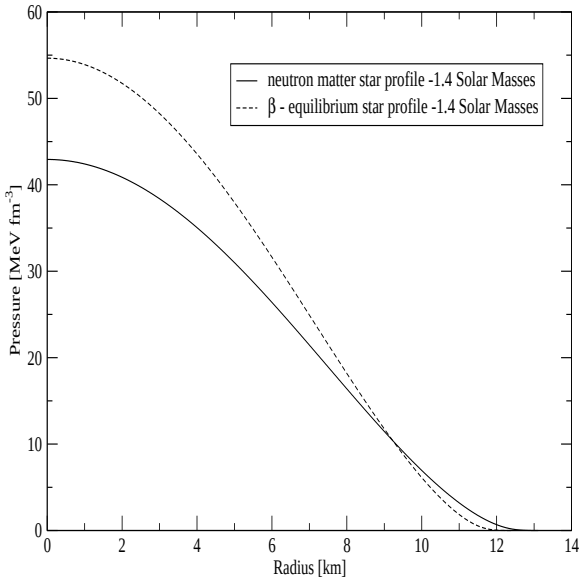

Figure 7.3: Profiles of typical mass (1.4 $M_\odot$) neutron stars (solid line) and npe stars (dashed line) from the NJL model, using a quark - scalar-diquark model of the nucleon.

of General Relativity to describe compact stars. The method for performing calculations for non-rotating stars was developed by Tolman, Oppenheimer and Volkoff in 1939 [23, 24]. These authors derived the equations for hydrostatic equilibrium (now referred to as the TOV equations) using Einstein's equations,

$$G^{\mu\nu} = R^{\mu\nu} - \frac{1}{2} g^{\mu\nu} R = 8\pi T^{\mu\nu}(\mathcal{E}, P(\mathcal{E})). \tag{7.1}$$

These equations relate the components of the curvature tensor, $R^{\mu\nu}$, and the Ricci scalar (scalar curvature), $R = R^{\mu\nu} g_{\mu\nu}$, to the components of the stress-energy tensor (energy-momentum tensor), $T^{\mu\nu}$. Note that $T^{\mu\nu}$ depends on the equation of state, $P(\mathcal{E})$. The unique relationship between pressure and energy density will determine the macroscopic properties of compact stars. The stress-energy tensor for a perfect fluid is given by,

$$T^{\mu\nu} = u^\mu u^\nu (\mathcal{E} + P) + g^{\mu\nu} P, \tag{7.2}$$

where $g^{\mu\nu}$ is the Schwarzschild metric and $u^\mu = d\,x^\mu / d\tau$ is the local fluid four-velocity satisfying the relation $u^\mu u_\mu = 1$. The equation for the Ricci tensor

General Relativity and Quantum Mechanics in the context of black holes is considered to be one of the greatest challenges in physics.

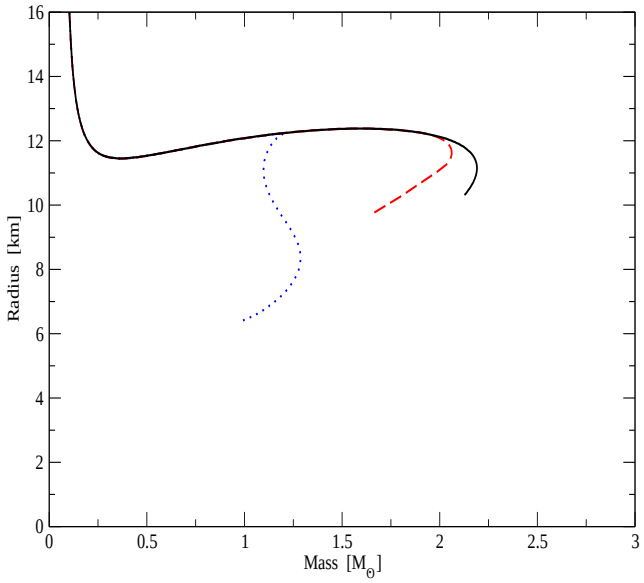

Figure 7.4: Mass vs radius configurations for npe stars (solid line) and hybrid stars in the NJL model. The dashed line has a transition to normal quark matter (NQM) and the dotted line has a transition to color superconducting quark matter (SQM) with pairing strength $r_s = 0.25$.

is,

$$R^{\mu\nu} = \Gamma^{\alpha}_{\mu\alpha,\nu} - \Gamma^{\alpha}_{\mu\nu,\alpha} - \Gamma^{\alpha}_{\mu\nu}\Gamma^{\beta}_{\alpha\beta} + \Gamma^{\alpha}_{\mu\beta}\Gamma^{\beta}_{\nu\alpha}, \tag{7.3}$$

where the Christoffel symbols (Gammas) and their derivatives are defined in Appendix F. The TOV equations give the rate of change of the pressure inside the star with respect to radial position,

$$\frac{dP(r)}{dr} = -\frac{G[P(r) + \mathcal{E}(r)][M(r) + 4\pi r^3 P(r)]}{r[r - 2M(r)G]} \tag{7.4}$$

and an expression that defines the mass contained within a radius, r,

$$M(r) = 4\pi \int_0^r \mathcal{E}(r')r'^2 dr'. \tag{7.5}$$

Integrating the TOV equations from $r = 0$ (the centre of the star) until $P(r = R) = 0$ (the surface of the star) gives $M(R)$, the mass of the star. We use the Runge-Kutta method to perform this integration [151].

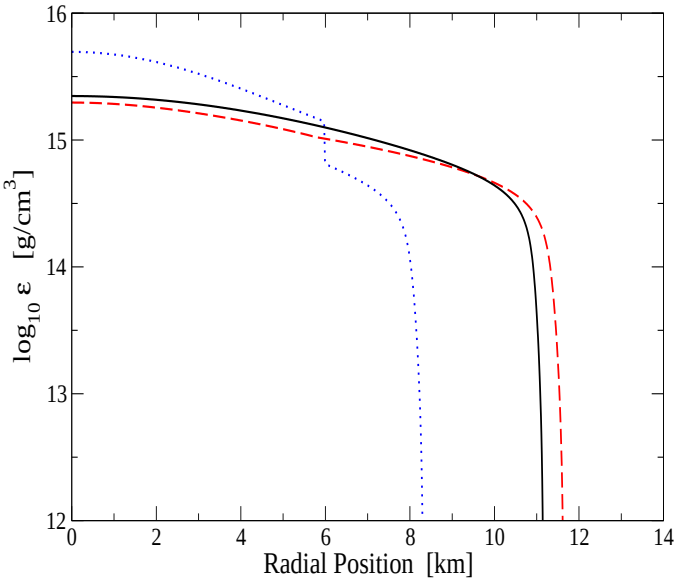

Figure 7.5: Profiles of maximum mass stars in the NJL model. The solid line is a 2.2 $M_\odot$ npe star. The dashed line is a 2.1 $M_\odot$ hybrid star which has a normal quark matter (NQM) core. The dotted line is a 1.3 $M_\odot$ hybrid star which has a transition to color superconducting quark matter (SQM) with pairing strength $r_s = 0.25$, corresponding to the rapid drop in energy density at approximately 6 kilometres from the centre of the star.

7.3 Results

Through the Tolman Oppenheimer Volkoff (TOV) equations [23, 24], any equation of state specifies a unique set of non-rotating relativistic stars. In Fig. 7.1 the results for neutron star masses as a function of central density (solid line) are shown for the NJL model equation of state derived in Ref. [1]. The dashed line in this figure shows the effects of introducing protons and electrons (in equal numbers) and imposing chemical equilibrium ($\mu_p = \mu_n - \mu_e$). These are referred to as "npe stars" in the literature [152, 153]. The results in Fig. 7.1 correspond to the equations of state presented in Fig. 4.3. Including protons and electrons softens the equation of state, reducing the masses of the stars for all possible central densities. The radii are also reduced, as shown in Fig 7.2. These results are discussed in Ref. [139]. Clearly the traditional description of compact stars as a giant sphere of neutron matter is significantly modified just by allowing for

protons. The masses are reduced by up to 0.25 $M_\odot$ for a given density, while the radii are reduced by almost a kilometre for any given mass.

In Fig. 7.3, the pressure profiles of typical mass (1.4 $M_\odot$) neutron and npe stars are shown. The pressure decreases monotonically until it reaches zero at the surface of the star. Note that the star with the higher pressure in the centre turns out to have the smaller radius. This may seem counter-intuitive, but it can be understood in terms of Eqn. (7.4), since in this equation, the rate of change of pressure is proportional to the pressure itself. Therefore, the higher the pressure in the centre of the star, the faster it will decrease. This is characteristic of relativistic stars, but it is not the case for classical objects (like our sun and the planets in our solar system), where larger pressures will tend to support larger masses and radii[3]. Equations of state and hybrid star properties for two cases ($r_s = 0$ and $r_s = 0.25$ in quark matter) are illustrated in Figs. 7.4 - 7.6.

The equation of state with a phase transition to SQM has a plateau in the central density vs mass curve (Fig.7.6). For this configuration there are two sets of stable solutions, which in the literature are referred to as twins [154] (since for these configurations there can be stars that have the same mass but different radii, as illustrated in Fig. 7.4). Qualitatively similar results are also found in Ref. [155]. It has recently been shown that solutions in the second set are indeed stable and may give rise to an observable signature for the occurance of phase transitions in compact stars [156]. It is interesting to note that such phase transitions to SQM can give rise to plateaus in the compact star masses. This phenomenon may be the reason that so many observed neutron stars lie within such a narrow mass range (See Fig. 7.7). Fig. 7.4 shows the mass to radius relationship of npe and hybrid stars. Notice that the maximum mass hybrid star (twin) with an SQM core has a much smaller radius than the corresponding npe star. The profile of this maximum mass star is illustrated in Fig. 7.5. Here we can see very clearly where the phase transition takes place. In fact, there is a 6 kilometre radius core of quark matter, surrounded by a 2 kilometre thick exterior of hadronic matter. The other lines in this figure are the maximum mass star profiles for npe matter (solid line) and npe matter with a transition to NQM (dashed line). It is clear from this figure that the presence of color superconductivity in quark matter can have a dramatic effect on hybrid star structure (a much more dramatic effect than normal quark matter, for example).

The hybrid star configurations represented by the dotted line on the right hand side of Fig. 7.6 correspond to the largest reasonable pairing strength ($r_s = 0.25$) for the phase diagrams shown in Fig. 6.1. As noted previously, the

[3]In the weak field limit (Newtonian limit) the curvature tensor vanishes and the TOV equations simplify to the form $dP/dr = -GM(r)\ \mathcal{E}(r)/r^2$, where $M(r)$ is given by Eqn. (7.5).

value of r_s used in the hadronic part of the equation of state (the solid line in Fig. 7.6) is approximately double this value. However, it is clear from Fig. 7.6 that even if we could increase the pairing strength in quark matter, it would only lead to smaller masses for the hybrid stars. The hybrid star masses are already too low compared with the observed compact star masses presented in Fig. 7.7, which are certainly at least 1.4 $M_\odot$. Assuming that our description of quark matter (i.e. a soup of up and down quarks with scalar pairing at the Fermi surface) is approximately correct in the density regime where we are applying it, the discrepancy in the value of r_s between the confined and the deconfined phases must be addressed by improving our hadronic equation of state. In the next chapter we consider how we may improve our model for the nucleon and how this effects the equation of state.

7.4 Rotation

The rotation of astrophysical objects is a beautiful feature of the universe. Outside the familiar realm of the Earth's atmosphere there is very little friction. All of the stars are rotating and most of them will continue to rotate through their entire life cycles. The rotation rate depends on the initial conditions during star formation, as matter swirls into the gravitational well of a star forming region. Our sun rotates rather slowly, about once every 26 days. This corresponds to an equatorial speed of approximately 2 kms^{-1}, but many observed main sequence stars have equatorial speeds in excess of 400 kms^{-1}. Upon collapse of a main sequence star the radius of the collapsed portion can decrease by 4 or 5 orders of magnitude, while the mass remains the same order of magnitude. As a result the angular velocity is dramatically increased. Thus compact stars rotate much faster than their progenitors, simply because of conservation of angular momentum. The fastest known pulsar rotates approximately 716 times per second - i.e. the rotation period is just 1.4 milliseconds [157]. The effects of rapid rotation on the properties of a relativistic star are naturally very important. For an introduction to rotating, relativistic stars, see Ref. [158].

In a classical star[4] the poles are slightly flattened by rotation and the star will have an expanded radius at the equator due to the centrifugal force. The same is true for a relativistic star, but there is also a distortion of the space-time metric itself. Local inertial frames will be dragged along by the motion of the star. This is known as the Lense-Thirring effect [22]. The effect is strongest at

[4]i.e. a star that has relatively low energy density and almost flat space-time, so that the Schwarzschild radius associated with the star is far smaller than the physical radius of the star.

the centre of the star and diminishes essentially to zero at great distances from the star. In a sense, the gravitational field is twisted by the star's rotation. The complexity of the problem arises because this gravitational field determines the distribution of matter and energy in the star, while the mass-energy distribution effects the gravitational field. The interplay of these features of the theory must be self-consistently resolved. As matter is spread away from the centre of the star, the central density can be reduced though the mass increases. However, a star that is rotating rapidly is more vulnerable to instability in the form of mass shedding. The outcome of including rotation thus depends on the equation of state. Strange quark matter, for example, will allow more rapid rotation rates, because it is self-bound [159]. In general, the most rapid (observed) rotation rates would lead to a 10% increase in the maximum mass predicted by typical equations of state [22]. However, the majority of stars that have known masses have much slower rotation rates. Thus we cannot account for the mass discrepancy between our hybrid stars (with $M \sim 1.3$) and the observed masses presented in Fig. 7.7, by introducing stellar rotation. Again, this prompts us to consider how we may improve our equation of state for hybrid stars.

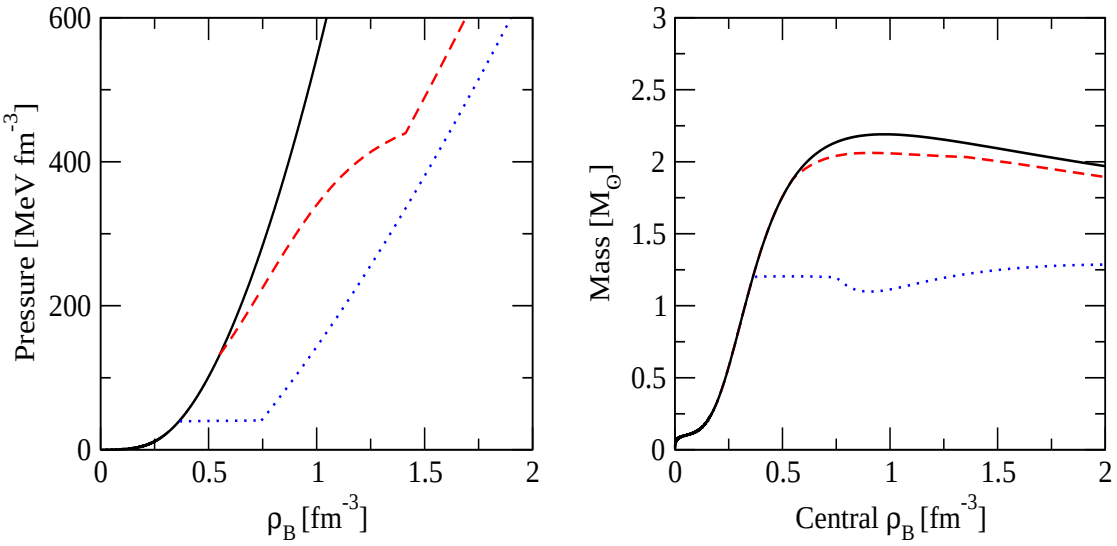

Figure 7.6: Equations of state and stellar masses for npe stars (solid line) and hybrid stars in the NJL model, using a quark - scalar-diquark model of the nucleon. The dashed line has a transition to normal quark matter (NQM) and the dotted line has a transition to color superconducting quark matter (SQM) with pairing strength $r_s = 0.25$.

NOTE: This image is included on page 80 in the print copy of the thesis held in the University of Adelaide Library.

Figure 7.7: Observed compact star masses as of 2004, plotted with 1σ uncertainties. This illustration is taken from Lattimer et. al. [148]. The letters (a) to (o) refer to the journal articles where these measurements are published. The result for J0751+1807 has since been published as M = 2.1 ± 0.2 M□ at the 68% confidence level [160].

8

Revisiting the Nucleon

In order to build on our simple description of the nucleon as a quark - scalar diquark state there are two immediately obvious improvements we can make. Firstly, within the formalism we have developed we can extend the model to include the axial vector diquark channel. Secondly, we can calculate the nucleon self-energy and consider how this effects the dynamics of the system at finite density. It turns out that these two improvements have opposing effects on the behaviour of the saturation curve (i.e. Fig. 3.5). The inclusion of the axial vector diquark stiffens the equation of state, while the finite pion cloud softens the equation of state. When we include both of these effects, the saturation point of the model remains very good. Moreover, there can be considerable benefit to the saturation properties, when we use a more realistic model of the nucleon. Since both improvements lead to decreases in the value of r_s, it actually becomes comparable to the value implied by the phase diagrams in our preliminary version of the model (quark - scalar diquark). In this chapter we present an improved model of the nucleon and use it to fix the scalar pairing strength in quark matter. We have some flexibility in setting the overall strength of the pion cloud, so it is treated as a variable parameter. In this way we study the evolution of the phase diagrams as a function of the strength of the pion cloud.

8.1 Axial Vector Diquarks

As we have seen in Chapter 3, it is possible to describe some features of the nucleon without the axial vector diquark channel. In fact for some purposes it can be neglected. Mineo *et. al.* found that the axial vector diquark correlations occur with less than 10% probability [161]. The scalar diquark correlations are favoured because they have a much lighter mass and have total spin zero. On the other hand for some calculations, such as the determination of spin dependent structure functions [162], the axial vector diquark channel is essential. In the present case, the inclusion of the axial vector diquark channel leads to the important effect that the pairing strength in the scalar channel (r_s) is diminished due to the presence of this alternative pairing channel, characterised by

the ratio, $r_a = G_a/G_\pi$. One may well ask whether there are any other active pairing channels inside the nucleon, such as vector or tensor terms, for example. However, only the scalar and axial vector channels involve s-wave interactions. All other interaction terms should be suppressed.

Actually, the value of the scalar pairing strength for quarks inside the nucleon is not important in itself, because there are no direct constraints on this quantity from experiment. If we had only considered hadronic matter in this model there would be no immediate reason to question the value of r_s. However, through calculating the properties of (colour superconducting) quark matter and investigating the phase diagram, we have found that a relatively small value of r_s is required in the quark matter phase so that colour superconducting quark matter does not become more stable than the two flavour hadronic matter at low density[1].

We wish to make a quantitative comparison of the scalar pairing strength in hadronic matter and color superconducting quark matter and examine the possibility that it is the same in both phases. We use the properties of the nucleon to calculate r_s. Therefore, any aspect of nucleon dynamics that effects this parameter must be included. With this in mind we consider again the Faddeev equation for the nucleon. This can be expressed as [163],

$$\Gamma^a_N(p) = Z^{aa'}\,\Pi^{a'b}_N(p)\,\Gamma^b_N(p) \equiv K^{ab}(p)\Gamma^b_N(p), \tag{8.1}$$

where Z is the quark exchange kernel[2],

$$Z^{aa'} = \frac{3}{M}\begin{pmatrix} 1 & \sqrt{3}\gamma_5\gamma^\mu \\ \sqrt{3}\gamma^{\mu'}\gamma_5 & -\gamma^{\mu'}\gamma^\mu \end{pmatrix}. \tag{8.2}$$

$\Pi_N(p)$ is the product of the quark and diquark propagators [82]. With both pairing channels included the quark-diquark bubble graph becomes,

$$\Pi^{a'b}_N(p) = \int_{PT}\frac{d^4k}{(2\pi)^4}\tau^{a'b}(p-k)S(k) \tag{8.3}$$

$$= \int_{PT}\frac{d^4k}{(2\pi)^4}\begin{pmatrix} \tau_s(p-k) & 0 \\ 0 & \tau_a^{\mu'\nu}(p-k) \end{pmatrix} S(k), \tag{8.4}$$

where τ_s and $\tau_a^{\mu\nu}$ refer to the scalar and axial vector components of the diquark t-matrix[3] and $S(k)$ is the constituent quark propagator. The nucleon mass follows

[1] i.e. In the density region where we are certain that two flavour quark matter is not favoured, because we observe stable two flavour hadronic matter.

[2] Using the proper time regularisation scheme, the calculation is somewhat more complicated than in the 3-momentum cut-off scheme, for example. Therefore, we use the static approximation (i.e. momentum independent approximation) to the quark exchange kernel [9].

[3] We use the approximate "constant + pole" forms of the diquark t-matrices as outlined in Appendix B.

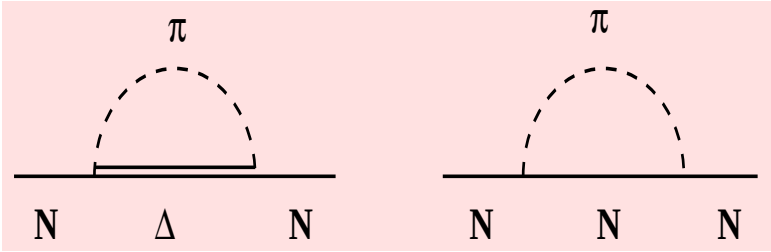

Figure 8.1: The dominant processes associated with the nucleon self-energy.

from the solution to Eqn. (8.1). That is, the requirement that the Faddeev kernel, $K \equiv Z\,\Pi_N$, has eigenvalue 1. For further details of this calculation, see Appendix C.

With both pairing channels included, we now need an additional constraint (apart from the value of the nucleon mass) to determine the variables r_a and r_s. For this purpose we consider the Δ^{++}. This baryon is composed of three up quarks. Any diquark correlations in such a baryon, must be symmetric in flavour and anti-symmetric in colour. Therefore, to produce an anti-symmetric wavefunction, the diquark state must be symmetric in spin. In this case the scalar diquark correlations are prohibited ($r_s = 0$) and we can use the empirical mass of the Δ^{++} (1232 MeV) to fix the value of r_a. This pairing strength ($r_a = G_a/G_\pi$) is calculated by looking for the value of M_a using bisection method, such that the pole condition for the axial vector diquark, $1+2G_a\Pi_a(q^2 = M_a^2) = 0$ and the Faddeev Equation for the delta baryon is satisfied (see Appendix C). Before we incorporate the self-energy of the nucleon (and the self-energy of the Δ^{++}), the pairing strength in the axial vector diquark channel is about 0.27 as shown in the second line of Table 8.2. Once r_a is fixed we may solve the Faddeev equation for the nucleon to determine r_s, such that we obtain the correct physical nucleon mass (940 MeV). r_s is fixed by the pole condition $1+2r_sG_\pi\Pi_s(q^2 = M_s^2) = 0$ and the solution to the Faddeev equation for the nucleon (Eqn. (8.1)). We obtain the value $r_s = 0.3$ when the pion cloud is not included.

8.2 Nucleon Self-Energy

In any model where the nucleon mass is calculated it is important to remember that the nucleon is a quasiparticle. It is actually dressed with pion loops, so

that what we measure as the nucleon mass may be defined as,

$$M_N = M_N^0 + \Sigma_N, \tag{8.5}$$

where M_N^0 is the "bare" nucleon mass and Σ_N is the nucleon self-energy. The main contribution to Σ_N comes from processes of the form $N \rightarrow \Delta\,\pi \rightarrow N$ and $N \rightarrow N\,\pi \rightarrow N$, illustrated in Fig. 8.1. For discussions on one-loop mesonic corrections to the nucleon mass see Refs. [164] and [165]. The pion loop diagrams dominate Σ_N because the pion is the by far the lightest meson (it actually plays the role of a Goldstone boson) and therefore has the longest range. The corresponding self-energies are given by [166],

$$\Sigma_N = \sigma_{NN}^{\pi} + \sigma_{N\Delta}^{\pi} \tag{8.6}$$

$$\Sigma_\Delta = \sigma_{\Delta\Delta}^{\pi} + \sigma_{\Delta N}^{\pi}, \tag{8.7}$$

where,

$$\sigma_{BB'}^{\pi} = \frac{-3\ g_A^2}{16\pi^2 f_\pi^2} c_{BB'} \int_0^\infty dk \frac{k^4 u^2(k)}{\omega(k)[\omega_{BB'} + \omega(k)]} \tag{8.8}$$

where $\omega_{BB'} = (M_B - M_{B'})$ is the physical baryon mass splitting (e.g. $\omega_{N\Delta} = 1232 - 939$ MeV), and $\omega(k) = \sqrt{k^2 + m_\pi^2}$ is the intermediate pion energy. The coefficients $c_{BB'}$ come from the standard SU(6) couplings (i.e. $c_{NN} = 1$, $c_{N\Delta} = 32/25$ [167]). For the $\pi BB'$ vertex we assume the phenomenological dipole form [168],

$$u(k) = \Lambda^4/(\Lambda^2 + k^2)^2. \tag{8.9}$$

The dipole cut-off Λ should not be confused with Λ_{IR} and Λ_{UV} which are the cut-off parameters on the quark level in this model. We assume that the ratio g_A/f_π in EQN. (8.8) is independent of density. This is supported by a recent analysis of the pion-nucleus optical potential [169], which has shown that the pion decay constant in nuclear matter is reduced by 20%, which is the same as the quenching of g_A derived from Gamow-Teller matrix elements [170]. The pion mass in the medium is constrained by chiral symmetry which leads to the relation[4] $m_\pi(\rho)^2 = m_\pi^2 M_0/M$ [1]. This small enhancement of the pion mass in the medium is taken into account in the calculation but its effect is not very important.

The value of the self-energy of the nucleon, Σ_N, is not precisely known, but it is known to be large and negative. In fact, it is predicted to be an attractive contribution between about 150 and 400 MeV (at zero density) [164, 167, 171–173]. In the present work Σ_N is varied by changing the dipole cut-off, Λ, within

[4]The pion mass in this relation is defined at zero momentum.

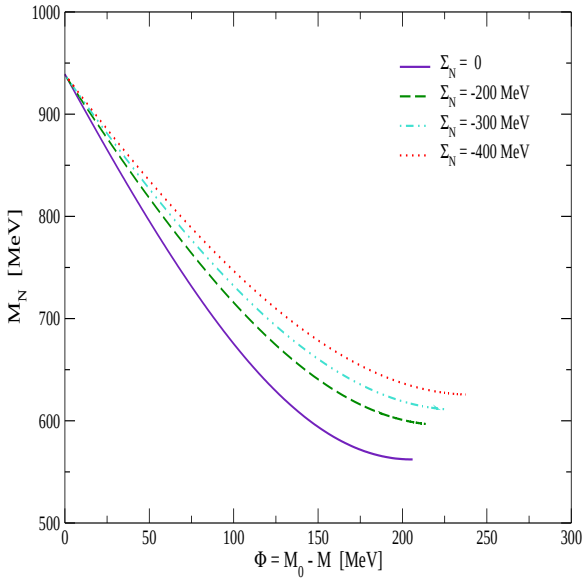

Figure 8.2: The quark mass dependence of the nucleon mass, for various choices of the nucleon self-energy, Σ_N (in free space).

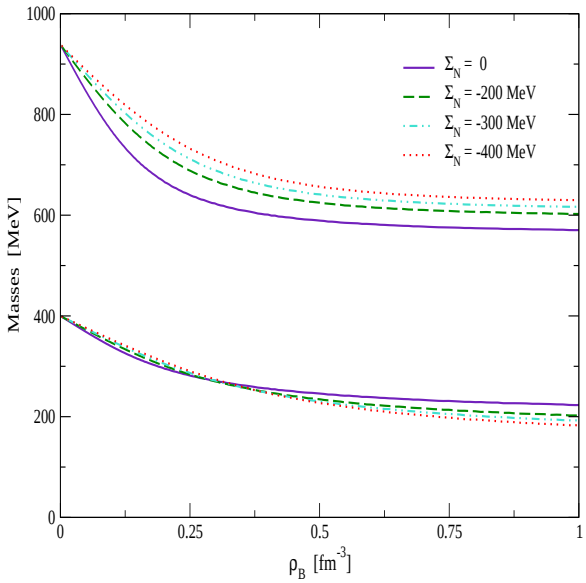

Figure 8.3: The quark mass (lower lines) and the nucleon mass (upper lines) as a function of baryon density, for various choices of the nucleon self-energy, Σ_N.

physically acceptable limits, in order to investigate how the pion cloud of the nucleon influences the equation of state of the system.

The pion cloud contribution to the nucleon is incorporated as follows. First, we must consider what pairing strengths, r_a and r_s, are required to give the bare nucleon mass, M_N^0, for a given nucleon self-energy, Σ_N, in accordance with Eqn. (8.5). As mentioned in Section 8.1, it is convenient to establish r_a first using the mass of the Δ^{++} (since this baryon should have no contribution from the scalar diquark channel). For consistency we must also incorporate the pion cloud of the Δ^{++} in this calculation. The experimental mass is given by $M_\Delta = M_\Delta^0 + \Sigma_\Delta$, where $M_\Delta^{(0)}$ is the "bare" mass which follows from the quark-diquark equation.

The first step is to choose a reasonable value for the nucleon self-energy. For example if we choose $\Sigma_N = -200$ MeV, this corresponds to a specific choice for the dipole cut-off ($\Lambda \approx 710$ MeV) which enters into Eqn. (8.8). Using the same value of Λ we calculate the corresponding self-energy of the Δ^{++}. In this case, the bare mass is thus given by,

$$M_\Delta^0 = M_\Delta - \Sigma_\Delta = 1232 + 183 = 1415 \text{ MeV}. \tag{8.10}$$

We use this value of the bare mass to fix r_a. Again we use the Faddeev equation for the nucleon to fix r_s, using the bare mass ($940 + 200 = 1140$ MeV). As usual, the parameter G_ω is fixed to give the empirical binding energy per nucleon of symmetric nuclear matter ($E_B = 17$ MeV), and the parameter G_ρ is adjusted to the symmetry energy ($a_{sym} = 32.5$ MeV at $\rho_0 = 0.17$ fm^{-3}). For the static parameter in the quark exchange kernel we use $c = 450$ MeV. This calculation of baryon masses is carried out for several initial choices of the dipole cut-off Λ, which controls the magnitude of the pion loop contributions to the nucleon mass, Σ_N. We will show the results for three different values of Λ, chosen to give Σ_N = -200, -300 and -400 MeV. The resulting parameter sets are shown in Table 1. The first and second lines in this Table correspond to cases where the nucleon and delta masses are produced without pion cloud contributions.

8.3 Improved Equation of State

Now that we have improved our model for the nucleon, there are some important implications for the equation of state. Though the effective potentials for hadronic matter and quark matter have exactly the same form as before, the behaviour of the masses of quarks and hadrons will be different (in the hadronic phase), because the input function for the mass, $M_N(M)$, has changed. Fig. 8.2

Λ	Σ_N	Σ_Δ	r_a	r_s	r_ω	r_ρ	ρ_0	K	M_N*
-	0	0	-	0.51	0.37	0.89	0.22	560	695
-	0	0	0.27	0.30	0.48	0.70	0.14	426	689
710	-200	-183	0.21	0.27	0.30	0.74	0.19	314	741
803	-300	-266	0.18	0.24	0.24	0.76	0.21	205	764
877	-400	-346	0.15	0.22	0.19	0.77	0.25	124	783

Table 8.1: Parameters and results corresponding to different choices of Σ_N. We define $r_\alpha = G_\alpha/G_\pi$ ($\alpha = a, s, \omega, \rho$). Λ, Σ_N, Σ_Δ the compressibility, K, and the effective nucleon mass at saturation density, M_N^*, are all in units of MeV. The first line corresponds to the quark - scalar-diquark model of the nucleon.

shows how the scalar polarisability[5] of the nucleon depends on the value of the nucleon self-energy. As the magnitude of Σ_N increases, the repulsion (G_ω) decreases and the masses shift upward. The curvature (which corresponds to the scalar polarisability) is comparatively decreased. At finite density, this is illustrated in Fig. 8.3, which also shows the decreasing curvature in the nucleon mass as the effect of the pion cloud increases. This behaviour translates directly to the saturation properties of the model outlined in Table 8.2. As the magnitude of Σ_N increases, the saturation point moves to higher densities, while the compressibility decreases. In fact, this represents a significant improvement in the model, since experimental evidence implies $K \sim 200$ - 300 MeV [22, 93]. Because the scalar pairing strength is significantly reduced by the inclusion of the axial vector diquark (See Table 8.2), the model now produces non-trivial phase diagrams when we apply the same scalar pairing strength in both phases.

8.4 Phase Diagrams and Compact Stars

The phase diagrams presented in Fig. 8.4 illustrate the effect of the pion cloud on the phases of QCD, based on our NJL model calculations. As the magnitude

[5] In models which use point-like nucleons (e.g. QHD), the effective mass of the nucleon has the form $M_N^* = M_{N_0} - g_\sigma\sigma$, where σ is the scalar field. When nucleon structure is introduced this linear expression in σ develops curvature, so that, $M_N^* \approx M_{N_0} - g_\sigma\sigma - g_{\sigma\sigma}\sigma^2$. The coefficient $g_{\sigma\sigma}$ is known as the scalar polarisability [89].

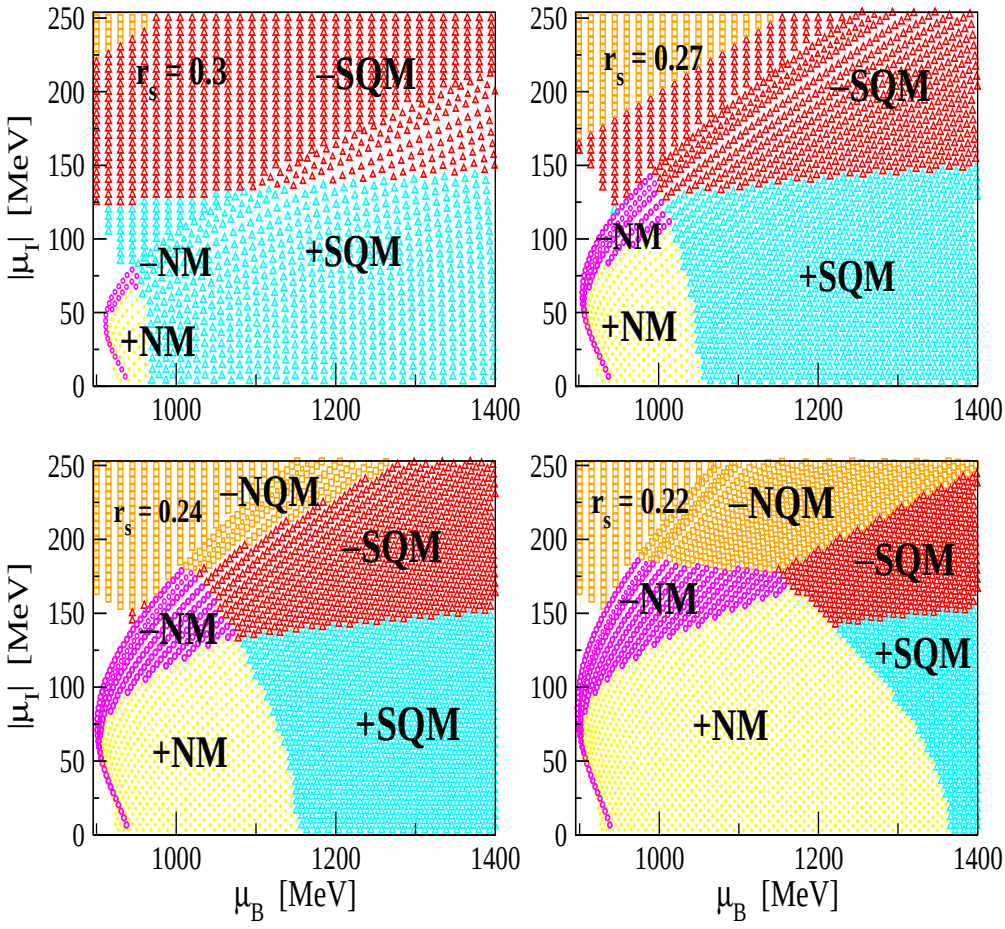

Figure 8.4: Phase diagrams with $r_s(NM) = r_s(QM)$. The nucleon self-energies (Σ_N) are 0, -200, -300 and -400 MeV respectively. The labels NM, NQM and SQM refer to nuclear matter (a mixture of neutrons, protons and electrons), normal quark matter and color superconducting quark matter. The plus and minus signs indicate the sign of the charge density in each region.

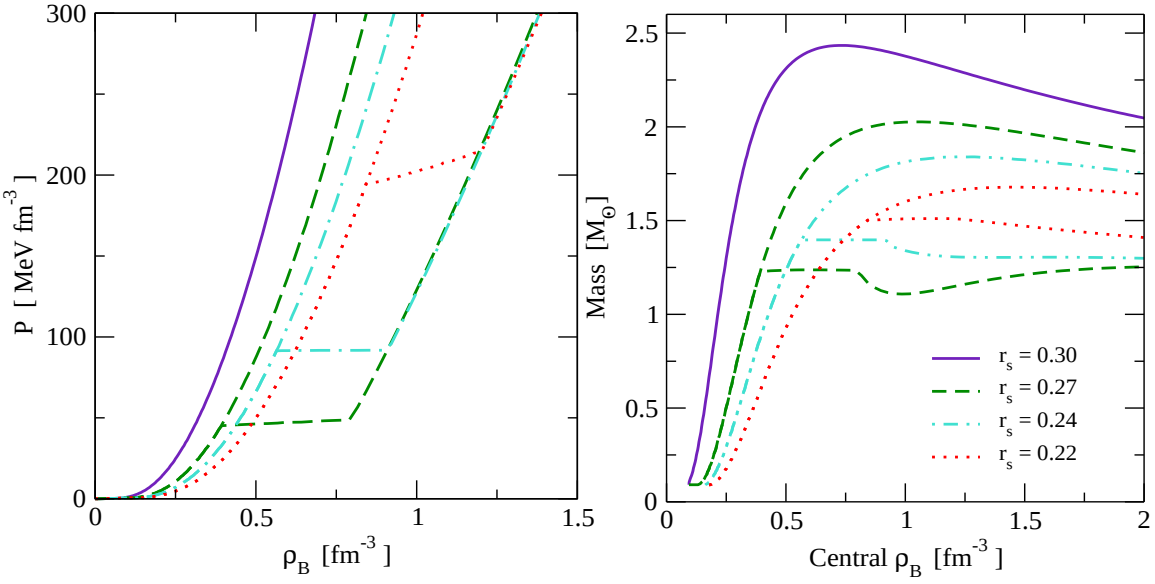

Figure 8.5: Equations of state (with and without transitions to quark matter) and compact star masses corresponding to four different choices of the nucleon self-energy. With Σ_N = 0, -200, -300 and -400 MeV, the pairing strengths are r_s = 0.30, 0.27, 0.24 and 0.22 respectively.

of the pion cloud increases, the SQM phase shrinks. There are two effects that are competing in this process. The pressure in the NM phase is reduced when we increase the pion cloud (the NM equation of state is softened, as shown in Fig. 8.5). However, since the value of r_s is decreasing, this leads to a decrease in the pressure of the SQM phase as well (as we saw earlier in Figs. 5.3 and 6.1). The latter effect is much stronger and has a greater influence on the phase diagrams. This highlights the importance of using a physically motivated choice for the coupling in models of colour superconducting quark matter (which has been achieved for the first time using this NJL model).

An interesting feature of the phase diagrams in Fig. 8.4 is that the phase transitions from NM to SQM can be qualitatively different, depending on the size of the pion cloud. At r_s = 0.27 (Σ_N = -200 MeV) the mixed phase involves negatively charged hadronic matter (-NM) and positively charged quark matter (+SQM). In the last diagram (Σ_N = -400 MeV) the transition moves in the opposite direction, generating a +NM/-SQM mixed phase. These two possibilities are curious if we consider the microscopic behaviour of matter in mixed phases, as it may be quite different in each case (forming different shapes etc). In the

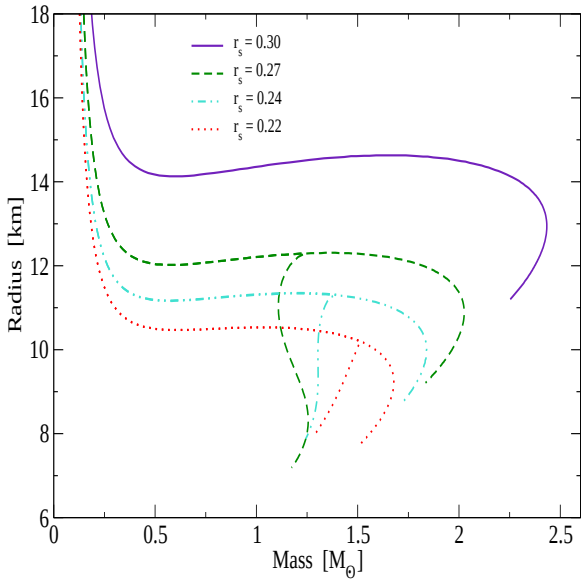

Figure 8.6: Compact star masses and radii corresponding to four different choices of the nucleon self-energy. With Σ_N = 0, -200, -300 and -400 MeV, the pairing strengths are r_s = 0.30, 0.27, 0.24 and 0.22 respectively.

intermediate diagram (Σ_N = -300 MeV), the mixed phase is confined almost to a point. Thus the equation of state will have a very flat phase transition (i.e. almost constant in pressure). This is illustrated on the left hand side of Fig. 8.5.

Without the pion cloud, there is no stable transition to quark matter (c.f. the first diagram in Fig. 8.4). The positively charged quark matter phase (+SQM) separates the charge neutral equations of state for hadronic matter and quark matter, so that there is no charge neutral line running through this diagram. This represents an interesting scenario for the phase diagram of QCD. Supposing that nature has a phase diagram of this form (which is quite possible, though not favoured by this model, since we anticipate a large negative value for the pion cloud). Then we may consider what happens if we begin with charge neutral nuclear matter and try to increase the density. This scenario could be important in a supernova, for example. When a star is collapsing, we assume that the density continues to increase until it reaches hydrostatic equilibrium (where it satisfies the TOV equations). However, if the QCD equation of state has a charge discontinuity (as in the first diagram in Fig. 8.4), then matter may be forced (by gravity) into a positively charged state. The star will surely encounter a massive source of internal Coulomb repulsion when the core density reaches the positively charged transition region of the phase diagram.

In a compact star the formation of matter with a net positive charge must lead to mass shedding. The reason is that the net Coulomb force will become much more powerful than the gravitational force [132]. For illustration, consider a compact star with a net positive charge, $Z_{net}e$. For an additional positively charge particle (charge = e, mass = m) to be introduced, for stability we must have the gravitational force larger than the Coulomb force on that particle,

$$\frac{(Z_{net}e)e}{R^2} < \frac{GMm}{R^2}. \tag{8.11}$$

For example, if the particle is a proton, and the baryon number of the star is A, we have, $Z_{net}e^2 < GAm^2$. With $m = 940$ MeV and $e = 1.44$ MeV fm^{-3}, we obtain the requirement (in gravitational units),

$$Z_{net} < 10^{-36}A. \tag{8.12}$$

Therefore, the net charge must be extremely small for the system to be stable against Coulomb repulsion. Since the first diagram in Fig. 8.4 does not allow a charge neutral phase transition to quark matter, it cannot give rise to a stable hybrid star. However, for comparison we show the results for npe stars (solid line) on the right hand side of Fig. 8.5. The maximum mass is relatively large because the equation of state is quite stiff. Once the nucleon self-energy is included, the equations of state soften and the compact star masses decrease substantially.

The equations of state for charge neutral matter are shown in the left diagram of Fig. 8.5. The lines which run smoothly to zero pressure correspond to the hadronic equations of state and produce the four upper lines (npe stars) in the diagram on the right. The other equations of state include transitions to quark matter and produce the corresponding hybrid stars (lower lines) in the central density vs mass diagram. The hybrid star maximum mass for the $r_s = 0.27$ (Σ_N = -200 MeV) case is about 1.25 $M_\odot$. This is too small to account for the observed masses of compact stars. The other configurations are more realistic, with maximum masses of approximately 1.4 and 1.5 $M_\odot$. The highest mass hybrid stars (lower dotted line) may only have a mixed phase in the core, while the other curves allow for pure quark matter to form.

The effect of the pion cloud has important implications for hadronic matter. This is clear from the equations of state, but it is highlighted in a very tangible way by the properties of npe stars. The configuration based on a $\Sigma_N = 0$ equation of state (solid line), has a maximum mass of approximately 2.4 $M_\odot$. This is dramatically reduced when the pion cloud is included. For example, the (upper) dotted line (Σ_N = -400 MeV) has a maximum mass of about 1.7 $M_\odot$. Furthermore, the central densities sustained in these stars can be up to double

the maximum central density of the densest stable $\Sigma_N = 0$ star. Obviously this must have a significant effect on the radius. Fig. 8.6 shows the npe star and hybrid star radii. Indeed, when the pion cloud is included the radii are reduced by approximately 2 - 4 km. From these results it is clear that the self-energy of the nucleon can have substantial effects on the properties of compact stars.

The mass vs radius relationships for two flavour colour superconducting quark stars are presented in Fig. 8.7. These stars are quite small ($R \sim 6$ km). In fact, they are approximately half the size of the corresponding npe stars shown in Fig. 8.6. This is an interesting feature from an observational point of view. Indeed, most equations of state for quark matter predict comparatively small stars (though not all of them [174]). However, as pointed out earlier, two flavour hadronic matter is more stable than two flavour quark matter at low density (i.e. $\rho_B < 2\rho_0$, say). So in practice there must be some region of hadronic matter surrounding a star of two flavour quark matter. In our model pure two flavour quark stars are not massive enough to agree with observational data and of course, they are not favoured by the phase diagrams. For reasonable values of the pion cloud, the phase diagrams produce hybrid stars.

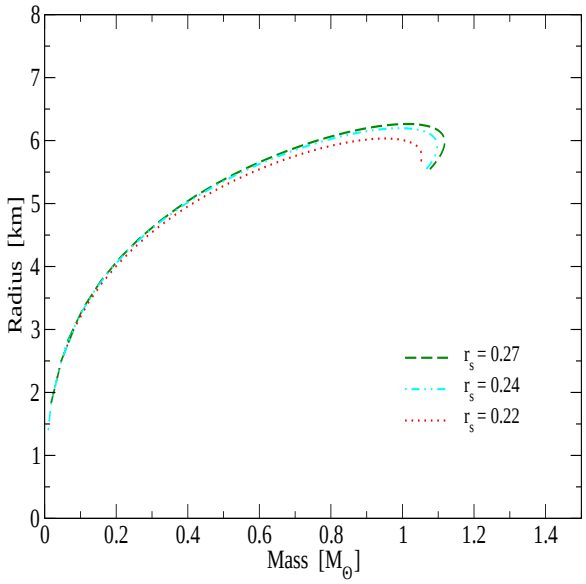

Figure 8.7: Mass vs Radius relationship for hypothetical two flavour quark stars from the NJL model with color superconducting pairing strength fixed by the properties of the nucleon. With nucleon self-energy Σ_N = -200, -300 and -400 MeV, the pairing strengths are r_s = 0.27, 0.24 and 0.22 respectively.

9

Conclusion

To accurately describe matter at high densities is a very challenging task. A great deal of work has been done using models of nuclear matter and quark matter to predict the behaviour of QCD under extreme conditions. It is clear that a relativistic description of nuclear matter is preferable and becomes increasingly so as we move to higher densities. Most models of nuclear matter treat nucleons as point like particles. However, it is now apparent that quark degrees of freedom are an indispensable aspect of the system. In this sense, Quantum Hadrodynamics does not provide a complete picture of the hadronic phase. The dynamics at the scale of nuclei (i.e. the nucleon-nucleon interaction), influences and is affected by the internal structure of the nucleon. The purpose of this thesis was to develop an existing model (the NJL model) to describe asymmetric matter, with the particular aim of using quark degrees of freedom to describe both confined and deconfined matter, appropriate to the description of compact stars.

The main advantages of the NJL model lie in its similarities with the underlying theory of the finite density system, which is QCD. It is chirally symmetric, relativistic and is based on quark degrees of freedom. As with all models it has limitations. Though it is mathematically beautiful and shares some important qualities of QCD it does not explicitly incorporate gluon degrees of freedom and it is not renormalisable. However, in some respects, non-renormalisability may actually be interpreted as a positive attribute of the NJL model. It means that we have the freedom to choose a regularisation scheme that is, in effect, connected with the underlying physics of quarks and gluons. Essentially, an infra-red cut-off can restrict the behaviour of quarks, stabilising the free nucleon against decay. Thus the model can mimic the QCD description of a nucleon in a very simple way. Of itself this is a remarkable discovery, but on top of this it has also been shown, more recently, that this prescription for the regularisation of the NJL model actually leads to the stabilisation of symmetric nuclear matter (something which has eluded chiral models for many decades).

Apart from recent progress in the description of the hadronic phase, there have also been significant theoretical advances in our understanding of the quark matter phase, especially during the last few years. In particular, it is now well documented that in two flavour quark matter, a colour superconducting phase

(2SC) may be favourable at high densities, depending on the strength of the scalar pairing between quarks. In light of these significant developments, this work has been aimed at exploring the phase diagram of the NJL model. We have calculated the properties of the quark matter phase using the same regularisation method (proper-time) as in the hadronic phase, except that the (confining) infra-red cut-off is set to zero. We can confirm from this work, that the phase diagram has a strong dependence on the pairing strength between quarks in deconfined matter. In particular, Cooper pairing increases the pressure of quark matter substantially.

As a first step we have studied the phase diagram using a quark - scalar-diquark model for the nucleon (neglecting the nucleon self-energy). We found that the saturation properties of nuclear matter are not sensitive to the initial choices of the infra-red cut-off or the constituent quark mass at zero density. Using the quark - scalar-diquark model of the nucleon the outcome for the saturation density is surprisingly good, at $\rho_0 = 0.22$ fm^{-3}, but the compressibility ($K = 560$ MeV) is much too high compared to experimental estimates. We also found that the pairing strength in quark matter had to be at least a factor of two smaller than the value derived for the scalar diquark state inside the nucleon, otherwise two flavour quark matter would be the ground state, even in the low density region of the phase diagram (where it is physically excluded).

Treating r_s(QM) as a free parameter allowed us to study the properties of hybrid stars using the quark - scalar-diquark model in the hadronic phase. We found that the phase diagrams revealed some novel scenarios for hybrid stars. The charge neutral equations of state could proceed through several different mixed phases, depending on the pairing strength in quark matter. When the Cooper pairing is completely switched off there is a transition to normal quark matter leading to massive hybrid stars, which look very similar to conventional neutron stars. As the pairing strength increases, the hybrid star configurations have smaller maximum masses. For the strongest pairing, r_s(QM)= 0.25, the hybrid stars lie along a plateau in the mass vs density plot, at approximately 1.25 $M_\odot$. In other words, over a large range of densities all the hybrid stars have very similar masses. Though this equation of state is not stiff enough to reproduce observed compact star masses, it does suggest a qualitative explanation of why the most accurately measured compact star masses are all clustered around a value of 1.4 $M_\odot$. In other words, it could be indicative of a phase transition to quark matter, like the one we are exploring here.

Using the Faddeev approach to baryons, we have also studied the effects of including the axial vector diquark channel in the nucleon. Though the scalar diquark accounts for the dominant interaction within the nucleon, the axial vector diquark is also very important in the context of the equation of state. It

shifts the saturation point of the model to a much lower density ($\rho_0 = 0.14$ fm^{-3}) and improves the compressibility somewhat ($K = 426$ MeV). However, a better result emerges once we take into account the self-energy of baryons. For a broad range of values of Σ_N, the compressibility is in agreement with the experimental range ($K \sim 200$ - 300 MeV).

Curiously, the inclusion of pion exchange and axial vector diquarks for the nucleon mass allows a common value of r_s, for the single nucleon and for colour superconducting quark matter, while maintaining a physically reasonable prediction for the phase diagram of QCD. This result has enabled us to use the properties of baryons at zero density to calculate the pairing between quarks operative in the 2SC phase of quark matter. The conclusion is that the scalar pairing strength, $r_s = G_s/G_\pi$, lies approximately within the range 0.2 - 0.3 for two flavour quark matter. We also found that the properties of compact stars have a strong dependence on the magnitude of the pion cloud, through the equation of state for hadronic matter. Clearly, this effect should be taken into account in other finite density calculations that incorporate nucleon structure.

In closing we would like to point out that the results for the properties of nuclear matter and for the properties of hybrid stars are quite reasonable in this model. Indeed, the model has many attractive features. However, the hybrid star configurations will not account for observational data if recent estimates for larger mass X-ray binary candidates are confirmed, or if other larger mass stars are discovered in the future. This remains to be seen, but it is important to recognise that in compact star physics we are dealing with the behaviour of matter at very high densities, far in excess of our experimental limits. Yet all of the physical input we have must be obtained from our knowledge and understanding of nuclei and nucleons from Earthbound experiments. Therefore, we always rely very heavily on the predictive power of models, in producing compact star configurations. With this model we can only hope to provide a rough approximation of the true system. We do not include gluons explicitly and we have implemented the deconfinement transition in an elementary way (switching off the infra-red cut-off). We have also made some pivotal approximations and assumptions along the way, including the mean field approximation and the assumption that the strange quark is too massive to feature in the composition of compact stars. Such issues may be analysed in detail in the future. In fact, there are many ideas which deserve further investigation within the framework of this model. However, the main purpose of this work is to gain insight into the possible working of QCD at extreme densities. Particular points we wish to highlight are the qualitative findings within this model and the possibilities that have become apparent through this study, which may not have been anticipated.

The impact of including the nucleon self-energy is especially striking. This

qualitative behaviour should be relevant for other approaches to the equation of state. The evolution of the phase diagram showed the potential for different types of charge neutral mixed phases. In the transitions from hadronic matter to colour superconducting quark matter we observed an interesting plateau effect in the hybrid star masses, including the possibility of twins (stars which have the same mass, but different density profiles). By using one Lagrangian density to derive the properties of both phases (and using the Faddeev approach to the nucleon), for the first time we have made a connection between the pairing of quarks inside the nucleon and the pairing of quarks in quark matter.

A

Conventions

A.1 Dirac Algebra

The Dirac Matrices are given by,

$$\gamma^\mu = (\gamma^0, \vec{\gamma}), \quad \gamma^0 = \gamma_0 = \begin{pmatrix} \mathbf{1} & 0 \\ 0 & -\mathbf{1} \end{pmatrix}, \quad \vec{\gamma} = \begin{pmatrix} 0 & \vec{\sigma} \\ -\vec{\sigma} & 0 \end{pmatrix}, \quad \gamma^5 = \gamma_5 = \begin{pmatrix} -\mathbf{1} & 0 \\ 0 & \mathbf{1} \end{pmatrix}$$

with $\mathbf{1}$ representing the 2 x 2 unit matrix and $\vec{\sigma} = (\sigma_1, \sigma_2, \sigma_3)$ is defined by the Pauli spin matrices,

$$\sigma_1 = \begin{pmatrix} 0 & 1 \\ 1 & 0 \end{pmatrix}, \quad \sigma_2 = \begin{pmatrix} 0 & -i \\ i & 0 \end{pmatrix}, \quad \sigma_3 = \begin{pmatrix} 1 & 0 \\ 0 & -1 \end{pmatrix}.$$

The matrices for isospin are defined in the usual way,

$$\vec{\tau} = (\tau_1, \tau_2, \tau_3), \quad \tau_\pm = \frac{1}{2}(\tau_1 \pm i\tau_2), \tag{A.1}$$

$$\tau_1 = \begin{pmatrix} 0 & 1 \\ 1 & 0 \end{pmatrix}, \quad \tau_2 = \begin{pmatrix} 0 & -i \\ i & 0 \end{pmatrix}, \quad \tau_3 = \begin{pmatrix} 1 & 0 \\ 0 & -1 \end{pmatrix},$$

The Gell-Mann SU(3) matrices for colour or flavour are given by,

$$\lambda_1 = \begin{pmatrix} 0 & 1 & 0 \\ 1 & 0 & 0 \\ 0 & 0 & 0 \end{pmatrix}, \quad \lambda_2 = \begin{pmatrix} 0 & -i & 0 \\ i & 0 & 0 \\ 0 & 0 & 0 \end{pmatrix}, \quad \lambda_3 = \begin{pmatrix} 1 & 0 & 0 \\ 0 & -1 & 0 \\ 0 & 0 & 0 \end{pmatrix},$$

$$\lambda_4 = \begin{pmatrix} 0 & 0 & 1 \\ 0 & 0 & 0 \\ 1 & 0 & 0 \end{pmatrix}, \quad \lambda_5 = \begin{pmatrix} 0 & 0 & -i \\ 0 & 0 & 0 \\ i & 0 & 0 \end{pmatrix}, \quad \lambda_6 = \begin{pmatrix} 0 & 0 & 0 \\ 0 & 0 & 1 \\ 0 & 1 & 0 \end{pmatrix},$$

$$\lambda_7 = \begin{pmatrix} 0 & 0 & 0 \\ 0 & 0 & -i \\ 0 & i & 0 \end{pmatrix}, \quad \lambda_8 = \frac{1}{\sqrt{3}} \begin{pmatrix} 1 & 0 & 0 \\ 0 & 0 & 0 \\ 0 & 0 & -2 \end{pmatrix},$$

The Gell-mann matrices satisfy the commutation relations $[\lambda_a, \lambda_b] = 2if_{abc}\lambda_c$, where the non-zero permutations of f_{abc} are:

$$f_{123} = 2f_{147} = 2f_{257} = 2f_{345} = -2f_{156} = -2f_{367} = \frac{2}{\sqrt{3}} f_{458} = \frac{2}{\sqrt{3}} f_{678} = 1. \tag{A.2}$$

B

NJL model Derivations

B.1 The Gap Equation

$$\langle\bar{\psi}\psi\rangle = -i\,Tr\,S_F(0) \tag{B.1}$$

$$= -i\,Tr\int\frac{d^4p}{(2\pi)^4}\frac{1}{\not{p}-M+i\epsilon} \tag{B.2}$$

$$= -i\,Tr\int\frac{d^4p}{(2\pi)^4}\frac{\not{p}+M}{\not{p}^2-M^2+i\epsilon} \tag{B.3}$$

$$= -i\,4M\int\frac{d^4p}{(2\pi)^4}\frac{1}{\not{p}^2-M^2+i\epsilon}\ \big(\text{since } Tr(\gamma_\mu)=0 \text{ and } Tr(I)=4\big) \tag{B.4}$$

$$\text{Wick rotation gives } \int_M \to i\int_E \quad \text{and} \quad \not{p}^2 \to -p_E^2 \tag{B.5}$$

$$= \quad 4M\int\frac{d^4p_E}{(2\pi)^4}\frac{1}{-p_E^2-M^2} \tag{B.6}$$

$$= -4M\frac{2\pi^2}{(2\pi)^4}\int_0^\infty dp_E\,p_E^3\,\frac{1}{p_E^2+M^2}\ \text{(using 4D polar coordinates)} \tag{B.7}$$

$$= -\frac{M}{2\pi^2}\int_0^\infty dp_E\,p_E^3\,\frac{1}{p_E^2+M^2} \tag{B.8}$$

$$\text{Use proper time replacement:}\quad \frac{1}{A^n} \to \frac{1}{(n-1)!}\int_{\frac{1}{\Lambda_{UV}^2}}^{\frac{1}{\Lambda_{IR}^2}} d\tau\tau^{n-1}e^{-\tau A} \tag{B.9}$$

$$= -\frac{M}{2\pi^2}\int_0^\infty dp_E\,p_E^3\int_{\frac{1}{\Lambda_{UV}^2}}^{\frac{1}{\Lambda_{IR}^2}} d\tau e^{-\tau(p_E^2+M^2)} \tag{B.10}$$

$$= -\frac{M}{2\pi^2}\int_{\frac{1}{\Lambda_{UV}^2}}^{\frac{1}{\Lambda_{IR}^2}} d\tau\left[e^{-\tau M^2}\int_0^\infty dp_E\,p_E^3\,e^{-\tau p_E^2}\right] \tag{B.11}$$

$$= -\frac{M}{2\pi^2}\int_{\frac{1}{\Lambda_{UV}^2}}^{\frac{1}{\Lambda_{IR}^2}} d\tau\left[e^{-\tau M^2}\frac{1}{2\tau^2}\right]. \tag{B.12}$$

Thus the gap equation for the NJL model in the proper-time regularisation

scheme is given by,

$$M = m_q - 2G_\pi N_c N_F \langle\bar{\psi}\psi\rangle \tag{B.13}$$

$$= m_q + G_\pi N_c N_F \frac{M}{2\pi^2} \int_{\frac{1}{\Lambda_{UV}^2}}^{\frac{1}{\Lambda_{IR}^2}} \frac{d\tau}{\tau^2} e^{-\tau M^2}. \tag{B.14}$$

B.2 Proper Time Derivation of V_{vac}

$$V_{vac} = i\gamma_q \int \frac{d^4k}{(2\pi)^4} ln\left[\frac{k^2 - M^2 + i\epsilon}{k^2 - M_0^2 + i\epsilon}\right] \tag{B.15}$$

$$= -\gamma_q \frac{2\pi^2}{(2\pi)^4} \int_0^\infty dk_E k_E^3 ln\left[\frac{-k_E^2 - M^2}{-k_E^2 - M_0^2}\right] \tag{B.16}$$

$$= -\frac{2\gamma_q}{16\pi^2} \int_0^\infty dk_E k_E^3 \left[ln(k_E^2 + M^2) - ln(k_E^2 + M_0^2)\right] \tag{B.17}$$

$$\text{Use proper time replacement:} \quad ln\, A \to -\int_{\frac{1}{\Lambda_{UV}^2}}^{\frac{1}{\Lambda_{IR}^2}} \frac{d\tau}{\tau} e^{-\tau A} \tag{B.18}$$

$$= -\frac{2\gamma_q}{16\pi^2} \int_0^\infty dk_E k_E^3 \left[-\int_{\frac{1}{\Lambda_{UV}^2}}^{\frac{1}{\Lambda_{IR}^2}} \frac{d\tau}{\tau} \left(e^{-\tau(k_E^2+M^2)} - e^{-\tau(k_E^2+M_0^2)}\right)\right] \tag{B.19}$$

$$= \frac{2\gamma_q}{16\pi^2} \int_{\frac{1}{\Lambda_{UV}^2}}^{\frac{1}{\Lambda_{IR}^2}} \frac{d\tau}{\tau} \left[\left(e^{-\tau M^2} - e^{-\tau M_0^2}\right) \int_0^\infty dk_E k_E^3 e^{-\tau k_E^2}\right] \tag{B.20}$$

$$= \frac{2\gamma_q}{16\pi^2} \int_{\frac{1}{\Lambda_{UV}^2}}^{\frac{1}{\Lambda_{IR}^2}} \frac{d\tau}{2\tau^3} \left(e^{-\tau M^2} - e^{-\tau M_0^2}\right) \tag{B.21}$$

$$= \frac{\gamma_q}{16\pi^2} \left(C_3(M^2) - C_3(M_0^2)\right) \tag{B.22}$$

B.3 The Pion Decay Constant

The pion decay constant, f_π, is defined by the matrix element for pion decay,

$$f_\pi q_\mu = -i < 0|\bar{\psi}(0)\gamma_\mu\gamma_5\psi(0)|\pi(q) > \tag{B.23}$$

$$= -i3\sqrt{g_\pi} \int \frac{d^4k}{(2\pi)^4} Tr[\gamma_5 S(k)\gamma_\mu\gamma_5 S(k-q)] \tag{B.24}$$

$$= -i3\sqrt{g_\pi} \int \frac{d^4k}{(2\pi)^4} Tr\left[\gamma_5 \left(\frac{\not{k} + M}{\not{k}^2 - M^2 + i\epsilon}\right) \gamma_\mu\gamma_5 \left(\frac{\not{k} - \not{q} + M}{(\not{k} - \not{q})^2 - M^2 + i\epsilon}\right)\right]. \tag{B.25}$$

Note that $\gamma_\mu\gamma_5 = -\gamma_5\gamma_\mu$, $\gamma_5^2 = \mathbf{1}$, $Tr[\text{odd } \#\gamma\text{'s}] = 0$ and $Tr[\gamma_\mu\gamma_\nu] = 4g_{\mu\nu}$.

$$Tr[\gamma_5(k^\nu\gamma_\nu + M)\gamma_\mu\gamma_5(k^\nu\gamma_\nu - q^\nu\gamma_\nu + M)] \tag{B.26}$$
$$= Tr[k^\nu\gamma_\nu\gamma_\mu M - M\gamma_\mu(k^\nu\gamma_\nu - q^\nu\gamma_\nu)] \tag{B.27}$$
$$= Tr[M\gamma_\mu\gamma_\nu q^\nu] = M4g_{\mu\nu}q^\nu = 4Mq_\mu. \tag{B.28}$$

Combining this result with Eqn. B.25 we obtain the relation,

$$f_\pi = -12i\sqrt{g_\pi}\int\frac{d^4k}{(2\pi)^4}\frac{M}{\big(k^2 - M^2 + i\epsilon\big)\big((k-q)^2 - M^2 + i\epsilon\big)}. \tag{B.29}$$

The integrand has the form 1/AB and we introduce the Feynman parameter, x, to this expression using the following formula,

$$\frac{1}{AB} = \int_0^1 dx\frac{1}{[xA + (1-x)B]^2}. \tag{B.30}$$

The denominator in Eqn. B.29 becomes,

$$\mathcal{D} = \big[x(k^2 - M^2 + i\epsilon) + (k-q)^2 - M^2 + i\epsilon - x((k-q)^2 - M^2 + i\epsilon)\big]^2 \tag{B.31}$$
$$= \big[k^2 - 2k\cdot q + q^2 - M^2 + i\epsilon + 2k\cdot qx - q^2x\big]^2 \tag{B.32}$$

Performing a shift in the momentum, k $\longrightarrow$ k - xq + q, eliminates the k·q dot products and we obtain,

$$\mathcal{D} = \big[k^2 + q^2(x - x^2) - M^2 + i\epsilon\big]^2. \tag{B.33}$$

Thus the expression for the pion decay constant becomes,

$$f_\pi = -12i\sqrt{g_\pi}M\int\frac{d^4k}{(2\pi)^4}\int_0^1 dx\frac{1}{[k^2 + q^2(x-x^2) - M^2 + i\epsilon]^2} \tag{B.34}$$
$$= 12\sqrt{g_\pi}M\int\frac{d^4k_E}{(2\pi)^4}\int_0^1 dx\frac{1}{[-k_E^2 + q^2(x-x^2) - M^2]^2} \tag{B.35}$$
$$= 12\sqrt{g_\pi}M\frac{2\pi^2}{(2\pi)^4}\int_0^\infty dk_E\int_0^1 dx\frac{k_E^3}{[k_E^2 + q^2(x^2-x) + M^2]^2}. \tag{B.36}$$
Now use the proper-time replacement (Eqn. B.9). (B.37)
$$= \frac{3}{2\pi^2}\sqrt{g_\pi}M\int_0^1 dx\int_{\frac{1}{\Lambda_{UV}^2}}^{\frac{1}{\Lambda_{IR}^2}} d\tau\,\tau\int_0^\infty dk_E\,k_E^3 e^{-\tau(k_E^2 + q^2(x^2-x) + M^2)} \tag{B.38}$$
$$= \frac{3}{2\pi^2}\sqrt{g_\pi}M\int_0^1 dx\int_{\frac{1}{\Lambda_{UV}^2}}^{\frac{1}{\Lambda_{IR}^2}} d\tau\,\tau\left(\frac{1}{2\tau^2}\right)e^{-\tau(q^2(x^2-x) + M^2)} \tag{B.39}$$
$$= \frac{3}{4\pi^2}\sqrt{g_\pi}M\int_0^1 dx\int_{\frac{1}{\Lambda_{UV}^2}}^{\frac{1}{\Lambda_{IR}^2}} d\tau\frac{1}{\tau}e^{-\tau(q^2(x-x^2) + M^2)} \tag{B.40}$$

The remaining integrals over x and τ are solved numerically. The value of g_π is obtained from the expression,

$$g_\pi = \frac{-2}{\partial\Pi_\pi(q^2)/\partial q^2}\Big|_{q^2=M_\pi^2}, \tag{B.41}$$

where the pseudoscalar bubble graph is,

$$\Pi_\pi(k^2) = i\,tr\int\frac{d^4q}{(2\pi)^4}[\gamma_5 S(\not{q})\gamma_5 S(\not{q}-\not{k}))]. \tag{B.42}$$

Applying exactly the same techniques that are used to find the expression for f_π, we obtain,

$$g_\pi^{-1} = \frac{3}{4\pi^2}\int_0^1 dy\int_{\frac{1}{\Lambda_{UV}}}^{\frac{1}{\Lambda_{IR}}} d\tau\left(\frac{1}{\tau} - q^2(y^2-y)\right)e^{-\tau(q^2(y^2-y)+M^2))}, \tag{B.43}$$

where y is a Feynman parameter.

B.4 The Pole Approximation

The form for the couplings g_π, g_s and g_a arises from the pole approximation to the t-matrix. For example, expanding about the pole, $q^2 = M_s^2$, for the scalar channel t-matrix we obtain,

$$\tau_s(q^2) = \frac{4iG_s}{1+2G_s\Pi_s(q^2)} \tag{B.44}$$

$$= 4iG_s - \frac{8iG_s^2\Pi_s(q^2)}{1+2G_s\Pi_s(q^2)} \tag{B.45}$$

$$= 4iG_s - \frac{8iG_s^2\Pi_s(q^2)}{1+2G_s\left[\Pi_s(M_s^2) + (q^2-M_s^2)\,\frac{\partial\Pi_s(q^2)}{\partial q^2}\Big|_{q^2=M_s^2} + \ldots\right]} \tag{B.46}$$

$$= 4iG_s - \frac{8iG_s^2\Pi_s(q^2)}{2G_s(q^2-M_s^2)\,\frac{\partial\Pi_s(q^2)}{\partial q^2}\Big|_{q^2=M_s^2} + \ldots}. \tag{B.47}$$

Near the pole, $\Pi_s(q^2) \approx -1/2G_s$ and we may approximate the t-matrix as,

$$\tau_s(q^2) \approx 4iG_s - \frac{ig_s}{(q^2-M_s^2)}, \tag{B.48}$$

where we have defined,

$$g_s = \frac{-2}{\frac{\partial\Pi_s(q^2)}{\partial q^2}}\Bigg|_{q^2=M_s^2}. \tag{B.49}$$

C

The Faddeev Approach to Baryons

C.1 The quark - scalar-diquark model

The bubble graph for a quark - scalar diquark system is given by,

$$\Pi_N(p) = \int \frac{d^4k}{(2\pi)^4} S(\not{k})\tau_s(\not{p}-\not{k}) \tag{C.1}$$

$$= \int \frac{d^4k}{(2\pi)^4}\left[\left(\frac{\not{k}+M}{\not{k}^2-M^2+i\epsilon}\right)\left(4iG_s - \frac{ig_s}{(\not{p}-\not{k})^2-M_s^2+i\epsilon}\right)\right] \tag{C.2}$$

$$= \int \frac{d^4k}{(2\pi)^4}\left[\frac{4iG_sM}{\not{k}^2-M^2+i\epsilon} - \frac{ig_s(\not{k}+M)}{(\not{k}^2-M^2+i\epsilon)((\not{p}-\not{k})^2-M_s^2+i\epsilon)}\right] \tag{C.3}$$

Using the proper-time prescription given in Eqn. B.9 the first term simplifies to,

$$\frac{1}{4\pi^2}\int_{\frac{1}{\Lambda_{UV}}}^{\frac{1}{\Lambda_{IR}}} d\tau \frac{G_sM}{\tau^2} e^{-\tau(M^2)}. \tag{C.4}$$

For the second term in Eqn. C.3 we introduce a Feynman parameter, x. Using Eqn. B.30, the denominator can be expressed as,

$$\mathcal{D} = [x((\not{p}-\not{k})^2 - M_s^2 + i\epsilon) + (1-x)(\not{k}^2 - M^2 + i\epsilon)]^2 \tag{C.5}$$

$$= [\not{p}^2x - 2\not{p}\cdot\not{k}x + (M^2-M_s^2)x + \not{k}^2 - M^2 + i\epsilon]^2 \tag{C.6}$$

Shifting $\not{k} \longrightarrow \not{k} + \not{p}x$, we obtain,

$$\mathcal{D} = [\not{k}^2 - M^2 + (M^2-M_s^2)x + p^2x(1-x) + i\epsilon]^2 \tag{C.7}$$

and the second term in Eqn. C.3 simplfies to,

$$\int \frac{d^4k}{(2\pi)^4}\int_0^1 dx \frac{-ig_s(\not{p}x+M)}{[\not{k}^2 - M^2 + (M^2-M_s^2)x + p^2x(1-x) + i\epsilon]^2} \tag{C.8}$$

$$= \int \frac{d^4k_E}{(2\pi)^4}\int_0^1 dx \frac{g_s(\not{p}x+M)}{[k_E^2 + M^2 + (M_s^2-M^2)x + p^2x(x-1)]^2} \tag{C.9}$$

Integrating this using the proper-time prescription (Eqn. B.9), and combining the result with Eqn. C.4, we obtain an expression for the bubble graph, of the form,

$$\Pi_N(p) = a_1 + \frac{\not{p}}{M} a_2. \tag{C.10}$$

The factors a_1 and a_2 are given by,

$$a_1 = \frac{1}{16\pi^2} \int_{\frac{1}{\Lambda_{UV}}}^{\frac{1}{\Lambda_{IR}}} d\tau \left[\frac{4G_s M}{\tau^2} e^{-\tau M^2} + \frac{g_s M}{\tau} \int_0^1 dx e^{-\tau A} \right] \tag{C.11}$$

$$a_2 = \frac{g_s M}{16\pi^2} \int_{\frac{1}{\Lambda_{UV}}}^{\frac{1}{\Lambda_{IR}}} d\tau \int_0^1 dx \frac{x}{\tau} e^{-\tau A} \tag{C.12}$$

where A $= M^2 + (M_s^2 - M^2)x + p^2 x(x-1)$. Thus the Faddeev equation for the quark - scalar-diquark model of the nucleon is given by,

$$\Gamma(p) = Z\, \Pi_N(p)\Gamma(p) = \frac{12}{M}(a_1 + \frac{\not{p}}{M} a_2)\Gamma(p), \tag{C.13}$$

where Z is the quark exchange kernel in the static approximation and Γ(p) is the vertex function of the nucleon. The nucleon mass is the solution to,

$$\frac{12}{M}(a_1 + \frac{M_N}{M} a_2) = 1 \tag{C.14}$$

for which $\not{p}^2 = M_N^2$.

C.2 Axial Vector Diquarks

The Bethe-Salpeter equation for the axial vector diquark is given by,

$$1 + 2G_a \Pi_a(\not{k}^2 = M_a^2) = 0, \tag{C.15}$$

which corresponds to the pole in the t-matrix. In order to solve for G_a and M_a, we require a second constraint to combine with this equation. We use the Faddeev equation for the Δ^{++} for this purpose.

C.3 The quark - diquark model of the Δ^{++}

The Faddeev equation for the Δ^{++} requires that

$$K^{\mu\nu}\Gamma_\nu = \Gamma^\mu, \tag{C.16}$$

where the kernel, $K^{\mu\nu} = Z^{\mu}_{\ \rho}\Pi^{\rho\nu}$, is given by,

$$K^{\mu\nu}(p) = \frac{6}{M}\gamma^{\mu}\gamma_{\rho}\int\frac{d^4k}{(2\pi)^4}\tau_a^{\rho\nu}(\not{p}-\not{k})S(\not{k}). \tag{C.17}$$

The quark propagator is S($\not{k}$)=1/($\not{k}$-M+iϵ) and the axial vector t-matrix is given by [163],

$$\tau_a^{\rho\mu}(k) = 4iG_a\left[g^{\mu\nu} - \frac{2G_a\Pi_a(k^2)}{1+2G_a\Pi_a(k^2)}\left(g^{\mu\nu}-\frac{k^{\mu}k^{\nu}}{k^2}\right)\right]. \tag{C.18}$$

The bubble graph is determined by,

$$\Pi_a(k^2)\left(g^{\mu\nu}-\frac{k^{\mu}k^{\nu}}{k^2}\right) = 6i\int\frac{d^4k}{(2\pi)^4}Tr[\gamma^{\mu}S(q)\gamma^{\nu}S(k+q)]. \tag{C.19}$$

After performing the trace and applying proper-time regularisation, this expression is used to obtain the kernel for the Δ^{++},

$$K^{\mu\nu}(p) = \frac{6}{M}\gamma^{\mu}\gamma_{\rho}g^{\rho\nu}(b_1+\frac{\not{p}}{M}b_2). \tag{C.20}$$

This leads to the requirement for G_a (with $\not{p}^2 = M_{\Delta}^2$),

$$\frac{12}{M}(b_1+\frac{\not{p}}{M}b_2) = 1, \tag{C.21}$$

where b_1 and b_2 are defined by,

$$b_1 = \frac{1}{16\pi^2}\int_{\frac{1}{\Lambda_{UV}}}^{\frac{1}{\Lambda_{IR}}}d\tau\Big[\frac{4G_aM}{\tau^2}e^{-\tau M^2} + g_aM\int_0^1 dx\frac{e^{-\tau B}}{\tau}\Big] \tag{C.22}$$

$$b_2 = \frac{g_aM}{16\pi^2}\int_{\frac{1}{\Lambda_{UV}}}^{\frac{1}{\Lambda_{IR}}}d\tau\int_0^1 dx\frac{x}{\tau}e^{-\tau B}, \tag{C.23}$$

$$\tag{C.24}$$

and we define $B = M^2+(M_a^2-M^2)x+p^2x(x-1))$. We use Eqns. C.15 and C.21 to solve for M_a and G_a in the Δ^{++} system.

C.4 The Two - Channel Faddeev Equation

Including both the scalar and axial vector channels in the nucleon, the Faddeev equation can be written as,

$$\Gamma^a(p) = K^{ab}(p)\Gamma^b(p) = Z^a_{\ a'}\Pi^{a'b}(p)\Gamma^b(p), \tag{C.25}$$

where the quark exchange kernel is given by,

$$Z^{a}{}_{a'} = \frac{3}{M}\begin{pmatrix} 1 & \sqrt{3}\gamma_5\gamma^\mu \\ \sqrt{3}\gamma_\nu\gamma_5 & -\gamma_\nu\gamma^\mu \end{pmatrix} \tag{C.26}$$

and the nucleon bubble graph is given by,

$$\begin{aligned} \Pi_N^{a'b}(p) &= \int \frac{d^4k}{(2\pi)^4}\tau^{a'b}(p-k)S(k) && \text{(C.27)} \\ &= \int \frac{d^4k}{(2\pi)^4}\begin{pmatrix} \tau_s(p-k) & 0 \\ 0 & \tau_a^{\mu\nu}(p-k) \end{pmatrix} S(k) && \text{(C.28)} \\ &= \begin{pmatrix} a_1 + \frac{\not{p}}{M}a_2 & 0 \\ 0 & b_1 + \frac{\not{p}}{M}b_2 \end{pmatrix} && \text{(C.29)} \end{aligned}$$

using the results obtained in Eqns. C.10 and C.20. Thus the Faddeev equation requires that,

$$\Gamma^a(p) = \frac{3}{M}\begin{pmatrix} 1 & \sqrt{3}\gamma_5\gamma^\mu \\ \sqrt{3}\gamma_\nu\gamma_5 & -\gamma_\nu\gamma^\mu \end{pmatrix}\begin{pmatrix} a_1 + \frac{\not{p}}{M}a_2 & 0 \\ 0 & b_1 + \frac{\not{p}}{M}b_2 \end{pmatrix}\Gamma^b(p), \tag{C.30}$$

where $\Gamma^a = (\Gamma_N^5, \Gamma_N^\mu)$. The scalar component of the vertex function has the form,

$$\Gamma_N^5(p,s) = \beta_1 u_N(p,s), \tag{C.31}$$

where β_1 is an unknown coefficient and $u_N(p,s)$ is a Dirac spinor, with spin projection s, normalised according to $\bar{u}_N u_N = 1$. The axial vector component of the vertex function is given by,

$$\Gamma_N^\mu(p,s) = \beta_2\frac{p^\mu}{M}u_N(p,s) + \beta_3\gamma^\mu\gamma_5 u_N(p,s). \tag{C.32}$$

Therefore, Eqn. C.30 (the Faddeev equation) can be expressed as,

$$\begin{aligned} &\begin{pmatrix} \beta_1 \\ \beta_2\frac{p^\mu}{M} + \beta_3\gamma^\mu\gamma_5 \end{pmatrix} u_N(p,s) && \text{(C.33)} \\ &= \frac{3}{M}\begin{pmatrix} \beta_1(a_1 + \frac{\not{p}}{M}a_2) + \sqrt{3}\gamma_\nu\gamma_5(b_1 + \frac{\not{p}}{M}b_2)(\beta_2\frac{p^\mu}{M} + \beta_3\gamma^\mu\gamma_5) \\ \sqrt{3}\gamma_\nu\gamma_5(b_1 + \frac{\not{p}}{M}b_2)\beta_1 - \gamma_\nu\gamma^\mu(b_1 + \frac{\not{p}}{M}b_2)(\beta_2\frac{p^\mu}{M} + \beta_3\gamma^\mu\gamma_5) \end{pmatrix} u_N(p,s) && \text{(C.34)} \\ &= \frac{3}{M}\begin{pmatrix} X_1 \\ (X_2)\frac{p^\mu}{M} + (X_3)\gamma^\mu\gamma_5 \end{pmatrix} u_N(p,s). && \text{(C.35)} \end{aligned}$$

This yields three equations for the coefficients β_1, β_2 and β_3,

$$\beta_1 = \frac{3}{M}[X_1] = \frac{3}{M}[\beta_1(a_1 + \frac{M_N}{M}a_2) + \sqrt{3}\gamma_\nu\gamma_5(b_1 + \frac{M_N}{M}b_2)(\beta_2\frac{p^\mu}{M} + \beta_3\gamma^\mu\gamma_5)] \quad \text{(C.36)}$$

$$\beta_2 = \frac{3}{M}[X_2] = \frac{3}{M}[-2\beta_2(b_1 - \frac{M_N}{M}b_2) - 4\beta_3\frac{M_N}{M}b_2] \quad \text{(C.37)}$$

$$\beta_3 = \frac{3}{M}[X_3] = \frac{3}{M}[-\beta_1\sqrt{3}(a_1 + \frac{M_N}{M}a_2) - \beta_2(b_1 - \frac{M_N}{M}b_2) + 2\beta_3 b_1]. \quad \text{(C.38)}$$

These three equations can be expressed in matrix form,

$$\begin{pmatrix} M_{11} & M_{12} & M_{13} \\ M_{21} & M_{22} & M_{23} \\ M_{31} & M_{32} & M_{33} \end{pmatrix} \begin{pmatrix} \beta_1 \\ \beta_2 \\ \beta_3 \end{pmatrix} = M(p^2) \begin{pmatrix} \beta_1 \\ \beta_2 \\ \beta_3 \end{pmatrix} = 0.$$

The nucleon mass is then determined by the condition $det\ [M(p^2 = M_N^2)] = 0$.

D

Hadronization

Here we show how the NJL lagrangian density for quarks (Eqn. 3.14) is translated into a theory of mesons and baryons, using the path integral formalism.

D.1 Functional Integration

Since quantum field theory was developed to a large extent in analogy with the theories of thermodynamics and statistical mechanics, there are considerable similarities in the terminology and notation. In analogy with the partition function of statistical mechanics the generating functional for the NJL model is denoted,

$$Z[\psi,\bar{\psi}] = \mathcal{N}\int \mathcal{D}\bar{\psi}\mathcal{D}\psi \;\; exp\left[i\int d^4x\, \mathcal{L}_{NJL}\right], \tag{D.1}$$

where $\bar{\psi}$ and ψ are the quark fields and $\mathcal{N}$ is a normalization factor which does not influence the outcome of the method, but is included here for completeness. Note that after Fierz transformation the interaction part of the Lagrangian density ($\mathcal{L}_{NJL} = \mathcal{L}_0 + \mathcal{L}_{int}$) can be written as a sum of mesonic and diquark interaction channels,

$$\mathcal{L}_{int} = G_\alpha(\bar{\psi}M_\alpha\psi)(\bar{\psi}M^\alpha\psi) + H_\alpha(\bar{\psi}D_\alpha\bar{\psi})(\psi D^\alpha\psi), \tag{D.2}$$

where M_α are the gamma matrices associated with the mesonic interactions and D_α are the gamma matrices associated with diquark interactions and G_α and H_α are the corresponding coupling constants. These quantities appear in Eqn (3.14) where the gamma matrices are given explicitly as,

$$M^\alpha = \mathbf{1}, \gamma_5\tau_i, \gamma^\mu, \gamma^\mu\tau_i, \tag{D.3}$$

$$D_\alpha = \gamma_5 C\tau_2\beta^A,\ \gamma_\mu C\tau_i\tau_2\beta^A, \tag{D.4}$$

corresponding to the scalar, psuedoscalar, vector, pseudovector, scalar diquark and axial vector diquark channels respectively. At this stage the model is defined purely in terms of quarks and their interactions. In order to reformulate the model in terms of physical meson and baryon fields we introduce colourless

auxiliary quark - anti-quark and three-quark fields, θ^α and N^α, as well as colour-antisymmetric fields for diquarks, χ^α. We define the meson fields such that they satisfy the relation,

$$\begin{aligned}\mathbf{1} &= \int \prod_\alpha \mathcal{D}\varphi_\alpha \, \delta(\varphi_\alpha - \bar{\psi} M_\alpha \psi) \\ &= \int \prod_\alpha \mathcal{D}\varphi_\alpha \mathcal{D}\theta_\alpha \;\; exp\left[i \int d^4x \;\; \theta^\alpha(x) \;\left(\varphi_\alpha(x) - \bar{\psi}(x) M_\alpha \psi(x)\right)\right], \end{aligned} \tag{D.5}$$

where we have introduced additional auxiliary fields for the mesons, φ_α. As will become clear, the purpose of introducing these fields is to assist in eliminating quark fields from the Lagrangian density through the process of functional integration. Introducing the diquark auxiliary fields, Δ_α, we define a similar relation for the diquarks,

$$\begin{aligned}\mathbf{1} &= \int \prod_\alpha \mathcal{D}\chi_\alpha \mathcal{D}\chi^*_\alpha \, \delta\Big(\chi^{\alpha *} - (\bar{\psi} D^\alpha \bar{\psi})\Big) \, \delta\Big(\chi^\alpha - (\psi D^\alpha \psi)\Big) \\ &= \int \prod_\alpha \mathcal{D}\chi_\alpha \mathcal{D}\chi^*_\alpha \mathcal{D}\Delta_\alpha \mathcal{D}\Delta^*_\alpha \\ &\exp\left[\frac{i}{2} \int d^4X \left(\chi^{\alpha *}(X) - \bar{\psi}(X) D^\alpha \bar{\psi}(X)\right) \Delta_\alpha(X) \right. \\ &\qquad \left. + \Delta^*_\alpha(X) \Big(\chi^\alpha(X) - \psi(X) D^\alpha \psi(X)\Big) \right], \end{aligned} \tag{D.6}$$

where χ^* is the complex conjugate of χ and Δ^* is the complex conjugate of Δ. Finally, the baryon field $N^\alpha(x, X)$ is defined as a colourless combination of a quark and a diquark such that,

$$\begin{aligned}\mathbf{1} &= \int \prod_\alpha \mathcal{D}N^\alpha \mathcal{D}\bar{N}^\alpha \;\; \delta\Big(\bar{N}^\alpha - \bar{\psi}(\bar{\psi} D^\alpha \bar{\psi})\Big) \, \delta\Big(N^\alpha - (\psi D^\alpha \psi)\psi\Big) \\ &= \int \prod_\alpha \mathcal{D}N^\alpha \mathcal{D}\bar{N}^\alpha \mathcal{D}\Phi^\alpha \mathcal{D}\bar{\Phi}^\alpha \\ &exp\left[i \int d^4x d^4X \left(\Big(\bar{N}^\alpha_\mu(x, X) - \bar{\psi}_\mu(x)\big(\bar{\psi}(X) D^\alpha \bar{\psi}(X)\big)\Big) \Phi^\mu_\alpha(x, X) \right. \right. \\ &\qquad \left. \left. + \bar{\Phi}^\mu_\alpha(x, X) \Big(N^\alpha_\mu(x, X) - \big(\psi(X) D^\alpha \psi(X)\big)\psi_\mu(x)\Big) \right) \right]. \end{aligned} \tag{D.7}$$

Note that φ, θ, Δ and χ are bose fields, while N and Φ are fermion fields. Inserting Eqn. D.5 into the generating functional, $Z[\psi, \bar{\psi}]$, and making use of

the δ function in Eqn. D.5 we obtain,

$$Z = \mathcal{N} \int \mathcal{D}\bar{\psi}\mathcal{D}\psi\mathcal{D}\varphi\mathcal{D}\theta \; exp\left[i \int \; \mathcal{L}_0 + H_\alpha(\bar{\psi}D_\alpha\bar{\psi})(\psi D^\alpha\psi)\right] \\ .exp\left[i \int \; G_\alpha(\varphi_\alpha\varphi^\alpha) + \theta^\alpha\varphi_\alpha - \bar{\psi}\theta^\alpha M_\alpha\psi\right], \qquad \text{(D.8)}$$

where the notation is condensed here, so that $\int \; d^4x \; \rightarrow \; \int$ and the x-dependence of the fields is not shown explicitly (i.e. $\theta = \theta(x)$ etc). We use Eqns D.6 and D.7 to eliminate the remaining terms that are higher than second order in the quark fields. The resulting generating functional is given by,

$$Z = \mathcal{N} \int \mathcal{D}\bar{\psi}\mathcal{D}\psi\mathcal{D}\varphi\mathcal{D}\theta\mathcal{D}\chi^*\mathcal{D}\chi\mathcal{D}\Delta^*\mathcal{D}\Delta\mathcal{D}\bar{N}\mathcal{D}N\mathcal{D}\bar{\Phi}\mathcal{D}\Phi \\ exp\left[i \int \; \mathcal{L}_0 + G_\alpha(\varphi_\alpha\varphi^\alpha) + \theta^\alpha\varphi_\alpha - \bar{\psi}\theta^\alpha M_\alpha\psi\right] \\ exp\left[i \int \; H_\alpha(\chi^*_\alpha\chi^\alpha) + \frac{1}{2}(\chi^*_\alpha\Delta^\alpha + \Delta^*_\alpha\chi^\alpha) - \frac{1}{2}(\bar{\psi}D_\alpha\Delta^\alpha\bar{\psi} + \psi\Delta^*_\alpha D^\alpha\psi)\right] \\ exp\Bigg[i \int d^4x\, d^4X \Big(\bar{N}_\alpha(x,X)\Phi^\alpha(x,X) + \bar{\Phi}_\alpha(x,X)N^\alpha(x,X)\Big) \\ - \Big(\bar{\psi}(x)\chi^*_\alpha(X)\Phi^\alpha(x,X) + \bar{\Phi}_\alpha(x,X)\chi^\alpha(X)\psi(x)\Big)\Bigg]. \qquad \text{(D.9)}$$

The path integral of a Gaussian function may be performed exactly through the relation,

$$\int \mathcal{D}\phi \; exp\left[i \int d^4x \; (\pm A\phi - B\phi^2)\right] = \mathcal{N}' \, exp\left[i \int d^4x \; \frac{A^2}{4B}\right]. \qquad \text{(D.10)}$$

In this way the auxiliary fields φ, χ and χ^* are integrated out, where we use the fact that $\chi^*\chi = (\chi^{*2} + \chi^2)/2$, for the complex conjugate fields. The generating

functional becomes,

$$
\begin{aligned}
Z = \mathcal{N} \int & \mathcal{D}\bar{\psi}\mathcal{D}\psi\mathcal{D}\theta\mathcal{D}\Delta^*\mathcal{D}\Delta\mathcal{D}\bar{N}\mathcal{D}N\mathcal{D}\bar{\Phi}\mathcal{D}\Phi \\
& exp\left[i \int d^4x\, \bar{\psi}\Big(i\partial\!\!\!/ - m - \theta^\alpha M_\alpha - \frac{1}{2}(D_\alpha\Delta^\alpha + \Delta^*_\alpha D^\alpha)\Big)\psi \right] \\
& exp\left[i \int d^4x\, \frac{1}{4G_\alpha}\theta_\alpha\theta^\alpha \right] \\
& exp\Bigg[i \int d^4X\, \frac{1}{4H_\alpha}\Big(\Delta^*_\alpha(X) - 2\int d^4x\, \bar{\Phi}_\alpha(x,X)\psi(x)\Big) \\
& \qquad\qquad \Big(\Delta^\alpha(X) - 2\int d^4y\, \Phi^\alpha(y,X)\bar{\psi}(y)\Big)\Bigg] \\
& exp\left[i \int d^4x\, d^4X \Big(\bar{N}_\alpha(x,X)\Phi^\alpha(x,X) + \bar{\Phi}_\alpha(x,X)N^\alpha(x,X)\Big)\right]. \qquad \text{(D.11)}
\end{aligned}
$$

Integrating over the quark fields gives rise to a "trace-log" term in the generating functional through the Nambu-Gorkov formula,

$$
\int \mathcal{D}\bar{\psi}\mathcal{D}\psi \;\; exp(i[\bar{\psi}S^{-1}\psi + \bar{\psi}\xi + \bar{\xi}\psi]) = exp(i[-iTr\, lnS^{-1} + \bar{\xi}S\xi]). \qquad \text{(D.12)}
$$

Integrating over the diquark and nucleon auxiliary fields (using Eqn. D.12) the fully hadronised generating functional has the form,

$$
Z = \mathcal{N} \int \mathcal{D}\theta\mathcal{D}\Delta\mathcal{D}\Delta^*\mathcal{D}\Phi\mathcal{D}\bar{\Phi} \;\; exp\left(S_{eff}[\theta,\Delta,\Delta^*,N,\bar{N}]\right) + i(\bar{\Phi}N + \bar{N}\Phi), \quad \text{(D.13)}
$$

where the effective action is given by,

$$
\begin{aligned}
S_{eff} = & -i\,(Tr\, ln\, S_0^{-1} - Tr\, ln\, D_0^{-1} - Tr\, ln\, \mathcal{M}_0^{-1} - Tr\, ln\, G_N^{-1}) \\
& + \bar{N}G_N N + \int d^4x \left[\frac{1}{4G_\alpha}\theta_\alpha\theta^\alpha + \frac{1}{4H_\alpha}\Delta^*_\alpha\Delta^\alpha \right]. \qquad \text{(D.14)}
\end{aligned}
$$

Neglecting the "trace-log" terms for the diquarks and the mesons which correspond to vacuum loop diagrams (ring contributions) the effective action for our model simplifies to (see Ref. [12]),

$$
\begin{aligned}
S_{eff} = & -i\,(Tr\, ln\, S_0^{-1} - Tr\, ln\, G_N^{-1}) \\
& + \bar{N}G_N N + \int d^4x \left[-\frac{(\Sigma^2+\pi^2)}{4G_\pi} + \frac{\omega^2}{4G_\omega} + \frac{\rho^2}{4G_\rho} \right], \qquad \text{(D.15)}
\end{aligned}
$$

where we have substituted the scalar, pseudoscalar, vector and pseudovector meson fields (i.e. $\theta^\alpha \rightarrow \Sigma, \pi, \omega$ and ρ) which are determined within the mean field approximation, as explained in the text.

E

Quark Matter Derivations

E.1 Effective Potential

The NJL Lagrangian density is given by Eqns. (3.14)-(3.18). In quark matter the terms associated with meson exchange and axial vector diquark condensation are zero. Using Nambu-Gorkov formalism [175,176], the quark fields are written as,

$$\Psi = \frac{1}{\sqrt{2}} \begin{pmatrix} \psi \\ C\tau_2 \bar{\psi}^T \end{pmatrix}, \quad \bar{\Psi} = \frac{1}{\sqrt{2}} \begin{pmatrix} \bar{\psi}, & -\psi^T \tau_2 C^{-1} \end{pmatrix},$$

where $C = i\gamma_0\gamma_2$. Introducing the quark and isospin chemical potentials, $\mu_q = (\mu_u + \mu_d)/2$ and $\mu_I = (\mu_u - \mu_d)/2$, for quark matter, it is sufficient to use the Lagrangian density,

$$\mathcal{L} = \bar{\Psi}(i\partial\!\!\!/ - m + \gamma_0\sigma_3\mu_q + \gamma_0\tau_3\mu_I)\Psi + G_\pi(\bar{\Psi}\Psi)^2 + G_s(\bar{\Psi}i\gamma_5\sigma_1\beta_1\Psi)^2. \quad \text{(E.1)}$$

To obtain the effective action one may use the functional integration techniques outlined in Appendix D. An equivalent procedure is to subtract terms of the form,

$$(2G_\alpha\bar{\Psi}\Gamma_\alpha\Psi + b_\alpha)^2/4G_\alpha, \quad \text{(E.2)}$$

which are equal to zero, since we require that the auxiliary fields, b_α, satisfy the constraints $\partial\mathcal{L}/b_\alpha = 0$. In this way the 4-fermi interaction terms are eliminated from Eqn. (E.1). In particular, by subtracting

$$(2G_\pi\bar{\Psi}\Psi + \Sigma)^2/4G_\pi \quad \text{and} \quad (2G_s\bar{\Psi}i\gamma_5\sigma_1\beta_1\Psi + \hat{\Delta})^2/4G_s, \quad \text{(E.3)}$$

the Lagrangian density simplifies to,

$$\mathcal{L} = \bar{\Psi}(i\partial\!\!\!/ - m + \gamma_0\sigma_3\mu_q + \gamma_0\tau_3\mu_I - \Sigma - i\gamma_5\sigma_1\beta_1\hat{\Delta})\Psi - \frac{\Sigma^2}{4G_\pi} - \frac{\hat{\Delta}^2}{4G_s} \quad \text{(E.4)}$$

$$\equiv \bar{\Psi}S^{-1}\Psi - \frac{(M-m)^2}{4G_\pi} - \frac{\hat{\Delta}^2}{4G_s}. \quad \text{(E.5)}$$

Taking into account the Dirac structure, colour, flavour and Nambu-Gorkov components, S^{-1} is a 48×48 matrix. Integrating over the quark fields gives rise

to the usual trace log term in the effective action (where the trace has to be evaluated over each component of the 48 dimensional space),

$$S_{eff} = -\frac{i}{2} Tr\ ln\ S^{-1} - \int d^4x \left[\frac{(M-m)^2}{4G_\pi} + \frac{\hat{\Delta}^2}{4G_s} \right]. \tag{E.6}$$

Note that the effective potential satisfies the expression, $S_{eff} = -\int\ d^4x\ V$. Thus the quark loop term is given by,

$$V_l = \frac{i}{2} \int \frac{d^4p}{(2\pi)^4} Tr\ ln\ S^{-1} \tag{E.7}$$

$$= \frac{i}{2} \int \frac{d^4p}{(2\pi)^4} Tr\ ln\ \left[\not{p} - M + \gamma_0(\sigma_3\mu_q + \tau_3\mu_I) - i\gamma_5\sigma_1\beta_1\hat{\Delta} \right]. \tag{E.8}$$

Using σ_1 and σ_3 as defined in Appendix A,

$$V_l = \frac{i}{2} \int \frac{d^4p}{(2\pi)^4} Tr\ ln \begin{bmatrix} \not{p} - M + \gamma_0(\mu_q + \tau_3\mu_I) & -i\gamma_5\beta_1\hat{\Delta} \\ -i\gamma_5\beta_1\hat{\Delta} & \not{p} - M - \gamma_0(\mu_q - \tau_3\mu_I) \end{bmatrix}. \tag{E.9}$$

We simplify this expression using the relation,

$$Tr\, ln \begin{pmatrix} A & B \\ C & D \end{pmatrix} = Tr\, ln(-BC + BDB^{-1}A). \tag{E.10}$$

Note that $\beta_1^2 = 3/2\ diag(0,1,1) = 3/2\ C_1$ and we define $\Delta = \sqrt{3/2}\ \hat{\Delta}$. For the integrand we obtain,

$$Tr\ ln\left[\Delta^2 C_1 + (-\not{p} - M + \gamma_0(\mu_q - \tau_3\mu_I))\,(\not{p} - M + \gamma_0(\mu_q + \tau_3\mu_I))\right] \tag{E.11}$$

$$= Tr\ ln\ [\Delta^2 C_1 - \not{p}^2 + M^2 + \mu_q^2 - \mu_I^2 - \mu_q(\not{p}\gamma_0 - \gamma_0\not{p}) - \tau_3\mu_I(\not{p}\gamma_0 + \gamma_0\not{p}) - 2M\gamma_0\mu_q] \tag{E.12}$$

$$= Tr\ ln\ [\Delta^2 C_1 - \not{p}^2 + M^2 + \mu_q^2 - \mu_I^2 - \mu_q(-2\gamma^3\gamma_0 p^3) - \tau_3\mu_I(2p_0) - 2M\gamma_0\mu_q] \tag{E.13}$$

where we have used $\not{p}\gamma_0 - \gamma_0\not{p} = -2\gamma^3\gamma_0 p^3$ and $\not{p}\gamma_0 + \gamma_0\not{p} = 2p_0$. Note that $\not{p}^2 = p^2 = {p_0}^2 - \vec{p}^{\,2}$. Taking $\vec{p} = (0,0,p)$ we have,

$$Tr\ ln\ [\Delta^2 C_1 - p_0^2 + p^2 + M^2 + \mu_q^2 - \mu_I^2 + 2\mu_q\gamma^3\gamma_0 p - 2\tau_3\mu_I p_0 - 2M\gamma_0\mu_q]. \tag{E.14}$$

The trace over isospin is simplified by the relation,

$$Tr_I\ ln \begin{bmatrix} a+b & 0 \\ 0 & a-b \end{bmatrix} = ln\ Det_I \begin{bmatrix} a+b & 0 \\ 0 & a-b \end{bmatrix} = ln\ (a^2 - b^2). \tag{E.15}$$

In this case,

$$a = \Delta^2 C_1 - (p_0^2 + \mu_I^2) + p^2 + M^2 + \mu_q^2 + 2\mu_q \gamma^3 \gamma_0 p - 2M\gamma_0 \mu_q, \tag{E.16}$$
$$b = -2\mu_I p_0 \tag{E.17}$$

and the integrand for Eqn. (E.9) becomes,

$$\begin{aligned} &Tr\ ln\left[\Delta^2 C_1 - (p_0 + \mu_I)^2 + E_p^2 + \mu_q^2 + 2\mu_q(p\gamma^3\gamma_0 - M\gamma_0)\right] \\ &+\ Tr\ ln\left[\Delta^2 C_1 - (p_0 - \mu_I)^2 + E_p^2 + \mu_q^2 + 2\mu_q(p\gamma^3\gamma_0 - M\gamma_0)\right], \end{aligned} \tag{E.18}$$

where $E_p = \sqrt{p^2 + M^2}$. Finally, using the explicit representations for γ_0 and γ^3 given in Appendix A and using $C_1 = diag(0, 1, 1)$, it is straightforward to take the trace over Dirac and colour space. We get a factor of 2 from the Dirac trace and Eqn. (E.18) reduces to,

$$\begin{aligned} &2\,Tr_c\ ln\left[(\Delta^2 C_1 - (p_0 + \mu_I)^2 + E_p^2 + \mu_q^2)^2 - 4E_p^2\mu_q^2\right] \ +\ (\mu_I \to -\mu_I)\text{ term} \\ &\quad = -\,2\left[2\ ln\left((p_0 + \mu_I)^2 - (E_p + \mu_q)^2 - \Delta^2\right)\right. \\ &\qquad + 2\ ln\left((p_0 + \mu_I)^2 - (E_p - \mu_q)^2 - \Delta^2\right) \\ &\qquad + ln\left((p_0 + \mu_I)^2 - (E_p + \mu_q)^2\right) \\ &\qquad \left. + ln\left((p_0 + \mu_I)^2 - (E_p - \mu_q)^2\right)\right] \\ &\qquad + (\mu_I \to -\mu_I)\text{ terms.} \end{aligned} \tag{E.19}$$

The four $(\mu_I \to -\mu_I)$ terms come from the second term in Eqn. (E.18). Defining $\varepsilon_\pm(p) = \sqrt{(E_p \pm \mu_q)^2 + \Delta^2}$ and $E_\pm = |E_p \pm \mu_q|$, this expression can be written in a more compact form. Note that,

$$ln\left[(p_0 + \mu_I)^2 - \varepsilon_+^2\right] + ln\left[(p_0 - \mu_I)^2 - \varepsilon_+^2\right] \tag{E.20}$$
$$= ln\left[(p_0 + \mu_I + \varepsilon_+)(p_0 + \mu_I - \varepsilon_+)(p_0 - \mu_I + \varepsilon_+)(p_0 - \mu_I - \varepsilon_+)\right] \tag{E.21}$$
$$= ln\left[p_0^2 - (\varepsilon_+ + \mu_I)^2\right] + ln\left[p_0^2 - (\varepsilon_+ - \mu_I)^2\right], \tag{E.22}$$

so we may rearrange the terms to obtain,

$$V_l = i\int\frac{d^4p}{(2\pi)^4}\sum_{\alpha=\pm}\Bigg[2\,ln\,(p_0^2-(\varepsilon_\pm+\mu_I)^2)+2\,ln\,(p_0^2-(\varepsilon_\pm-\mu_I)^2) + ln\,(p_0^2-(E_\pm+\mu_I)^2)+ ln\,(p_0^2-(E_\pm-\mu_I)^2)\Bigg] \tag{E.23}$$

$$= 2i\int\frac{d^4p}{(2\pi)^4}\sum_{\alpha=\pm}\left[ln\left(\frac{p_0^2-(\varepsilon_\pm+\mu_I)^2}{p_0^2-(E_\pm+\mu_I)^2}\right)+ln\left(\frac{p_0^2-(\varepsilon_\pm-\mu_I)^2}{p_0^2-(E_\pm-\mu_I)^2}\right)\right] + 3i\int\frac{d^4p}{(2\pi)^4}\sum_{\alpha=\pm}\left[ln\left(p_0^2-(E_\pm+\mu_I)^2\right)+ln\left(p_0^2-(E_\pm-\mu_I)^2\right)\right] \tag{E.24}$$

$$= 2i\int\frac{d^4p}{(2\pi)^4}\sum_{\alpha=\pm}\left[ln\left(\frac{p_0^2-(\varepsilon_\pm+\mu_I)^2}{p_0^2-(E_\pm+\mu_I)^2}\right)+ln\left(\frac{p_0^2-(\varepsilon_\pm-\mu_I)^2}{p_0^2-(E_\pm-\mu_I)^2}\right)\right] + 3i\int\frac{d^4p}{(2\pi)^4}\sum_{\alpha=\pm}\left[ln\left(\frac{p_0^2-(E_\pm+\mu_I)^2}{p_0^2-E_p^2}\right)+ln\left(\frac{p_0^2-(E_\pm-\mu_I)^2}{p_0^2-E_p^2}\right)\right] + 12i\int\frac{d^4p}{(2\pi)^4}\left[ln\,(p_0^2-E_p^2)\right]. \tag{E.25}$$

We put the second integral in terms of up and down quark chemical potentials using,

$$ln\,[p_0^2-(E_\pm+\mu_I)^2]+\,ln\,[p_0^2-(E_\pm-\mu_I)^2] \tag{E.26}$$

$$= ln\,[(p_0+E_\pm+\mu_I)(p_0-E_\pm-\mu_I)(p_0+E_\pm-\mu_I)(p_0-E_\pm+\mu_I)] \tag{E.27}$$

$$= ln\,[p_0-(E_p+\mu_q+\mu_I)^2]+\,ln\,[p_0-(E_p+\mu_q-\mu_I)^2] \tag{E.28}$$

$$= ln\,[p_0-(E_p+\mu_u)^2]+\,ln\,[p_0-(E_p+\mu_d)^2]. \tag{E.29}$$

Including the quark loop term and the last two terms in Eqn. (E.6) (where $\Delta=\sqrt{3/2}\hat{\Delta}$), we derive the effective potential for quark matter (which has the form $V^{QM}=V_\Delta+V_Q+V_{vac}$),

$$V^{QM} = 2i\int\frac{d^4p}{(2\pi)^4}\sum_{\alpha=\pm}\left[ln\left(\frac{p_0^2-(\varepsilon_\pm+\mu_I)^2}{p_0^2-(E_\pm+\mu_I)^2}\right)+ln\left(\frac{p_0^2-(\varepsilon_\pm-\mu_I)^2}{p_0^2-(E_\pm-\mu_I)^2}\right)\right]+\frac{\Delta^2}{6G_s} + 3i\int\frac{d^4p}{(2\pi)^4}\sum_{Q=u,d}\left[ln\left(\frac{p_0^2-(E_p+\mu_Q)^2}{p_0^2-E_p^2}\right)+ln\left(\frac{p_0^2-(E_p-\mu_Q)^2}{p_0^2-E_p^2}\right)\right] + 12i\int\frac{d^4p}{(2\pi)^4}\left[ln\,(p_0^2-E_p^2)-ln\,(p_0^2-E_{p0}^2)\right]+\frac{(M-m)^2}{4G_\pi}-\frac{(M_0-m)^2}{4G_\pi}. \tag{E.30}$$

In the last line, we have subtracted the zero density ($M = M_0$) contribution to the vacuum term, V_{vac}. The first line corresponds to V_Δ, the contribution from the gap. The second term, referred to as V_Q, is simplified using the relation,

$$\int dp_0 \; ln \left[\frac{p_0^2 - a^2 + i\epsilon}{p_0^2 - b^2 + i\epsilon}\right] = 2\pi i\Big(|a| - |b|\Big). \tag{E.31}$$

Indeed, this term corresponds to the Fermi motion of the quarks,

$$\begin{aligned} V_Q =& 3i \int \frac{d^4p}{(2\pi)^4} \sum_{Q=u,d} \left[ln\left(\frac{p_0^2 - (E_p + \mu_Q)^2}{p_0^2 - E_p^2}\right) + ln\left(\frac{p_0^2 - (E_p - \mu_Q)^2}{p_0^2 - E_p^2}\right)\right] \\ =& -3 \int \frac{d^3p}{(2\pi)^3} \sum_{Q=u,d} \Big[|E_p + \mu_Q| + |E_p - \mu_Q| - 2E_p \Big] \\ =& -6 \int \frac{d^3p}{(2\pi)^3} \sum_{Q=u,d} \Theta(\mu_Q - E_p)(\mu_Q - E_p). \end{aligned} \tag{E.32}$$

The contribution due to colour superconductivity in quark matter is given by,

$$V_\Delta = 2i \sum_{\alpha=\pm} \int \frac{d^4p}{(2\pi)^4} \left[ln\left(\frac{p_0^2 - (\varepsilon_\alpha + \mu_I)^2}{p_0^2 - (E_\alpha + \mu_I)^2}\right) + ln\left(\frac{p_0^2 - (\varepsilon_\alpha - \mu_I)^2}{p_0^2 - (E_\alpha - \mu_I)^2}\right)\right] + \frac{\Delta^2}{6G_s}.$$

To evaluate the integral we note that,

$$2i \int \frac{d^4p}{(2\pi)^4} F(p_0^2, p) = \frac{-2}{(2\pi)^4} \int_{-\infty}^{\infty} dp_0 \int d^3p \; F(-p_0^2, p) \tag{E.33}$$

$$= \frac{-2}{(2\pi)^4} \, 2 \int_0^{\infty} dp_0 \, (4\pi) \int_0^{\infty} p^2 dp \; F(-p_0^2, p) \tag{E.34}$$

$$= \frac{-1}{(\pi)^3} \int_0^{\infty} dp_0 \int_0^{\infty} p^2 dp \; F(-p_0^2, p). \tag{E.35}$$

We use the proper-time replacement (Eqn. (B.18)) for the log terms. Setting the infra-red cut-off to zero, the integral is given by,

$$\begin{aligned} \sum_{\alpha=\pm} \frac{1}{(\pi)^3} \int_0^{\infty} dp_0 \int_0^{\infty} p^2 dp \int_{\frac{1}{\Lambda_{UV}{}^2}}^{\infty} \frac{d\tau}{\tau} \Big[& e^{-\tau(p_0^2 + (\varepsilon_\alpha + \mu_I)^2)} - e^{-\tau(p_0^2 + (E_\alpha + \mu_I)^2)} \\ & + e^{-\tau(p_0^2 + (\varepsilon_\alpha - \mu_I)^2)} - e^{-\tau(p_0^2 + (E_\alpha - \mu_I)^2)} \Big] \end{aligned} \tag{E.36}$$

We can not solve this numerically, since the integral over τ diverges. However, it

can be solved after using partial integration over p_0. That is, using the relation,

$$\int dx\ \frac{d}{dx}(fg) = \int dx\ (f\frac{dg}{dx}) + \int dx\ (g\frac{df}{dx}), \tag{E.37}$$

where $x = p_0$, $g = p_0$ and f is the integrand of Eqn. (E.36). Differentiating with respect to p_0 gives a factor of $-2\tau p_0$ and we may now integrate over τ to obtain,

$$\frac{2}{(\pi)^3}\int_0^\infty p_0^2\, dp_0 \int_0^\infty p^2 dp \left[F_+ + F_- - F_{0+} - F_{0-}\right] \tag{E.38}$$

where we have defined,

$$F_\pm = \frac{e^{-\left(p_0^2+(\varepsilon_\pm-\mu_I)^2\right)/\Lambda_{UV}^2}}{p_0^2+(\varepsilon_\pm-\mu_I)^2}. \tag{E.39}$$

F_{0+} and F_{0-} have the same form as $F_\pm$ except that $\Delta = 0$. At this point the integrals still have divergences (i.e. zeros in the denominator which do not cancel in the numerator). Using the identity $p_0^2/(p_0^2+x^2) = 1 - x^2/(p_0^2+x^2)$ and making a subtraction at $p_0 = 0$, we rearrange the integral so that all divergences cancel. For example, the second term is expressed as,

$$\begin{aligned}
&\frac{2}{(\pi)^3}\int_0^\infty p_0^2\, dp_0 \int_0^\infty p^2 dp\ \frac{e^{-\left(p_0^2+(\varepsilon_- -\mu_I)^2\right)/\Lambda_{UV}^2}}{p_0^2+(\varepsilon_- -\mu_I)^2} \\
&= \frac{2}{(\pi)^3}\int_0^\infty p_0^2\, dp_0 \int_0^\infty p^2 dp \left[e^{-\left(p_0^2+(\varepsilon_- -\mu_I)^2\right)/\Lambda_{UV}^2} - \frac{(\varepsilon_- -\mu_I)^2}{p_0^2+(\varepsilon_- -\mu_I)^2} e^{-\left(p_0^2+(\varepsilon_- -\mu_I)^2\right)/\Lambda_{UV}^2}\right] \\
&= \frac{2}{(\pi)^3}\frac{\Lambda_{UV}\sqrt{\pi}}{2}\int_0^\infty p^2 dp \left[e^{-(\varepsilon_- -\mu_I)^2/\Lambda_{UV}^2}\right] \\
&- \frac{2}{(\pi)^3}\int_0^\infty p_0^2\, dp_0 \int_0^\infty p^2 dp \left[\frac{(\varepsilon_- -\mu_I)^2}{p_0^2+(\varepsilon_- -\mu_I)^2}\left(e^{-\left(p_0^2+(\varepsilon_- -\mu_I)^2\right)/\Lambda_{UV}^2} - e^{-\left((\varepsilon_- -\mu_I)^2\right)/\Lambda_{UV}^2}\right)\right] \\
&- \frac{2}{(\pi)^3}\frac{\pi}{2}\int_0^\infty p^2 dp\, |\varepsilon_- -\mu_I|\, e^{-(\varepsilon_- -\mu_I)^2/\Lambda_{UV}^2}.
\end{aligned} \tag{E.40}$$

Thus we derive the numerically integrable form,

$$
\begin{aligned}
V_\Delta = \frac{2}{\pi^3}\sum_{\alpha=\pm}\Bigg[& \frac{\Lambda_{UV}\sqrt{\pi}}{2}\int_0^\infty dp\, p^2\Big(e^{-\frac{(\varepsilon_\alpha+\mu_I)^2}{\Lambda_{UV}^2}}+e^{-\frac{(\varepsilon_\alpha-\mu_I)^2}{\Lambda_{UV}^2}}-e^{-\frac{(E_\alpha+\mu_I)^2}{\Lambda_{UV}^2}}-e^{-\frac{(E_\alpha-\mu_I)^2}{\Lambda_{UV}^2}}\Big) \\
& -\int_0^\infty dp_0\int_0^\infty dp\, p^2\Bigg(\frac{(\varepsilon_\alpha+\mu_I)^2}{p_0^2+(\varepsilon_\alpha+\mu_I)^2}(e^{-\frac{p_0^2+(\varepsilon_\alpha+\mu_I)^2}{\Lambda_{UV}^2}}-e^{-\frac{(\varepsilon_\alpha+\mu_I)^2}{\Lambda_{UV}^2}}) \\
& \qquad +\frac{(\varepsilon_\alpha-\mu_I)^2}{p_0^2+(\varepsilon_\alpha-\mu_I)^2}(e^{-\frac{p_0^2+(\varepsilon_\alpha-\mu_I)^2}{\Lambda_{UV}^2}}-e^{-\frac{(\varepsilon_\alpha-\mu_I)^2}{\Lambda_{UV}^2}}) \\
& \qquad -\frac{(E_\alpha+\mu_I)^2}{p_0^2+(E_\alpha+\mu_I)^2}(e^{-\frac{p_0^2+(E_\alpha+\mu_I)^2}{\Lambda_{UV}^2}}-e^{-\frac{(E_\alpha+\mu_I)^2}{\Lambda_{UV}^2}}) \\
& \qquad -\frac{(E_\alpha-\mu_I)^2}{p_0^2+(E_\alpha-\mu_I)^2}(e^{-\frac{p_0^2+(E_\alpha-\mu_I)^2}{\Lambda_{UV}^2}}-e^{-\frac{(E_\alpha-\mu_I)^2}{\Lambda_{UV}^2}})\Bigg) \\
& -\frac{\pi}{2}\int_0^\infty dp\, p^2\Bigg(|\varepsilon_\alpha+\mu_I|e^{-\frac{(\varepsilon_\alpha+\mu_I)^2}{\Lambda_{UV}^2}}+|\varepsilon_\alpha-\mu_I|e^{-\frac{(\varepsilon_\alpha-\mu_I)^2}{\Lambda_{UV}^2}} \\
& \qquad -|E_\alpha+\mu_I|e^{-\frac{(E_\alpha+\mu_I)^2}{\Lambda_{UV}^2}}-|E_\alpha-\mu_I|e^{-\frac{(E_\alpha-\mu_I)^2}{\Lambda_{UV}^2}}\Bigg)\Bigg]+\frac{\Delta^2}{6G_s}. \qquad \text{(E.41)}
\end{aligned}
$$

To avoid integrating over edges (discontinuous first derivatives), we split up the integration ranges, depending on the values of μ_q, μ_I, M and Δ. The first integral is OK, as is the double integral. In the second to last line edges occur when p equals $\sqrt{(\mu_q-\sqrt{\mu_I^2-\Delta^2})^2-M^2}$, $\sqrt{\mu_q^2-M^2}$ and $\sqrt{(\mu_q+\sqrt{\mu_I^2-\Delta^2})^2-M^2}$ (when these are real numbers, they define the integration ranges we use). Similarly for the last two ($\Delta=0$) terms, the edges are at $\sqrt{(\mu_q-|\mu_I|)^2-M^2}$, $\sqrt{\mu_q^2-M^2}$ and $\sqrt{(\mu_q+|\mu_I|)^2-M^2}$.

E.2 Baryon Density

The baryon density for quark matter is given by,

$$
\rho_B^{QM} = -\frac{\partial V^{QM}}{\partial\mu_B} = -\frac{1}{3}\frac{\partial V_Q}{\partial\mu_q}-\frac{1}{3}\frac{\partial V_\Delta}{\partial\mu_q} \qquad \text{(E.42)}
$$

The last term is evaluated using the same techniques as were used to obtain Eqn. (E.41). Here we just quote the final result,

$$\begin{aligned}
\frac{\partial V_\Delta}{\partial \mu_q} = -\frac{2}{\pi^3}\sum_\pm \Bigg[& \int_0^\infty dp_0 \int_0^\infty dp \\
& p^2 \Bigg(\pm \frac{(\varepsilon_\pm + \mu_I)(E_q(p) \pm \mu_q)}{\varepsilon_\pm (p_0^2 + (\varepsilon_\pm + \mu_I)^2)} (e^{-\frac{p_0^2 + (\varepsilon_\pm + \mu_I)^2}{\Lambda_{UV}^2}} - e^{-\frac{(\varepsilon_\pm + \mu_I)^2}{\Lambda_{UV}^2}}) \\
& \pm \frac{(\varepsilon_\pm - \mu_I)(E_q(p) \pm \mu_q)}{\varepsilon_\pm (p_0^2 + (\varepsilon_\pm - \mu_I)^2)} (e^{-\frac{p_0^2 + (\varepsilon_\pm - \mu_I)^2}{\Lambda_{UV}^2}} - e^{-\frac{(\varepsilon_\pm - \mu_I)^2}{\Lambda_{UV}^2}}) \\
& \mp \frac{(E_\pm + \mu_I)(E_q(p) \pm \mu q)}{E_\pm (p_0^2 + (E_\pm + \mu_I)^2)} (e^{-\frac{p_0^2 + (E_\pm + \mu_I)^2}{\Lambda_{UV}^2}} - e^{-\frac{(E_\pm + \mu_I)^2}{\Lambda_{UV}^2}}) \\
& \mp \frac{(E_\pm - \mu_I)(E_q(p) \pm \mu q)}{E_\pm (p_0^2 + (E_\pm - \mu_I)^2)} (e^{-\frac{p_0^2 + (E_\pm - \mu_I)^2}{\Lambda_{UV}^2}} - e^{-\frac{(E_\pm - \mu_I)^2}{\Lambda_{UV}^2}}) \Bigg) \\
& + \frac{\pi}{2} \int_0^\infty dp\, p^2 \Bigg(\pm \frac{sign[\varepsilon_\pm + \mu_I](E_q(p) \pm \mu_q)}{\varepsilon_\pm} e^{-\frac{(\varepsilon_\pm + \mu_I)^2}{\Lambda_{UV}^2}} \\
& \qquad \pm \frac{sign[\varepsilon_\pm - \mu_I](E_q(p) \pm \mu_q)}{\varepsilon_\pm} e^{-\frac{(\varepsilon_\pm - \mu_I)^2}{\Lambda_{UV}^2}} \\
& \qquad \mp \frac{sign[E_\pm + \mu_I](E_q(p) \pm \mu_q)}{E_\pm} e^{-\frac{(E_\pm + \mu_I)^2}{\Lambda_{UV}^2}} \\
& \qquad \mp \frac{sign[E_\pm - \mu_I](E_q(p) \pm \mu_q)}{E_\pm} e^{-\frac{(E_\pm - \mu_I)^2}{\Lambda_{UV}^2}} \Bigg) \Bigg]. \qquad \text{(E.43)}
\end{aligned}$$

The integrands in both the double integral and the single integral contain edges. Again they occur when p equals $\sqrt{(\mu_q - \sqrt{\mu_I^2 - \Delta^2})^2 - M^2}$, $\sqrt{\mu_q^2 - M^2}$ and $\sqrt{(\mu_q + \sqrt{\mu_I^2 - \Delta^2})^2 - M^2}$ for the Δ dependent terms. The $(\Delta = 0)$ terms contain edges, at p equals; $\sqrt{(\mu_q - |\mu_I|)^2 - M^2}$, $\sqrt{\mu_q^2 - M^2}$ and $\sqrt{(\mu_q + |\mu_I|)^2 - M^2}$.

E.3 Charge Density

Including electrons, the charge density for quark matter is given by,

$$\rho_c^{QM} = \frac{1}{2}(\rho_B^{QM} + \rho_I^{QM}) + \rho_e \qquad \text{(E.44)}$$

$$= \frac{1}{2}(\rho_B^{QM} - \frac{\partial V^{QM}}{\partial \mu_I}) + \rho_e \qquad \text{(E.45)}$$

$$\text{where} \quad \frac{\partial V^{QM}}{\partial \mu_I} = \frac{\partial V_Q}{\partial \mu_I} + \frac{\partial V_\Delta}{\partial \mu_I} \tag{E.46}$$

The last term is evaluated using the same techniques as were used to obtain Eqn. (E.41). Here we just quote the final result,

$$\begin{aligned}
\frac{\partial V_\Delta}{\partial \mu_I} = -\frac{2}{\pi^3} \sum_{\alpha=\pm} \Bigg[& \int_0^\infty dp_0 \int_0^\infty dp \; p^2 \\
& \left(\frac{\varepsilon_\alpha + \mu_I}{p_0^2 + (\varepsilon_\alpha + \mu_I)^2} \left(e^{-\frac{p_0^2 + (\varepsilon_\alpha + \mu_I)^2}{\Lambda_{UV}^2}} - e^{-\frac{(\varepsilon_\alpha + \mu_I)^2}{\Lambda_{UV}^2}} \right) \right. \\
& - \frac{\varepsilon_\alpha - \mu_I}{p_0^2 + (\varepsilon_\alpha - \mu_I)^2} \left(e^{-\frac{p_0^2 + (\varepsilon_\alpha - \mu_I)^2}{\Lambda_{UV}^2}} - e^{-\frac{(\varepsilon_\alpha - \mu_I)^2}{\Lambda_{UV}^2}} \right) \\
& - \frac{E_\alpha + \mu_I}{p_0^2 + (E_\alpha + \mu_I)^2} \left(e^{-\frac{p_0^2 + (E_\alpha + \mu_I)^2}{\Lambda_{UV}^2}} - e^{-\frac{(E_\alpha + \mu_I)^2}{\Lambda_{UV}^2}} \right) \\
& \left. + \frac{E_\alpha - \mu_I}{p_0^2 + (E_\alpha - \mu_I)^2} \left(e^{-\frac{p_0^2 + (E_\alpha - \mu_I)^2}{\Lambda_{UV}^2}} - e^{-\frac{(E_\alpha - \mu_I)^2}{\Lambda_{UV}^2}} \right) \right) \\
& + \frac{\pi}{2} \int_0^\infty dp \, p^2 \left(\frac{\varepsilon_\alpha + \mu_I}{|\varepsilon_\alpha + \mu_I|} e^{-\frac{(\varepsilon_\alpha + \mu_I)^2}{\Lambda_{UV}^2}} - \frac{\varepsilon_\alpha - \mu_I}{|\varepsilon_\alpha - \mu_I|} e^{-\frac{(\varepsilon_\alpha - \mu_I)^2}{\Lambda_{UV}^2}} \right. \\
& \left. - \frac{E_\alpha + \mu_I}{|E_\alpha + \mu_I|} e^{-\frac{(E_\alpha + \mu_I)^2}{\Lambda_{UV}^2}} + \frac{E_\alpha - \mu_I}{|E_\alpha - \mu_I|} e^{-\frac{(E_\alpha - \mu_I)^2}{\Lambda_{UV}^2}} \right) \Bigg].
\end{aligned} \tag{E.47}$$

The integrands in both the double integral and the single integral contain edges. Again for the Δ dependent terms they occur at;

$\sqrt{(\mu_q - \sqrt{\mu_I^2 - \Delta^2})^2 - M^2}$, $\sqrt{\mu_q^2 - M^2}$ and $\sqrt{(\mu_q + \sqrt{\mu_I^2 - \Delta^2})^2 - M^2}$.

And for the ($\Delta = 0$) terms the edges are at;

$\sqrt{(\mu_q - |\mu_I|)^2 - M^2}$, $\sqrt{\mu_q^2 - M^2}$ and $\sqrt{(\mu_q + |\mu_I|)^2 - M^2}$.

F

General Relativity

In general relativity, the curvature tensor (Ricci tensor) is given by,

$$R^{\mu\nu} = \Gamma^{\alpha}_{\mu\alpha,\nu} - \Gamma^{\alpha}_{\mu\nu,\alpha} - \Gamma^{\alpha}_{\mu\nu}\Gamma^{\beta}_{\alpha\beta} + \Gamma^{\alpha}_{\mu\beta}\Gamma^{\beta}_{\nu\alpha}, \tag{F.1}$$

where the Christoffel symbols are defined by,

$$\Gamma^{\alpha}_{\mu\nu} = \frac{1}{2}g^{\alpha\beta}\left(\frac{\partial}{\partial x^{\nu}}g_{\mu\beta} + \frac{\partial}{\partial x^{\mu}}g_{\nu\beta} - \frac{\partial}{\partial x^{\beta}}g_{\mu\nu}\right). \tag{F.2}$$

The contracted symbols are given by,

$$\Gamma^{\alpha}_{\beta\alpha} = \frac{1}{2}g^{\mu\nu}\frac{\partial}{\partial x^{\alpha}}g_{\mu\nu}. \tag{F.3}$$

and the derivatives in Eqn. F.1 have the form,

$$\Gamma^{\alpha}_{\mu\nu,\,\alpha} = \frac{\partial}{\partial x^{\alpha}}\Gamma^{\alpha}_{\mu\nu}. \tag{F.4}$$

The metric for a spherically symmetric object is given by,

$$ds = -e^{2\Phi(r)}dt^2 + e^{2\Lambda(r)}dr^2 + d\theta^2 + r^2 sin^2\theta \;\; d\phi^2 \tag{F.5}$$

$$\equiv g_{\mu\nu}dx^{\mu}dx^{\nu}. \tag{F.6}$$

From this metric we identify the covariant components of the metric tensor,

$$g_{tt} = -e^{2\Phi(r)}, \;\; g_{rr} = e^{2\Lambda(r)}, \;\; g_{\theta\theta} = r^2, \;\; g_{\phi\phi} = r^2 sin^2\theta. \tag{F.7}$$

Spherical symmetry ensures that all the off-diagonal components are zero. The contravariant components of the metric tensor are obtained using the relation,

$$g^{\mu\alpha}g_{\nu\alpha} = \delta^{\mu}_{\nu}, \tag{F.8}$$

where δ^{μ}_{ν} is the four-dimensional Kronecker delta. Using these expressions it is simple to derive the Christoffel symbols (Eqn. F.2) and the derivatives used to calculate each component of the curvature tensor (Eqn. F.1). The equations for a spherically symmetric star (i.e. the TOV equations) follow from Eqns. (7.1) and (7.2). For a derivation of the TOV equations, see Ref. [177].

Bibliography

[1] W. Bentz and A. W. Thomas, Nucl. Phys. **A696**, 138 (2001), nucl-th/0105022.

[2] M. H. Johnson and E. Teller, Phys. Rev. **98**, 783 (1955).

[3] M. G. Mayer and J. H. D. Jensen, New York, USA: John Wiley and Sons (1955).

[4] H. Duerr, Phys. Rev. **103**, 469 (1956).

[5] T. Muta, World Sci. Lect. Notes Phys. **57**, 1 (1998).

[6] J. B. Kogut, Phys. Rept. **67**, 67 (1980).

[7] S. Hands, S. Kim, and J.-I. Skullerud, (2006), hep-lat/0604004.

[8] J. S. Schwinger, Phys. Rev. **82**, 664 (1951).

[9] A. Buck, R. Alkofer, and H. Reinhardt, Phys. Lett. **B286**, 29 (1992).

[10] D. Ebert, T. Feldmann, C. Kettner, and H. Reinhardt, Int. J. Mod. Phys. **A13**, 1091 (1998), hep-ph/9601257.

[11] M. Buballa, Phys. Rept. **407**, 205 (2005), hep-ph/0402234.

[12] W. Bentz, T. Horikawa, N. Ishii, and A. W. Thomas, Nucl. Phys. **A720**, 95 (2003), nucl-th/0210067.

[13] M. G. Alford, K. Rajagopal, and F. Wilczek, Phys. Lett. **B422**, 247 (1998), hep-ph/9711395.

[14] R. Rapp, T. Schafer, E. V. Shuryak, and M. Velkovsky, Phys. Rev. Lett. **81**, 53 (1998), hep-ph/9711396.

[15] D. G. Ravenhall, C. J. Pethick, and J. R. Wilson, Phys. Rev. Lett. **50**, 2066 (1983).

[16] R. G. Arnold *et al.*, Phys. Rev. Lett. **52**, 727 (1984).

[17] J. R. Bergervoet *et al.*, Phys. Rev. **C41**, 1435 (1990).

[18] P. Moller, J. R. Nix, W. D. Myers, and W. J. Swiatecki, Atom. Data Nucl. Data Tabl. **59**, 185 (1995), nucl-th/9308022.

[19] V. R. Pandharipande, In *Cargese 1989, Proceedings, Hadrons and hadronic matter* 293-341. (see HIGH ENEGY PHYSICS INDEX 29 (1991) No. 7756).

[20] U. W. Heinz and M. Jacob, (2000), nucl-th/0002042.

[21] e. . Rischke, D. and e. . Levin, G., Prepared for Workshop on New Discoveries at RHIC: The Current Case for the Strongly Interactive QGP, Brookhaven, Upton, New York, 14-15 May 2004.

[22] N. K. Glendenning, New York, USA: Springer (1997).

[23] J. R. Oppenheimer and G. M. Volkoff, Phys. Rev. **55**, 374 (1939).

[24] R. C. Tolman, Phys. Rev. **55**, 364 (1939).

[25] M. Kramer, (2003), astro-ph/0306456.

[26] H. Reinhardt, Phys. Lett. **B244**, 316 (1990).

[27] N. K. Glendenning, Phys. Rev. **D46**, 1274 (1992).

[28] M. E. Peskin and D. V. Schroeder, Reading, USA: Addison-Wesley (1995) 842 p.

[29] I. J. R. Aitchison and A. J. G. Hey, BRISTOL, UK: HILGER (1989) 571p.

[30] T. Hatsuda and T. Kunihiro, Phys. Rept. **247**, 221 (1994), hep-ph/9401310.

[31] G. 't Hooft, Phys. Rev. Lett. **37**, 8 (1976).

[32] R. J. Crewther, Riv. Nuovo Cim. **2N8**, 63 (1979).

[33] R. B. Wiringa, R. A. Smith, and T. L. Ainsworth, Phys. Rev. **C29**, 1207 (1984).

[34] J. Carlson and R. Schiavilla, Rev. Mod. Phys. **70**, 743 (1998).

[35] R. B. Wiringa, V. G. J. Stoks, and R. Schiavilla, Phys. Rev. **C51**, 38 (1995), nucl-th/9408016.

[36] J. Carlson, V. R. Pandharipande, and R. B. Wiringa, Nucl. Phys. **A401**, 59 (1983).

[37] B. D. Day and R. B. Wiringa, Phys. Rev. C **32**, 1057 (1985).

[38] A. E. L. Dieperink, D. Van Neck, Y. Dewulf, and V. Rodin, (2003), nucl-th/0312012.

[39] F. Weber and N. K. Glendenning, (1996), astro-ph/9609074.

[40] J. D. Walecka, Annals Phys. **83**, 491 (1974).

[41] B. D. Serot and J. D. Walecka, Adv. Nucl. Phys. **16**, 1 (1986).

[42] J. F. Donoghue, (2006), nucl-th/0602074.

[43] M. R. Pennington, (2006), hep-ph/0604212.

[44] J. D. Walecka, Phys. Lett. **B59**, 109 (1975).

[45] European Muon, J. J. Aubert *et al.*, Phys. Lett. **B123**, 275 (1983).

[46] A. Bodek *et al.*, Phys. Rev. Lett. **51**, 534 (1983).

[47] J.-W. Chen and W. Detmold, Phys. Lett. **B625**, 165 (2005), hep-ph/0412119.

[48] C. H. Llewellyn Smith, Phys. Lett. **B128**, 107 (1983).

[49] M. Ericson and A. W. Thomas, Phys. Lett. **B128**, 112 (1983).

[50] M. C. Birse, Phys. Lett. **B299**, 186 (1993).

[51] J. R. Smith and G. A. Miller, Phys. Rev. **C65**, 055206 (2002), nucl-th/0202016.

[52] L. S. Kisslinger and M. B. Johnson, Phys. Lett. **B259**, 416 (1991).

[53] D. F. Geesaman, K. Saito, and A. W. Thomas, Ann. Rev. Nucl. Part. Sci. **45**, 337 (1995).

[54] I. C. Cloet, W. Bentz, and A. W. Thomas, Phys. Rev. Lett. **95**, 052302 (2005), nucl-th/0504019.

[55] J. R. Smith and G. A. Miller, Phys. Rev. Lett. **91**, 212301 (2003), nucl-th/0308048.

[56] M. Buballa, Nucl. Phys. **A611**, 393 (1996), nucl-th/9609044.

[57] M. Gell-Mann and M. Levy, Nuovo Cim. **16**, 705 (1960).

[58] A. Chodos, R. L. Jaffe, K. Johnson, C. B. Thorn, and V. F. Weisskopf, Phys. Rev. **D9**, 3471 (1974).

[59] P. A. M. Guichon, Phys. Lett. **B200**, 235 (1988).

[60] A. W. Thomas, A. Michels, A. W. Schreiber, and P. A. M. Guichon, Phys. Lett. **B233**, 43 (1989).

[61] K. Saito, K. Tsushima, and A. W. Thomas, (2005), hep-ph/0506314.

[62] D. Diakonov and V. Y. Petrov, (2000), hep-ph/0009006.

[63] L. D. Faddeev, Sov. Phys. JETP **12**, 1014 (1961).

[64] Y. Nambu and G. Jona-Lasinio, Phys. Rev. **122**, 345 (1961).

[65] Y. Nambu and G. Jona-Lasinio, Phys. Rev. **124**, 246 (1961).

[66] S. P. Klevansky, Rev. Mod. Phys. **64**, 649 (1992).

[67] U. Vogl and W. Weise, Prog. Part. Nucl. Phys. **27**, 195 (1991).

[68] S. Klimt, M. Lutz, U. Vogl, and W. Weise, Nucl. Phys. **A516**, 429 (1990).

[69] J. Goldstone, A. Salam, and S. Weinberg, Phys. Rev. **127**, 965 (1962).

[70] D. Ebert, T. Feldmann, and H. Reinhardt, Phys. Lett. **B388**, 154 (1996), hep-ph/9608223.

[71] J. Bardeen, L. N. Cooper, and J. R. Schrieffer, Phys. Rev. **106**, 162 (1957).

[72] N. N. Bogoliubov, V. V. Tolmachev, and D. V. Shirkov, Consultants Bureau, New York, 1959.

[73] M. Gell-Mann, R. J. Oakes, and B. Renner, Phys. Rev. **175**, 2195 (1968).

[74] M. L. Goldberger and S. B. Treiman, Phys. Rev. **110**, 1178 (1958).

[75] K. Kawarabayashi and M. Suzuki, Phys. Rev. Lett. **16**, 255 (1966).

[76] Riazuddin and Fayyazuddin, Phys. Rev. **147**, 1071 (1966).

[77] V. Koch, T. S. Biro, J. Kunz, and U. Mosel, Phys. Lett. **B185**, 1 (1987).

[78] A. H. Rezaeian and H.-J. Pirner, Nucl. Phys. **A769**, 35 (2006), nucl-th/0510041.

[79] T. Hatsuda and T. Kunihiro, Prog. Theor. Phys. **74**, 765 (1985).

[80] G. Hellstern, R. Alkofer, and H. Reinhardt, Nucl. Phys. **A625**, 697 (1997), hep-ph/9706551.

[81] R. D. Ball, Phys. Rept. **182**, 1 (1989).

[82] N. Ishii, W. Bentz, and K. Yazaki, Nucl. Phys. **A587**, 617 (1995).

[83] E. E. Salpeter and H. A. Bethe, Phys. Rev. **84**, 1232 (1951).

[84] C. J. Burden, R. T. Cahill, and J. Praschifka, Austral. J. Phys. **42**, 147 (1989).

[85] F. Wilczek, (2004), hep-ph/0409168.

[86] E. Santopinto, Phys. Rev. **C72**, 022201 (2005), hep-ph/0412319.

[87] S. Capstick and N. Isgur, Phys. Rev. **D34**, 2809 (1986).

[88] N. Ishii, W. Bentz, and K. Yazaki, Phys. Lett. **B318**, 26 (1993).

[89] A. W. Thomas, P. A. M. Guichon, D. B. Leinweber, and R. D. Young, Prog. Theor. Phys. Suppl. **156**, 124 (2004), nucl-th/0411014.

[90] C. F. Von Weizsacker, Z. Phys. **96**, 431 (1935).

[91] D. N. Basu and P. R. Chowdhury, (2004), nucl-th/0408013.

[92] K. Iida and K. Oyamatsu, Phys. Rev. **C69**, 037301 (2004), nucl-th/0401057.

[93] J. P. Blaizot, Phys. Rept. **64**, 171 (1980).

[94] U. Zuckert, R. Alkofer, H. Weigel, and H. Reinhardt, Phys. Rev. **C55**, 2030 (1997), nucl-th/9609012.

[95] D. J. Gross and F. Wilczek, Phys. Rev. **D8**, 3633 (1973).

[96] S. Bethke, (2006), hep-ex/0606035.

[97] S. Lawley, W. Bentz, and A. W. Thomas, Phys. Lett. **B632**, 495 (2006), nucl-th/0504020.

[98] J. Bardeen, L. N. Cooper, and J. R. Schrieffer, Phys. Rev. **108**, 1175 (1957).

[99] M. G. Alford, Ann. Rev. Nucl. Part. Sci. **51**, 131 (2001), hep-ph/0102047.

[100] K. Rajagopal, Prepared for Cargese Summer School on QCD Perspectives on Hot and Dense Matter, Cargese, France, 6-18 Aug 2001.

[101] J. C. Collins and M. J. Perry, Phys. Rev. Lett. **34**, 1353 (1975).

[102] B. C. Barrois, Nucl. Phys. **B129**, 390 (1977).

[103] D. Bailin and A. Love, Phys. Rept. **107**, 325 (1984).

[104] T. Schafer, Nucl. Phys. **B575**, 269 (2000), hep-ph/9909574.

[105] H. Grigorian, D. Blaschke, and D. Voskresensky, Phys. Rev. **C71**, 045801 (2005), astro-ph/0411619.

[106] F. Weber, Prog. Part. Nucl. Phys. **54**, 193 (2005), astro-ph/0407155.

[107] D. Blaschke, S. Fredriksson, H. Grigorian, A. M. Oztas, and F. Sandin, Phys. Rev. **D72**, 065020 (2005), hep-ph/0503194.

[108] S. B. Ruster, V. Werth, M. Buballa, I. A. Shovkovy, and D. H. Rischke, Phys. Rev. **D72**, 034004 (2005), hep-ph/0503184.

[109] M. Buballa, F. Neumann, M. Oertel, and I. Shovkovy, Phys. Lett. **B595**, 36 (2004), nucl-th/0312078.

[110] A. R. Bodmer, Phys. Rev. **D4**, 1601 (1971).

[111] E. Witten, Phys. Rev. **D30**, 272 (1984).

[112] N. Itoh, Prog. Theor. Phys. **44**, 291 (1970).

[113] M. Alford and K. Rajagopal, (2006), hep-ph/0606157.

[114] D. Bandyopadhyay, Pramana **66**, 817 (2006), nucl-th/0512100.

[115] M. G. Alford, AIP Conf. Proc. **806**, 293 (2006), nucl-th/0512005.

[116] P. Wang, S. Lawley, D. B. Leinweber, A. W. Thomas, and A. G. Williams, Phys. Rev. **C72**, 045801 (2005), nucl-th/0506014.

[117] L.-y. He, M. Jin, and P.-f. Zhuang, Phys. Rev. **D71**, 116001 (2005), hep-ph/0503272.

[118] A. Barducci, R. Casalbuoni, G. Pettini, and L. Ravagli, Phys. Rev. **D71**, 016011 (2005), hep-ph/0410250.

[119] D. Ebert and K. G. Klimenko, J. Phys. **G32**, 599 (2006), hep-ph/0507007.

[120] T. Maruyama, T. Muto, T. Tatsumi, K. Tsushima, and A. W. Thomas, Nucl. Phys. **A760**, 319 (2005), nucl-th/0502079.

[121] W. H. Dickhoff, A. Faessler, J. Meyer-Ter-Vehn, and H. Muther, Phys. Rev. **C23**, 1154 (1981).

[122] J. B. Kogut and D. Toublan, Phys. Rev. D **64**, 034007 (2001).

[123] H. J. Warringa, D. Boer, and J. O. Andersen, Phys. Rev. **D72**, 014015 (2005), hep-ph/0504177.

[124] W. Detmold, G. A. Miller, and J. R. Smith, Phys. Rev. **C73**, 015204 (2006), nucl-th/0509033.

[125] M. Huang, P.-f. Zhuang, and W.-q. Chao, Phys. Rev. **D67**, 065015 (2003), hep-ph/0207008.

[126] R. Xu, (2002), astro-ph/0211348.

[127] S. Lawley, W. Bentz, and A. W. Thomas, J. Phys. **G32**, 667 (2006), nucl-th/0602014.

[128] H. Heiselberg, C. J. Pethick, and E. F. Staubo, Phys. Rev. Lett. **70**, 1355 (1993).

[129] I. Shovkovy, M. Hanauske, and M. Huang, Phys. Rev. **D67**, 103004 (2003), hep-ph/0303027.

[130] P. K. Panda, D. P. Menezes, and C. Providencia, Phys. Rev. **C69**, 025207 (2004), nucl-th/0310075.

[131] T. Endo, T. Maruyama, S. Chiba, and T. Tatsumi, (2005), hep-ph/0502216.

[132] N. K. Glendenning, Astrophys. J. **293**, 470 (1985).

[133] D. N. Voskresensky, M. Yasuhira, and T. Tatsumi, Phys. Lett. **B541**, 93 (2002), nucl-th/0109009.

[134] N. K. Glendenning and S. Pei, Phys. Rev. **C52**, 2250 (1995).

[135] W. Baade and F. Zwicky, Phys. Rev. **45**, 138 (1934).

[136] J. Chadwick, Nature **129**, 312 (1932).

[137] V. Canuto, B. Datta, and G. Kalman, Astrophys. J. **221**, 274 (1978).

[138] G. Baym, C. Pethick, and P. Sutherland, Astrophys. J. **170**, 299 (1971).

[139] S. Lawley, W. Bentz, and A. W. Thomas, Nucl. Phys. Proc. Suppl. **141**, 29 (2005), nucl-th/0409073.

[140] F. X. Timmes, S. E. Woosley, and T. A. Weaver, Astrophys. J. **457**, 834 (1996), astro-ph/9510136.

[141] A. Hewish, S. J. Bell, J. D. H. Pilkington, P. F. Scott, and R. A. Collins, Nature **217**, 709 (1968).

[142] F. Pacini, Nature **219**, 145 (1968).

[143] T. Gold, Nature **218**, 731 (1968).

[144] F. Pacini, (2002), astro-ph/0208563.

[145] A. A. Svidzinsky, Astrophys. J. **590**, 386 (2003), astro-ph/0212367.

[146] M. Gedalin, E. Gruman, and D. B. Melrose, Mon. Not. Roy. Astron. Soc. **337**, 422 (2002), astro-ph/0205069.

[147] R. A. Hulse and J. H. Taylor, Astrophys. J. **195**, L51 (1975).

[148] J. M. Lattimer and M. Prakash, Phys. Rev. Lett. **94**, 111101 (2005), astro-ph/0411280.

[149] G. S. Bisnovatyi-Kogan, (2005), gr-qc/0511072.

[150] I. H. Stairs, ECONF **C0507252**, L004 (2005).

[151] E. Kreyszig, 7th Edition, John Wiley and sons, Inc. (1993).

[152] L. Brito *et al.*, (2006), nucl-th/0606059.

[153] P. Haensel, K. P. Levenfish, and D. G. Yakovlev, (2000), astro-ph/0004183.

[154] N. K. Glendenning and C. Kettner, Astron. Astrophys. **353**, L9 (2000), astro-ph/9807155.

[155] E. S. Fraga, R. D. Pisarski, and J. Schaffner-Bielich, Phys. Rev. **D63**, 121702 (2001), hep-ph/0101143.

[156] K. Schertler, C. Greiner, J. Schaffner-Bielich, and M. H. Thoma, Nucl. Phys. **A677**, 463 (2000), astro-ph/0001467.

[157] J. W. T. Hessels *et al.*, (2006), astro-ph/0601337.

[158] G. B. Cook, S. L. Shapiro, and S. A. Teukolsky, Astrophys. J. **424**, 823 (1994).

[159] J. Madsen, Phys. Rev. **D46**, 3290 (1992).

[160] D. J. Nice *et al.*, (2005), astro-ph/0508050.

[161] H. Mineo, W. Bentz, N. Ishii, A. W. Thomas, and K. Yazaki, Nucl. Phys. **A735**, 482 (2004), nucl-th/0312097.

[162] I. C. Cloet, W. Bentz, and A. W. Thomas, Phys. Lett. **B621**, 246 (2005), hep-ph/0504229.

[163] H. Mineo, W. Bentz, N. Ishii, and K. Yazaki, Nucl. Phys. **A703**, 785 (2002), nucl-th/0201082.

[164] N. Ishii, Phys. Lett. **B431**, 1 (1998).

[165] A. N. Kvinikhidze, M. C. Birse, and B. Blankleider, Phys. Rev. **C66**, 045203 (2002), hep-ph/0110060.

[166] A. W. Thomas and W. Weise, Berlin, Germany: Wiley-VCH (2001) 389 p.

[167] R. D. Young, D. B. Leinweber, A. W. Thomas, and S. V. Wright, Phys. Rev. **D66**, 094507 (2002), hep-lat/0205017.

[168] W. Detmold, D. B. Leinweber, W. Melnitchouk, A. W. Thomas, and S. V. Wright, Pramana **57**, 251 (2001), nucl-th/0104043.

[169] K. Suzuki *et al.*, Phys. Rev. Lett. **92**, 072302 (2004), nucl-ex/0211023.

[170] A. Arima, K. Shimizu, W. Bentz, and H. Hyuga, Adv. Nucl. Phys. **18**, 1 (1987).

[171] A. W. Thomas, S. Theberge, and G. A. Miller, Phys. Rev. **D24**, 216 (1981).

[172] B. C. Pearce and I. R. Afnan, Phys. Rev. **C34**, 991 (1986).

[173] M. B. Hecht *et al.*, Phys. Rev. **C65**, 055204 (2002), nucl-th/0201084.

[174] M. Alford *et al.*, (2006), astro-ph/0606524.

[175] L. P. Gorkov, Sov. Phys. JETP **7**, 993 (1958).

[176] Y. Nambu, Phys. Rev. **117**, 648 (1960).

[177] F. Weber, Bristol, UK: IOP (1999) 682 p.